

Characterization and Quantification of Magnetic Particles and Magnetically Labeled Cells by Magnetic Cytometry

by

Chen Zhou

A dissertation submitted to the Graduate Faculty of
Auburn University
in partial fulfillment of the
requirements for the Degree of
Doctor of Philosophy

Auburn, Alabama
May 6, 2017

Keywords: labeled cells, magnetic particles, magnetophoretic mobility,
chemistry of phagocytosis, characterization and quantification

Copyright 2017 by Chen Zhou

Approved by

Thomas Hanley, Chair, Professor of Chemical Engineering
Allan David, Professor of Chemical Engineering
Bart Prorok, Professor of Materials Engineering
Ram Gupta, Professor of Chemical Engineering
Paul Todd, Chief Scientist Emeritus at Techshot, Inc.

Abstract

Characterization of magnetic particles and labeled cells is in high demand in both medical research and clinical applications. A HyperfluxTM Velocimeter is utilized to directly measure the magnetophoretic mobility, size and other morphology parameters of magnetic particles and labeled cells. The magnetophoretic mobility analysis provides a better understanding and quality control of particles samples, serves as a key parameter in describing cell motion in a defined magnetic field and quantitatively determines the number of particles ingested per cell.

The Chinese hamster ovary (CHO-K1) cells were exposed in monolayer culture to approximated 50 and 100 nm iron oxide nanoparticles coated with starch, surface amine groups and polyethylene glycol (PEG) to study the chemistry of phagocytosis. Kinetic and dynamic studies were performed with varying incubation times and particle concentrations. At the conclusion of each exposure, cells were harvested into single-cell suspensions, and particle uptake was quantified by magnetic cytometry. By quantitatively determining the magnetophoretic mobility which is proportional to particle uptake per cell as measured by flow cytometry and by chemical analysis, the dependencies of phagocytosis on cell type, incubation time, particle composition, particle size and particle toxicity were determined. Particle uptake of surface aminated particles by CHO cells is larger than either starch-coated particles or uncoated particles. Amination of starch particles increased the positive zeta potential and cellular uptake. In contrast, PEGylation of aminated starch particles decreased the positive zeta potential and drastically reduced cellular uptake.

Magnetic cytometry can accurately measure properties of magnetic particles and labeled cells. Velocimetry analysis reveals that SPION surface charges and composition profoundly affect their uptake by cells in vitro. The labeled cell system can be optimized for special applications by controlling labeling conditions.

Acknowledgment

I would like to show my sincere gratitude to Dr. Thomas R. Hanley for giving me a good guideline for my whole PhD degree. He continually and convincingly conveyed a spirit in regard to research. Without his encouragement and persistent help, this dissertation would not have been possible.

I would also like to expand my deepest gratitude to Dr. Paul W. Todd for his valuable advice, technical support, paper revise and also for serving on my committee. I also want to thank you Dr. Allan E. David, who help and support in providing biological lab for the characterization of label cells. I would like to extend my thanks to Dr. Young Suk Choi for the cell culture training and problems troubleshooting.

I would also like to acknowledge my committee members, Dr. Allan E. David, Dr. Bart Prorok, Dr. Ram Gupta and my university reader, Dr. Robert D. "Rusty" Arnold for their brilliant comments and suggestions on my dissertation.

I would especially like to thank Allison Church Bird for her help and support when using the flow cytometry for label cell measuring.

I would like to express my thanks to many people, especially my classmates and team members itself, who have made valuable comment suggestions on my dissertation which gave me an inspiration to improve work.

A special thanks to my family, my beloved wife Liang Li, my new-born daughter Iris Li Zhou, my parent-in law, my parents for supporting and letting me through all the difficulties.

Table of Contents

Characterization and Quantification of Magnetic Particles and Magnetically Labeled Cells by Magnetic Cytometry	i
Abstract	I
Acknowledgment	iv
Chapter 1- Introduction.....	1
Chapter 2 – Literature Review.....	3
2.1 Introduction to Magnetic Particles.....	3
2.1.1 Types of Magnetic particle	3
2.1.2 Methods for Magnetic Particle Preparation	4
2.1.3 Magnetophoretic Mobility	5
2.1.4 Application of MNPs and importance of magnetophoretic mobility	8
2.2 Characterization of Magnetic Particles	13
2.2.1 Structural analysis.....	13
2.2.2 Magnetic Properties	14
2.3 Magnetic Cell Separation	20
2.3.1 Theory of Magnetic Separation	21
2.3.2 Analytical and Separation techniques.....	26
2.4 Label Cell	36
2.4.1 Cytotoxicity	36

2.4.2 Cell uptake	37
2.4.3 Culture Condition	38
References	39
Chapter 3 - Magnetic Particle Characterization – Magnetophoretic Mobility and Particle Size .	57
Abstract:	57
Key Words:.....	57
3.1 INTRODUCTION.....	58
3.2 Theory	59
3.3 Materials and Methods	61
3.3.1 Non-magnetic Particles and Magnetic Particles.....	61
3.3.2 Hyperflux Velocimeter	62
3.3.3 Procedure	64
3.4 Results and Discussion.....	65
3.4.1 Magnetophoretic Mobility Measurements.....	65
3.4.2 Characterization of Paramagnetic Particles	67
3.4.3 Particle counting.....	69
3.4.4 Threshold Settings	71
3.4.5 Size Calibration	75
3.5 Conclusion.....	76
References	79

Chapter 4 - Application of Magnetic Carriers to Two Examples of Quantitative Cell Analysis .	83
Abstract.....	83
Keywords:	83
4.1 Introduction	84
4.2 Experimental	85
4.2.1 Cells	85
4.2.2 Particles	86
4.2.3 Magnetophoretic mobility measurement	86
4.3 Results and Discussion.....	88
4.3.1 Magnetophoretic mobility of tumor cells labeled for flowing separation	88
4.3.2 Magnetophoretic mobility and nanoparticle phagocytosis.....	89
4.4. Conclusions	92
Acknowledgments	93
References	93
Chapter 5 - Magnetically Labeled Cell Characterization and Quantification	95
Abstract	95
5.1 - Introduction	95
5.2 - Theory	96
5.3 - Experimental	97
5.3.1 - SPIONs Surface Modifications	97

5.3.2 - Stained SPIONs.....	98
5.3.3 – CHO-K1 cell subculture (every 48 hours).....	98
5.3.4 - Labeling of cells.....	99
5.3.5 - Preparing test samples for Hyperflux analysis.....	99
5.3.6 - Further treatment for flow cytometry test.....	99
5.3.7 - Flow Cytometry Test.....	100
5.3.8 - Ferrozine assay.....	100
5.4 - Results and Discussion.....	102
5.4.1 - Chemistry of Phagocytosis.....	102
5.4.2 - Triplicate Experiments.....	113
5.4.3 - Flow cytometry analysis.....	116
5.4.4 - Ferrozine Assay.....	121
5.5 - Conclusions.....	123
References.....	124
Chapter 6 – Summary.....	125
Reference.....	126

List of Figures

Figure 2.1 – Particle suspended in a magnetic field. (a) Magnetic particle entering the magnetic field; (b) Magnetic particle reaching the final velocity, force balance;.....	6
Figure 2.2 – Quadrupole Magnetic Sorter (flow field in symmetry plane on left).....	9
Figure 2.3 - How MRI work: (http://ygoy.com/).....	10
Figure 2.4 - Sherwood Susceptibility Balance (Mk1)	15
Figure 2.5 The Major component of Hyperflux and the High-Definition Magnetic Cell-Tracking Velocimeter (www.ikotech.com).....	19
Figure 2.6 - Isodynamic field (the region in the box with parallel, same length pathlines)	23
Figure 2.7 - Diagram of the Hyperflux Velocimeter (Camera focused on region of interest)	28
Figure 2.8 - Quadrupole field. The black lines with arrow are the field lines. The red dashed lines represent the magnetic field contour (dark red-low field; light red-high field)	32
Figure 2.9 - QMS: (a) transport lamina; (b) schematic of quadrupole flow sorter: r_1 refers to the distance between inner splitting surface (ISS) and the core; r_2 is the distance from core to outer splitting surface (OSS). The space between ISS and OSS is called the transport lamina.	35
Figure 3.1 - Hyperflux TM Velocimeter instrument layout, image data analysis processing and mobility distribution display. (A) Velocimeter Layout. Three major parts are included: microscope and camera system, stopped-flow channel cell positioned in the isodynamic magnetic field, image analysis software. (B) Working window of Cytotest TM Image Analysis Software Display: The trajectory of each particle can be observed, and artefacts can be excluded (blue disks). Threshold and size gates are set before automatic track calculation. Size distribution and statistical summary are listed on the right. (C) Graphical Display: Magnetophoretic mobility histogram of medium-mobility calibration beads.	64
Figure 3.2 - Mobility Distribution Results displayed on a linear scale. (A) Mobility distribution for Standard Medium Mobility Calibration Beads, results of triplicate tests: average mobilities of tests 1, 2 and 3 are 6.87 ± 1.85 , 6.80 ± 1.89 , 6.89 ± 2.05 . (B) Magnetophoretic Mobility Distributions of B Magnetic Particles. (C) Magnetophoretic Mobility Distributions of P Magnetic Particles. (D) Magnetophoretic Mobility distributions of L Samples.	66
Figure 3.3 - Influence of Threshold Setting Value on Analysis Results. (A) Particle Count versus intensity threshold. (B) Diameter versus intensity threshold. (C) Magnetophoretic Mobility Distributions of L1, L2 and L3 beads with different intensity threshold values 25, 30, 40, 60 and 90, respectively.	74

Figure 3.4 – (A) Particle size calibration plots showing average calculated (Hyperflux Velocimeter) diameter versus vendor reported diameter with intensity threshold values from 30 to 50. The fitted linear equations apply to the intensity threshold values shown to the right of each of the equations. (B) Two-parameter scatter plot of calculated diameter using equation (4) vs. measured magnetophoretic mobility for magnetic beads designated L1. 78

Figure 4.1. Labeled photograph of the Hyperflux™ magnetic velocimeter demonstrated in this study..... 88

Figure 4.2. Screen shot of mobility histogram generated automatically by the Hyperflux™ velocimeter for magnetically labeled chicken lymphoma cells. Vertical solid line indicates peak mobility. Vertical dashed line indicates minimum magnetophoretic mobility ($1.3 \times 10^{-12} \text{ m}^3/\text{TAs}$) for 100% capture of cells in a modeled cell separator flowing at 1.0 mL/min..... 89

Figure 4.3. Magnetophoretic mobility distributions of CHO cells labeled for 24 h with 100 nm starch-coated Chemicell Fluid MAG-D magnetic particles measured using two intensity threshold settings of the Hyperflux™ velocimeter. Top: Screen shot of image analysis data at Threshold= 190. Lower: Mobility distributions at threshold = 130 and 190 on a linear mobility scale. 90

Figure 4.4. Magnetophoretic mobility distributions of CHO cells labeled for 24 hours with five concentrations of 100 nm starch-coated beads. There is a 15-fold increase in beads/cell over this concentration range. Unlabeled cells have no magnetophoretic mobility. 91

Figure 4.5. Average magnetophoretic mobility of CHO cells that ingested five concentrations of 50 nm or 100 nm starch-coated beads vs. concentration of beads as measured by iron content. . 92

Figure 5.1 - Approximately 50 and 100 nm superparamagnetic iron-oxide nanoparticles with various coatings after surface treatment. Starch coating supplied by Chemicell (fluidMAG-D), aminated-starch, 2k-PEG, 5k-PEG, 20k-PEG 98

Figure 5.2a. Magnetophoretic mobility distributions of CHO cells labeled by 100nm SPIONs coated with starch, primary amine groups or 2k/5k/20k Da polyethylene glycol (PEG), incubation time = 24h, incubation concentration= 10, 50, 100, 150, 200 µg/mL of iron..... 106

Figure 5.2b. Magnetophoretic mobility distribution of CHO cells labeled by 50nm SPIONs coated with starch, primary amine groups or 2k/5k/20k Da poly(ethylene glycol) (PEG). Incubation time = 24h, incubation concentration= 10, 50, 100, 150, 200 µg/mL. 108

*SE, standard error= $SD/(\text{track number})^{0.5}$ 108

Figure 5.2c. Magnetophoretic mobility distributions of CHO cells labeled by 100nm SPIONs coated with starch, primary amine groups or 2k/5k/20k Da polyethylene glycol (PEG). incubation time = 1, 4, 8, 24 h, incubation concentration= 100, 200 µg/mL iron..... 110

Figure 5.2d. Magnetophoretic mobility distributions of CHO cells labeled by 50 nm SPIONs coated with starch, primary amine groups or 2k/5k/20k Da polyethylene glycol (PEG). Incubation time = 1, 4, 8, 24 hours, incubation concentration= 100, 200 µg/mL. 111

Figure 5.3. Average mobility after 24 h vs iron concentration. A: 100nm, B: 50nm diameter
Average mobility vs. incubation time at 100 µg/mL C: 100nm, D: 50nm. 112

Figure 5.4 - Triplicate experiment: magnetophoretic mobility distributions of CHO cells labeled
by 100 and 50nm SPIONs coated with starch, primary amine groups or 2k/5k/20k Da PEG
PEGpoly(ethylene glycol) (PEG), iron incubation time = 24h, incubation concentration=
100 µg/mL 115

Figure 5.5 - Cell uptake study by flow cytometry (Accuri C6 Flow Cytometer®) and
Hyperflux™ Velocimetry. (A) Fluorescence intensity distributions of labeled cells before and
after fluorescent marking with different fluorescent SPIONs. (C) Magnetophoretic mobility
distribution of labeled cells captured by fluorescent SPIONs (100nm aminated, 2k, 5k and 20k
PEGylated MNPs-AF488). (B) Comparison of fluorescence intensities between labeled cells
capturing fluorescent SPIONs. (D) The linear relationship between mean fluorescence intensities
and average mobility suggest a good agreement between the two methods of phagocytosis assay.
..... 120

Figure 5.6 Side scatter and forward scatter dot plots..... 120

Figure 5.7 - Comparison between magnetophoresis and ferrozine assay 122

List of Tables

Table 2.1 - Devices which can detect magnetic susceptibility	26
Table 2.2 - Commercial magnetic cell separation products and devices	30
Table 3.1. Summary characteristics of beads used for calibrations and supplied by vendor, IKOTECH, LLC.	67
Table 3.2 – Particle Concentration Measurement by Hyperflux Imaging Compared to Hemacytometer Counts.....	70
Table 3.3 – Statistical Analysis of the Agreement between Hyperflux Velocimeter and Hemacytometer Particle Counts	71
Table 5.1 – Concentrations for BCA Analysis	100
Table 5.2 – SPION and Coatings for Cell Uptake Testing.....	101
Table 5.3 - Statistical calculations for results of triplicate experiments.....	114
Table 5.4 - Particles with and without fluorescent label used in phagocytosis assays	116
Table 5.5 - Fluorescent assay and magnetophoresis of cells	117
Table 5.6 - Comparison of the two analytical methods based on study of magnetic carriers	118
Table 5.7 - Results of Ferrozine Assay.....	121

Chapter 1- Introduction

Magnetic particles have been applied to a wide range of biological and biomedical applications, including MRI, labeled cell separation, drug delivery, medical diagnosis and therapy. Each application requires high-quality magnetic particles with specific properties. In addition to the preparation method, particle property measurement and separation techniques are key in the production of magnetic particles.

Characterization of magnetic particles is required for analysis and separation of labeled cells and magnetic particles. Most reported methods provide only limited, bulk-average information of the magnetic particle sample which is insufficient for quality evaluation and control of the magnetic particle product and separation design.

A HyperfluxTM Velocimeter directly measures the magnetophoretic mobility distribution, size and other morphology parameters of magnetic particles and labeled cells. The particle-by-particle analysis describes the properties of the sample in greater detail than is possible with other techniques. The instrument provides quantitative video analysis of cells and/or particles and their motion. The trajectories of magnetic particles in a uniform isodynamic magnetic field are recorded using a high-definition camera/microscope system for image collection. Image analysis software then converts the image data to the parameters of interest.

The primary objective of this research is to design, simulate and test an accurate, cost-effective, user-friendly velocimeter. The distribution of magnetophoretic mobility is determined by combining fast image analysis with velocimetry measurements. In addition, the particle size distribution is characterized to provide a better understanding of the sample quality.

This work focuses on the study of the particle/cell system and reveals the effect of particle surface chemistry on cell uptake. Flow cytometry has been utilized to monitor the cell uptake and cell health but can't detect labeled cells without producing a fluorescent signal. The velocimeter characterizes labeled cells without fluorescent emission. Also, the magnetophoretic mobility is proportional to cell uptake rate and can be used to investigate the cell uptake kinetics. This work provides a more convenient and accurate method to describe magnetic labeled cells and quantify nanoparticle phagocytosis.

Chapter 2 – Literature Review

2.1 Introduction to Magnetic Particles

Magnetic particles have attracted sharper focus for their considerable potential application in various fields such as cell separation, magnetic resonance imaging (MRI), hyperthermia/drug delivery, magnetic particle standards and magnetic particle quality control. To succeed in use in a specific field, magnetic particles are required to possess at least one of following properties: monodispersity, superparamagnetism, stability, or biocompatibility (Kim, Shin et al. 2012). Thus, researchers and manufacturers have invested significant time and effort to develop this technology.

2.1.1 Types of Magnetic particle

Many types of magnetic particle are being studied and utilized. The magnetic nanoparticle (MNP) has the size range from 0.5 to 1,000 nanometers. The first generation of metallic oxide/ferrite nanoparticle was developed in 1960s. Such particles consist of γ -Fe₂O₃ (with a cubic structure), Fe₃O₄ and MeFe₂O₄ (Me = Co, Ni, Mn). These particles received the most attention from researchers until recently (Ranganathan and Ray 2002, Gul and Maqsood 2007, Gul, Ahmed et al. 2008). At the same time, metallic particles were studied in the application of drug delivery (Freeman, Arrott et al. 1960, Meyers, Nice et al. 1963). The further research indicates that carriers in nanoscale can extravasate more easily (Jain 1987, Dvorak, Nagy et al. 1988). In 1993, the preparation of Fe₄N magnetic particles was first reported (Tang, Hadjipanayis et al. 1993). After that, FeN, Fe₂N, ϵ -Fe₃N, Fe₁₆N₂ and similar compounds were also studied (Jonsson, Mamiya et al. 2004, Huang, Lu et al. 2009, Masubuchi, Yamashita et al. 2011). To date, interest in core-shell structure supports the development of this type of magnetic particle since the shells could protect to the cores and bring in new properties to the hybrid

system (Fung, Qin et al. 2000, Burke, Stover et al. 2001, Seto, Koga et al. 2006, Riskin, Basnar et al. 2007, Rosicka and Sembera 2011, Li, Ma et al. 2012). To summarize, the main types being used are metallic particles, oxide/ferrite particles, and iron nitride particles. Based on these types, the core-shell structure is developed.

2.1.2 Methods for Magnetic Particle Preparation

The methods to synthesis magnetic particles have been subjected to extensive research as magnetic particles are introduced to more and more fields. The microemulsion method has been employed to prepare Fe_3O_4 MNPs since 1982 (Inouye, Endo et al. 1982). MeFe_2O_4 was also formed in micelles (Carpenter, O'Connor et al. 1999, Agnoli, Zhou et al. 2001). The use of Nanoemulsions, a non-equilibrium system, was proposed for nanoparticle preparation 20 years ago with many successful applications in pharmacy and cosmetics (Gutierrez, Gonzalez et al. 2008). Katepetch (Katepetch and Rujiravanit 2011) use an in situ co-precipitation method to synthesis Fe_3O_4 MNP inside bacterial cellulose. $\alpha''\text{-Fe}_{16}\text{N}_2$ was produced by Masubuchi by using non-aqueous synthesis (Masubuchi, Yamashita et al. 2011). Gong used thermal decomposition and sol-gel methods to get Ni nanoparticles and Co-doped Ni nanoparticles with different grain sizes (Gong, Liu et al. 2010). Flame spray synthesis (FSS) was used as a large-scale powder processing technique to produce nanoscale $\text{La}_{0.6}\text{Sr}_{0.4}\text{CoO}_3$ -delta powder for solid oxide fuel cell cathodes from water-based nitrate solutions (Heel, Holtappels et al. 2010). Keng synthesized polymer-coated ferromagnetic cobalt nanoparticles via the method of radical polymerization (Keng, Shim et al. 2007). The core/shell nanoparticles can also be prepared by sol-gel method (Kobayashi, Kakinuma et al. 2009), self-assembly (Agnoli, Zhou et al. 2001), deposition (Binns, Prieto et al. 2012), in-situ polymerization (Deng, He et al. 2003), emulsion polymerization (You, Zhou et al. 2012), intercalation (Li, Chen et al. 2011), and chemical

coprecipitation (Ma, Dosev et al. 2009). Overall, more than fourteen methods are being studied and used for MNPs synthesis.

2.1.3 Magnetophoretic Mobility (Chalmers, Zhao et al. 1999, Todd, Cooper et al. 2001, Moore, Milliron et al. 2004)

Magnetophoretic mobility is an important parameter to describe the motion ability of magnetic particle in magnetic field. Suppose that a particle is suspended in a fluid in high magnetic fields, as illustrated in Figure 2.1. The magnetic force, F_m , acting on the magnetic particle (assume the particle is spherical) could be defined as (Jones 1995):

$$F_m = 2\pi\mu_s R^3 \frac{\mu_p - \mu_s}{\mu_p + 2\mu_s} \nabla H_0^2 \quad (2-1)$$

where μ_s and μ_p are permeability of the solution and particle, R is the radius of the spherical particle, and H_0 is the field intensity. The permeability can be expressed as susceptibilities (χ):

$$\mu = \mu_0(\chi + 1) \quad (2-2)$$

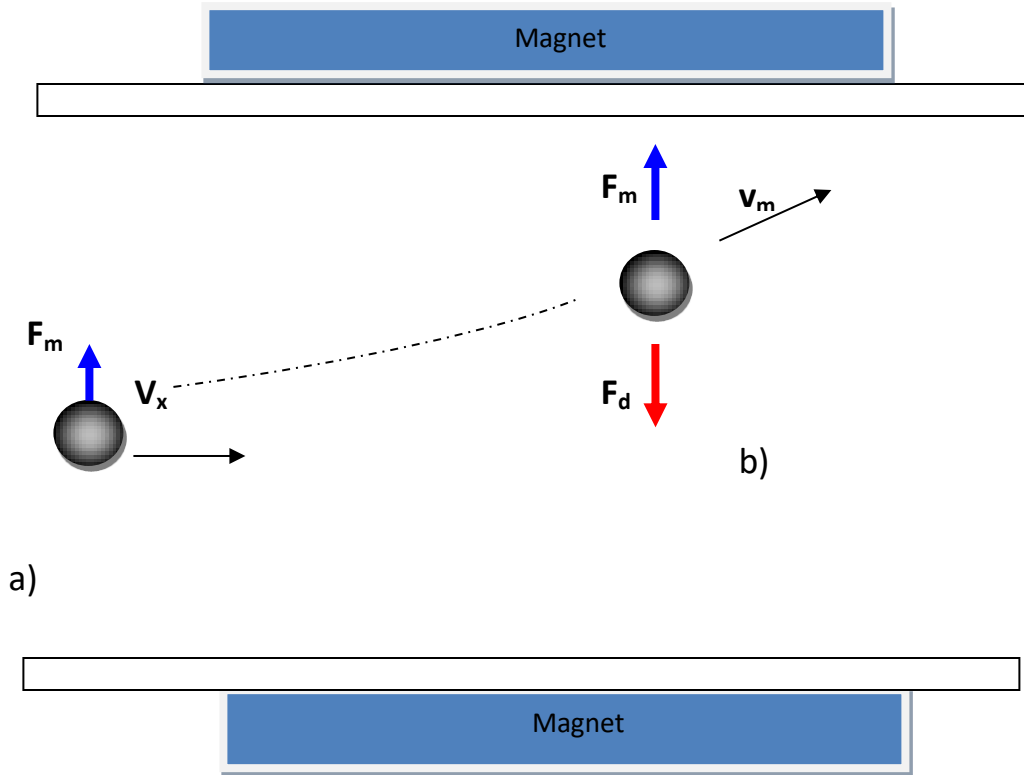


Figure 2.1 – Particle suspended in a magnetic field. (a) Magnetic particle entering the magnetic field; (b) Magnetic particle reaching the final velocity, force balance;

The gradient term can be expressed as

$$\nabla H_0^2 = \nabla(B_0/\mu_0)^2 \quad (2-3)$$

The volume of the magnetic particle is:

$$V = \frac{4}{3}\pi R^3 \quad (2-4)$$

Combining equations 2-1 through 2-4, the magnetic force is:

$$F_m = 3V(\chi_s + 1) \frac{\chi_p - \chi_s}{\chi_p + 2\chi_s + 3} \frac{\nabla B_0^2}{2\mu_0} \quad (2-5)$$

Assuming χ_s and χ_p are much smaller than one, so equation 2-5 can be simplified as:

$$F_m = V(\chi_p - \chi_s) \frac{\nabla B_0^2}{2\mu_0} \quad (2-6)$$

where the term ∇B_0^2 is the magnetic energy gradient.

The drag force, F_d , counteracts the effect of the magnetic field. F_d can be expressed based on Stokes law:

$$F_d = 6\pi R v_m u \quad (2-7)$$

where v_m is velocity of the magnetic particle, and u is the viscosity of the fluid. At equilibrium, the velocity of the particle remains constant. Assuming that the gravity and buoyance are negligible, the force balance on the magnetic particle can be expressed as

$$F_m - F_d = 0 \quad (2-8)$$

Combining equations 2-6 through 2-8, the terminal velocity of the particle v_m (the velocity of particle at equilibrium) is

$$v_m = \frac{V(\chi_p - \chi_s) \frac{\nabla B_0^2}{2\mu_0}}{6\pi R u} = \frac{2R^2 \Delta\chi}{9u} \frac{\nabla B_0^2}{2\mu_0} \quad (2-9)$$

The term $\frac{2R^2 \Delta\chi}{9u}$, related to the properties (magnetic susceptibility) of magnetic particle, is independent of the term $\frac{\nabla B_0^2}{2\mu_0}$, which is a result of the applied magnetic field. The

magnetophoretic mobility of a particle, μ_m , is defined as

$$\mu_m = \frac{2R^2 \Delta\chi}{9u} \quad (2-10)$$

Then one obtain the final definition of magnetophoretic mobility

$$\mu_m = \frac{v_m}{\frac{\nabla B_0^2}{2\mu_0}} \quad (2-11)$$

The expression of magnetophoretic mobility indicates that, for a given particle and fluid system, the terminal velocity is determined by the gradient of the magnetic field. When the magnetic field stays constant, particles with different magnetophoretic mobilities will be separated.

2.1.4 Application of MNPs and importance of magnetophoretic mobility

The following section discusses the five prevalent applications of magnetic particles and the need to know magnetophoretic mobility.

2.1.4.1 Cell Separation

Cell separation is an important application of magnetic particles. The target cell such as stem cells (Reece, Sanders et al. 2010), islet cells (Sajja, Hanley et al. 2011), blood progenitor cells (Jing, Moore et al. 2007), rare, circulating cancer cells (Xu, Aguilar et al. 2011), glial cells (Marek, Caruso et al. 2008) were labeled with magnetic reagents and then could be separated from unlabeled cells using a magnetic sorter.

The extensive study of magnetic cell separation technology places increasing demand on instruments and methods of cell separation. Since 1960, Giddings et al developed two separation techniques: field flow fraction (FFF) (Giddings 1993, Schimpf, Caldwell et al. 2000) and split-flow thin channel (SPLITT) (Giddings 1985, Giddings 1992). Using chromatography, the FFF brought in field-driven technology which can lead to different stream layers in a thin channel. Quadrupole Magnetic FFF, developed on the base of the FFF and SPLITT technology, proved successful for cell separation. Inside the quadrupole channel, the magnetic field increases

linearly from the axis in all directions. In other words, the field gradient is constant and directed away from the axis, as shown in Figure 2.2.

Sajja, Hanley et al. (2011) used a new commercially available high speed magnetic cell sorting system (IKOTECH LLC). The Quadrupole QMS is a high-throughput, high-gradient, continuous magnetic cell-sorting solution designed for clinical-grade cell sorting applications.

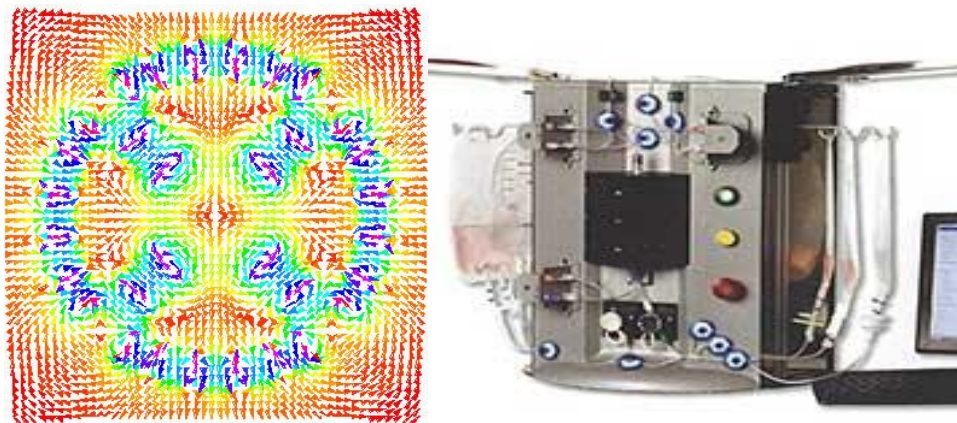


Figure 2.2 – Quadrupole Magnetic Sorter (flow field in symmetry plane on left)

2.1.4.2 MRI

Magnetic resonance imaging is a medical imaging technique used to take pictures of the organs and structures inside the body such as brain, muscle, heart and cancers. The protons in the body tissue will align parallel or anti-parallel to the direction of the field if a magnetic field is applied. When a radio frequency current is turned on, an electromagnetic field will be produced. The protons will absorb the energy and the spin of protons will change in new surroundings. After the current is turned off, the protons will re-aligned with the magnetic field and release the absorbed energy with different relaxation times (T_1 and T_2). A frequency signal which generated during the relaxation will be recorded by the MRI machines (Edelman and Warach 1993, Edelman and Warach 1993). The function of an MRI is shown in Figure 2.3.

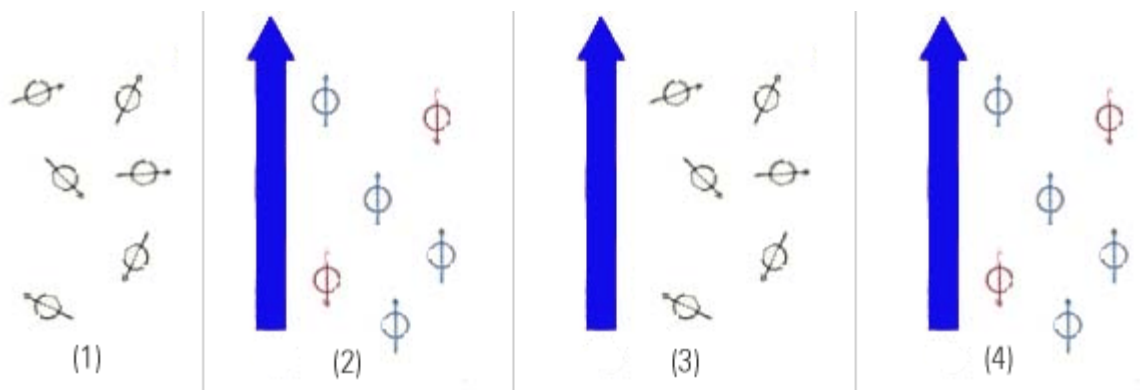


Figure 2.3 - How MRI work: (<http://ygoy.com/>)

1-Randomly oriented spinning protons; 2-The protons align along the magnetic field direction; 3-The protons are activated when the radio waves of the MRI are turned on; 4-The protons are inactivated when the radio waves are turned off.

Many different magnetic nanostructures have been developed as contrast agents for MRI application. Biocompatibility is the first requirement for the design of MNP. Among the contrast agents, iron oxide-based core - shell structure is the most extensive studied to date due to its unique properties including low toxicity, biodegradability and low impact on cell activities (Wilhelm and Gazeau 2008). A superparamagnetic iron core can offer sufficient sensitivity for T_2 (Bulte and Kraitchman 2004) and don't retain any magnetism after removal of magnetic field. Around the iron core, a polymer or inorganic coating protects the core from agglomeration and allows a targetable delivery. Polyethylene glycol (PEG), Polyvinylpyrrolidone (PVP), Dextran, mannan, Poly(vinyl acetate) (PVA) and silica are used to produce stable and biodegradable coating (Yoo, Park et al. 2008, Prabhakar, Vijayaraghavan et al. 2011, Sadjadi, Fathi et al. 2011, Masoudi, Hosseini et al. 2012, Osborne, Atkins et al. 2012, Ye, Laurent et al. 2012). The surface modifications of MNP include: non-polymeric organic stabilizers, polymeric stabilizers, inorganic molecules, and targeting ligands (Gupta and Gupta 2005).

Magnetophoretic mobility is an important parameter to predict the efficient contrast and efficient delivery of MNPs. Particles with greater magnetic susceptibility can increase the detection sensitivity of MRI. What's more, higher magnetophoretic mobility can ensure the carrier a eligible candidate for delivering drugs to target location in body (Silva, Silva et al. 2007). Further, analysis of magnetophoretic mobility can indicate the delivery efficiency. Silva et al. quantify the intercellular transfer of magnetic nanoparticle by analyzing the magnetophoretic mobility of donor cell as well as that of recipient cells (Silva, Wilhelm et al. 2012).

2.1.4.3 Drug delivery/ Hyperthermia

As a useful therapeutic type of tumors treatment, hyperthermia, also known as thermal therapy, is able to kill cancer cell at high temperatures without or with minimal hurting the normal tissues as tumor cell is more sensitive than healthy cells to the higher temperatures. In this therapy, targeted nanoscale heaters are carried to the tumor location and heat malignant cells to death (Gazeau, Levy et al. 2008). MNPs play an important role during the delivery process as it can be driven to selective action by using an applied magnetic field. MNPs can overcome RES (reticuloendothelial system) clearance and make it possible to control drug targeting and releasing (Huang and Juang 2011). Thus, much attention has been focus on MNPs design for cancel therapy.

Various types of MNPs have been studied extensively. A nanoplatform which contains the Core/Shell Fe/Fe₃O₄ MNPs was reported. With low toxicity, the platform efficiently delivers the SN38 drug to the cancer site and provide localized magnetic hyperthermia to assist cancer treatment (Wang, Shrestha et al. 2012). To develop a long-circulating MNP, cross-linked starch-coated iron oxide MNPs were modified with PEG. PEGylation enhances the platform's ability

to resist RES and biocompatibility, and finally magnetic tumor targeting (Cole, David et al. 2011, Cole, David et al. 2011). The Pluronic-coated Fe₃O₄ NPs shows many advantages like no cytotoxic effect, high efficiency of HeLa cancer killing and undesirable side effects (Tomitaka, Yamada et al. 2012). In practical medical application, drug delivery, hyperthermia and magnetic resonance imaging are always combining together. Sherlock and Dai (2011) reported the multifunctional FeCo-graphitic carbon shell nanocrystals for highly effective cancer therapy through combined drug delivery, tumor-selective near-infrared photothermal therapy, and cancer imaging of breast cancer.

Measurement of magnetophoretic mobility is important in drug delivery. Magnetically targeted pharmaceuticals can be guided to specific treatment sites within the human body by a combination of well-chosen injection sites and extracorporeal magnetic guidance. Magnetic guidance requires knowledge of magnetophoretic mobility, which must be high if particles are to respond to external magnets. Magnetophoretic mobility can also help to quantify MNPs. Tresilwised, Pithayanukul et al. (2010), estimated virus binding to a well-characterized magnetic nanoparticle from a simple photometric magnetophoretic mobility assay.

2.1.4.4 Magnetic Particle Standards

National Institute of Standards and Technology (NIST) has maintained microsphere size standards. In NIST Traceable size standards, particles are divided into 3 size groupings: Nanobead (40 nm to 950 nm), Microbead (1.00 μm to 9.00 μm), and Megabead (10.0 μm to 80.0 μm). They are measured on in-house instruments calibrated with NIST (www.polysciences.com). The beads are sold specifically as size standards for calibration purposes in various applications, such as light scattering, electron microscopy and optical sizing. However, NIST does not provide any magnetic susceptibility measurements in their measurement services.

To date, no one is measuring magnetic susceptibility using magnetophoretic mobility, and no companies, including InVitrogen-Life Technologies-Dynal, are claiming particle uniformity based on magnetophoretic mobility. The famous Dynal Dynabeads, 4.5 micrometer, only claim uniformity of size. A standardized way of measuring magnetophoretic mobility is the equivalent of a means of measuring magnetic susceptibility.

2.1.4.5 Magnetic Particle Quality Control

Many companies manufacture and sell magnetic particles but usually cannot report their susceptibility. For example, the products of Chemicell FluidMag are classified by particle size: 50, 100, 200 nm etc. (www.Chemicell.com). Nano Diagnostics Inc. provide Gold nanoparticle products size from 5 to 100 nm, Fe₃O₄ NP in size from 5 to 20 nm, etc. (www.nanodiainc.com). There are no physical quantities by which companies can characterize their particles except size distribution. Companies can become competitive by reporting magnetophoretic mobility.

2.2 Characterization of Magnetic Particles

Characterization of magnetic particles is required both in research and production. Thus, various methods and instruments are developed.

2.2.1 Structural analysis

Dynamic light scattering (DSL) could be used to determine the particle size distribution of nanoparticles (Filippousi, Altantzis et al. 2013). Scanning electron microscopy (SEM) could be used to determine the particle size, chemical composition and external morphology (Popa, Van Hong et al. 2003, Gherca, Pui et al. 2012). Transmission electron microscopy (TEM) could be used to observe the microstructure of the particle (Li, Kawashita et al. 2012). Energy dispersive X-ray spectrometer (EDX) could be used to measure the element composition of sample. TEM-EDX-SAED (Transmission electron microscopic –Energy Dispersive spectrometer - small-area electron diffraction) combine analysis could quantitatively reveal element content and particle

size (Tarasov, Isupov et al. 2008). X-ray diffraction (XRD) could reveal the information about the crystalline phase, chemical composition and physical properties of the samples. Small-angle X-ray scattering could provide structure information such as particles/pores size and shape (Tarasov, Isupov et al. 2008).

2.2.2 Magnetic Properties

Measuring the magnetic property of magnetic particle is as essential step before its widely application in varies fields. Many methods have developed to describe the quality of magnetic sample. As follows, some methods most often used are introduced and compared with Hyperflux Velocimeter.

- **Magnetic susceptibility balance**

The Sherwood scientific magnetic susceptibility balance, shown in Figure 2-4, is used to describe the magnetic properties of the magnetic particles (Mt/CACH-MPs) coated by montmorillonite/N-(carboxyacyl) chitosan.(Anirudhan, Gopal et al. 2014). The principle is simple: a compensating force will be generated in one end to maintain the balance system when the magnetic material is introduced into the other end surrounding by magnetic field. The force will be recorded and converted to display data. The magnetic susceptibility values were expressed:

$$\chi_g = \frac{L(R_1 - R_0)}{W \times 10^9} \quad (2-12)$$

where L is the path length of the sample, R_1 is balance reading for sample in tube, R_0 is the calibration constant and W is the weight of the sample.



Figure 2.4 - Sherwood Susceptibility Balance (Mk1)
(<http://www.sherwood-scientific.com/msb/msbindex.html>)

- **Vibrating Sample Magnetometer (VSM)**

The vibrating sample magnetometer (VSM), since its invention by Foner (Foner 1959), is employed to reveal the magnetism properties of nanoparticle in the form of powders, liquids, thin films or bulk samples . By vibrating sample sinusoidally, a sinusoidal signal of the magnetic flux change could be detect, then the induced voltage is recorded by the lock-in amplifier. The hysteresis curve of the material, including the information saturation magnetization (Ms), remnant magnetization (Mr.) and coercive field strength or coercivity (Hc), could be obtained after the test (Kim, Park et al. 2007, Filippousi, Altantzis et al. 2013, Bhukal, Bansal et al. 2014).

Li, Greenberg et al. (2011) developed a magnetic filter system that could derive magnetic susceptibilities of different sizes of γ -Fe₂O₃ particles from measured penetration data. However, in this method, the particle should be size monodisperse; and the susceptibility should be gained from VSM before measurement.

- **Hysteresis loop tracer equipment**

The equipment is used to measure saturation magnetization (M_r), retentivity (M_s) and coercivity (H_c) (Tangsali, Budkuley et al. 2011).

- **Superconducting quantum interference device**

Superconducting quantum interference device (SQUID), a sensitive magnetometer, could detect extremely small magnetic fields from magnetic particles (Clarke 1994). Thus, SQUID is used widely to measure magnetic properties of samples. The SQUID is based on Josephson Effect. Magnetic flux in the superconducting loop could be estimated as a function of voltage change. A good example is its application on magnetic resonance imaging (MRI).

- **SQUID-based susceptometer**

(Hurt, Li et al. 2013) developed a SQUID-based susceptometer which supports two different measurement techniques: dc scan and VSM. Thus, this instrument could access to investigate wide variety of samples by choosing the proper method.

- **Magnetorelaxometry (MRX)**

MRX is very useful to detect immobilized magnetic nanoparticles (Lange, Kotitz et al. 2002, Schmidl, Weber et al. 2007). This technology is also based on SQUIDs. Two different magnetic relaxation mechanisms - in a liquid phase and immobilized. The former one, in which particle could be freely movable and magnetization decays mainly due to rotational diffusion of magnetic particle, is a Brownian relaxation mechanism, while the latter is Néel relaxation mechanism, in which particle is immobilized. When a magnetic particle is bound, Brownian relaxation is suppressed, and then MRX could distinguish them from unbound particles. During Magnetorelaxometry, MNPs is exposed in magnetic field for t_{mag} , the magnetic field is turned off

and the relaxation of magnetization is measured. The relaxation times of two different relaxations could be calculated (Ludwig, Heim et al. 2004) and compared to determine the degree nanoparticles are bound.

- **AFM**

(Park, Yoo et al. 2008) used atomic force microscope to find the magnetic moment per unit mass of magnetic nanoparticles. By detecting the magnetic forces, the scanning probe could reveal the magnetic properties of a variety of systems, from thin film surfaces to biological samples (Saenz, Garcia et al. 1987). The relation between magnetic force and magnetization could be expressed by:

$$\vec{F} = M(B)m \frac{d\vec{B}}{dz} \quad (2-13)$$

where m is the mass of magnetic material, $M(B)$ the magnetization per unit mass, $\frac{d\vec{B}}{dz}$ is the magnetic field gradient.

All these method are used for off-line analysis, which means it takes significant time to collect sufficient samples before the measurements can be performed.

- **Ferromagnetic resonance**

To measure the magnetization of ferromagnetic materials, FMR is a good choice, say nanoparticles of Co-Ni alloys (Tarasov, Isupov et al. 2008), ferromagnetic films (Seemann, Leiste et al. 2013), Mn-Fe nanoparticles (Branquinho, Carriao et al. 2013) and so on (Abracado, Esquivel et al. 2012, Usselman, Russek et al. 2012, Raj, Sharma et al. 2013, Wardal, Typek et al. 2013). FMR is a spectroscopic technique base on resonance phenomenon happened when the

frequency of external magnetic force similar to the frequency of sample's magnetization \vec{M} . The relation between the magnetization, resonance frequency and magnetic field could be expressed:

$$f = \frac{\mu_0 \gamma}{2\pi} \sqrt{(H + H_k)(H + H_k + M_s)} \quad (2-14)$$

The uniaxial anisotropy field H_k and saturation magnetization M_s could be obtained by fitting resonance frequency f_0 to the function of magnetic field H .

- **HyperFlux Velocimeter**

The HyperFlux, a product of IKOTECH Inc., is short for High-Definition Magnetic Cell-Tracking Velocimeter. It can automatically analyze cell and particle sizes, concentrations, and magnetophoretic mobility (particle velocity within a magnetic field). The HyperFlux is particularly useful for quantifying the magnetic labeling of cells, validating particle quality and consistency, and identifying distinctly labelled populations in a sample.

The previously mentioned methods can only provide bulk average magnetization/susceptibility of sample. By contrast, Hyperflux Velocimeter can track the motion of each particle in the magnetic field and describe the distribution of particle's size, magnetophoretic mobility and other 18 distinct parameters after statistic calculation by powerful software. The particle-by-particle-base method provides more useful and meaningful data to allow researchers and manufacturers to control the quality of the product.

The Hyperflux flow system contains a borosilicate glass channel with square (2 mm) cross-section and 6 cm length. One end of channel connects to the prime buffer and sample syringe while the other end connects to the waste bottle. In each connection, there is a solenoid pinch valve to control the sample flow or buffer. The Focus channel is placed within a magnet

assembly where magnetic force is perpendicular to the direction of gravitational force. The video microscope system consist a darkfield LED light and a high definition Grasshopper 2.0 MP monochrome FireWire camera, capturing images rapidly at high definition. The images are recorded by computer and sent to the image processing software. From there, video data are converted into useful parameter data. A program “Cytotest” could help to set image thresholds and set the size range of particle. This step can be used to reject spurious data tracking. The tracking particles are analyzed and statistical summary is produced. A program called “Magex” provides the histogram of magnetophoretic mobility. Figure 2.5 illustrates the three important parts of Hyperflux Velocimeter.

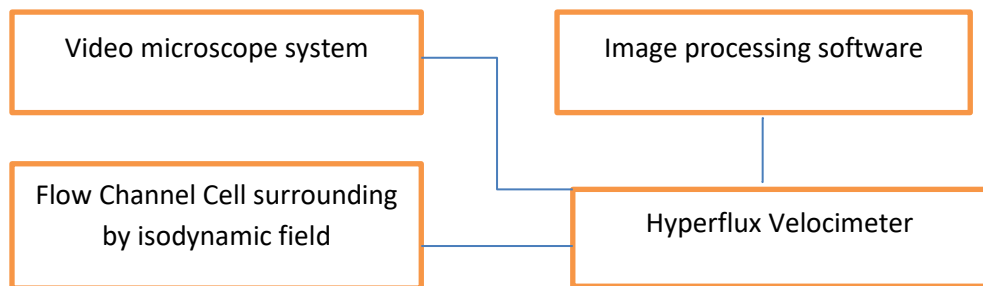


Figure 2.5 The Major component of Hyperflux and the High-Definition Magnetic Cell-Tracking Velocimeter (www.ikotech.com)

2.3 Magnetic Cell Separation

Cell separation is an essential step in both experimental cell science and applied biomedical technology. Cell separation methods have been developed rapidly in past decade. The contributions are not only come from academic lab but also commercial entrepreneurs. In other word, the market, currently, could offer a wide selection of cell separation methods and instruments to researcher and other users.

The commercially available cell separation methods could be classified into three groups by methodologies: adherence, density and antibody binding (Tomlinson, Tomlinson et al. 2013), The magnetic cell sorting technology is an antibody-binding method. The antibody is conjugated to micro particle which contains iron oxide. The magnetic field is required during the separation process: the labeled cells would be retained by the field while the unlabeled are depleted. Unlike other methods based on cell physical properties, the antigen-antibody reaction provides the potential for analyzing cells at a molecular level.

The magnetic cell separation method has many advantages compared to optical methods. First of all, the cell-labeling and separation process is simple. Moreover, it's more efficient as the time it takes much less time to prepare sample and process separation than that of fluorescence method. Last but most important, magnetic separation is more affordable for an individual laboratory due to the low capital and operation costs. On the other hand, magnetic separation is always combined with optical analysis of the fraction as only well-defined cell mixture system could lead to a meaningful result.

2.3.1 Theory of Magnetic Separation

2.3.1.1 Magnetic Susceptibility

Magnetic susceptibility (χ) is a dimensionless proportionality constant indicated the degree of magnetization (M) of a material in response to an applied magnetic field (H). In a word, the relationship between M and H is χ :

$$M = \chi H \quad (2-15)$$

The magnetic field could be described by magnetic field strength (H) and magnetic field induction. B indicates the effect of the magnetic source on the surrounding space. It can be expressed:

$$B = \mu H = \mu_0(1 + \chi)H = \mu_0(H + M) \quad (2-16)$$

where μ is the magnetic permeability and μ_0 is the magnetic permeability of the free space and the free space magnetic induction $B_0 = \mu_0 H$. The simple way to measure magnetic susceptibility is that of magnetic balance, which is to determine magnetic force:

$$F = \chi V H \frac{dB_0}{dx} \quad (2-17)$$

where F is the magnetic force, V is the volume material, H the magnetic field strength, B_0 the magnetic field induction of the free space. When $\chi > 0$, the material is paramagnetic, such as lathanide solution, hemoglobin; when $\chi < 0$, the material is diamagnetic, such as water and most of organic compounds.

2.3.1.2 Magnetic Force

A magnetic field will produce a stress on space, which is called Maxwell stress. In a homogeneous, isotropic, linear medium, Maxwell stresses reduce to a scalar, with the value $\frac{1}{2}HB$.

The local magnetic force density in matter, f , is equal to the divergence of the Maxwell stress tensor:

$$\mathbf{f} = \nabla \left(\frac{1}{2} \mathbf{H} \mathbf{B} \right) = \nabla \left(\frac{1}{2} M \mathbf{B}_0 \right) = \nabla \left(\frac{1}{2} \chi \mathbf{H} \mathbf{B}_0 \right) = \chi \nabla \left(\frac{1}{2} \mathbf{H} \mathbf{B}_0 \right) \quad (2-18)$$

So the total magnetic force acting on a particle is:

$$\mathbf{F} = fV = \chi V \nabla \left(\frac{1}{2} \mathbf{H} \mathbf{B}_0 \right) \quad (2-19)$$

Since $B_0 = \mu_0 H$, one can get the magnetic force in the x-direction:

$$F_x = \chi V \frac{d}{dx} \left(\frac{B_0^2}{2\mu_0} \right) \quad (2-20)$$

The term $\left(\frac{B_0^2}{2\mu_0} \right)$ is often referred to as magnetic pressure.

2.3.1.3 Isodynamic Field

In an isodynamic field, the force on a particle is essentially constant in magnitude. This characteristic makes it possible to measure the field-induced cell velocity as the cell velocity depends only on cell properties in the isodynamic field. The isodynamic field could be generated by two pole pieces. Figure 2.6 shows the domain we interested.

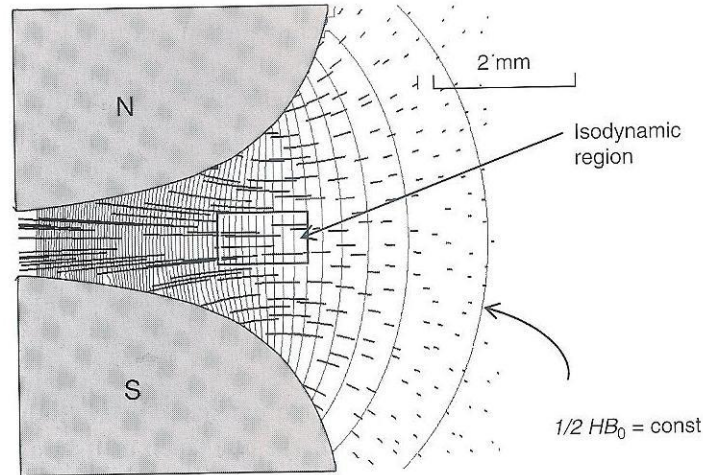


Figure 2.6 - Isodynamic field (the region in the box with parallel, same length pathlines) (Zborowski and Chalmers 2008)

2.3.1.4 Magnetophoretic Mobility

The magnetic force on a magnetic particle suspended in a diamagnetic fluid medium could be expressed:

$$\mathbf{F} = \Delta\chi V \nabla \left(\frac{B_0^2}{2\mu_0} \right) \quad (2-21)$$

where $\Delta\chi = \chi_p - \chi_f$, the difference of susceptibility between particle and fluid; V is the volume of the particle. Assuming the micro-sized particle is in a viscous creeping flow and reaches a terminal velocity, the drag force on the particle, according to Stokes law, should be

$$\mathbf{F}_d = 6\pi\eta R \mathbf{v} \quad (2-22)$$

where η is the viscosity of fluid, R is the radius of particle, and \mathbf{v} is the terminal velocity of the particle. If the magnetic force balances the drag force, $\mathbf{F} = \mathbf{F}_d$, one obtains the terminal velocity of the particle:

$$\mathbf{v} = \frac{\Delta\chi V}{6\pi\eta R} \nabla \left(\frac{B_0^2}{2\mu_0} \right) \quad (2-23)$$

The above expression is the form of a product of two quantities that are independent of each other. The left term, $\frac{\Delta\chi V}{6\pi\eta R}$, describes the properties of the particle and fluid medium; the right term, $\nabla\left(\frac{B_0^2}{2\mu_0}\right)$, is the magnetic pressure.

Then the magnetophoretic mobility and the magnetic pressure are defined as

$$m \equiv \frac{\Delta\chi V}{6\pi\eta R} \quad (2-24)$$

$$S_m = \nabla\left(\frac{B_0^2}{2\mu_0}\right) \quad (2-25)$$

In isodynamic field, S_m is constant. Then the value and direction of \mathbf{v} is fixed. In other word, the same particles will move in a nearly uniform motion.

2.3.1.5 Parameters that affect magnetophoretic mobility

Four parameters are reported to affect magnetophoretic mobility significantly of labeled cell: the antibody binding capacity (ABC) of a cell population, the secondary antibody amplification (ψ), the particle-magnetic field interaction parameter ($\Delta\chi V_m$), and the cell diameter (D_c) (McCloskey, Chalmers et al. 2003). For a two-step labeling cell, the magnetophoretic mobility could be expressed:

$$m = \frac{ABC\psi n_3 \phi}{3\pi D_c \eta} = \frac{(n_1 \theta_1 \lambda_1)(n_2 \theta_2 \lambda_2) n_3 \Delta\chi V_m}{3\pi D_c \eta} \quad (2-26)$$

where subscripts “1” and “2” refer to the primary and secondary labeling antibodies, respectively; n_1 is the number of antigen binding sites per cell, θ_1 is the fraction of antigen molecules on the particle surface bound by primary antibody, λ_1 is the valence of the primary antibody binding; $n_1 \theta_1 \lambda_1$ represents antibody binding capacity. n_2 is the number of binding sites on the primary

antibody, θ_2 is the fraction of binding sites on the primary antibodies that are bound by secondary antibodies, λ_2 is the valence of the secondary antibody binding; the combined term $n_2\theta_2\lambda_2$ is the secondary antibody amplification, $\psi \cdot n_3$ is the number of magnetic nanoparticles conjugated to the antibody. D_c is the diameter of the cell. η is the viscosity of the fluid. $\Delta\chi$ is the difference of magnetic susceptibility between magnetic particle and fluid. V_m is the volume of magnetic particle.

2.3.1.6 Settling Velocity versus Magnetic Velocity

When observing the magnetically induced velocity of magnetic particles in a magnetic energy gradient, the settling velocity (v_{setl}) of the particle should not be neglected. The settling velocity can be represented by:

$$v = \frac{\Delta\rho V}{6\pi\eta R} g \quad (2-27)$$

where $\Delta\rho$ is the density difference between particle and medium. Thus, the relation between the two velocities could be expressed:

$$\frac{v_{mag}}{v_{settling}} = \frac{\Delta\chi}{\Delta\rho g} S_m \quad (2-28)$$

The ratio should be constant if the magnetic field gradient is constant. All above is based on the assumption that the susceptibility and density of particle will not change. Susceptibility, which indicates the relationship between magnetization and applied field, can be regarded as constant value in a narrow range of applied field. The uniformity of particle will also impact the value of particle density. The size distribution of particle will contribute to data spread in magnetic and settling velocities (Xu, Mahajan et al. 2012)

2.3.2 Analytical and Separation techniques

2.3.2.1 Analytical technology

Further improvement of the methods of magnetic particle measurement and characterization is in demand due to the development and maturation of magnetic separation technology.

- **Measurement of Magnetic Susceptibility**

Several devices are employed to measure the magnetic susceptibility of materials, as shown in Table 2.1.

- **Measurement of Magnetophoretic mobility**

As discussed above, magnetophoretic mobility can describe the properties of particle if the fluid medium is fixed:

$$m = \frac{\Delta\chi V}{6\pi\eta R} \quad (2-29)$$

Table 2.1 - Devices which can detect magnetic susceptibility

Method	Sample	Mechanism	Reference
Superconducting Quantum-interference-device (SQUID)	Human Iron Stores	Magnetometer; Contain Josephson Junction which can tell tiny change of energy	(Brittenham, Farrell et al. 1982)
Faraday Microbalance	Ce ion	Faraday method	(Laachir, Perrichon et al. 1991)
CS-2 Apparatus and KLY-2 Kappabridge	Rock	Measurement of thermal variation of magnetic susceptibility	(Hrouda 1994)
Torque meter	Rock		(Kligfield, Owens et al. 1981)

Cryogenic Magnetometer			
Digico spinner magnetometer			
The Bartington Magnetic Susceptibility System sensors	Water Calibration sample 'Ferro' cassette tape Steel wool		(Dearing 1994)

If the particle is spherical, the relationship between the particle radius and the mobility is

$$m = \frac{2R^2}{9\eta} (\chi_p - \chi_f) \quad (2-30)$$

This parameter could help to characterize the process of magnetic separation and further assist to design the particle separation system. As the definition is given, instruments are developed to measure magnetophoretic mobility.

The cell-tracking velocimetry (CTV) can successfully monitor the movement of particles and/or labeled cells in an isodynamic fluid (S_m , magnetic field strength is constant). Unlike SQUID which can only measure the average properties of cells, CTV can provide a track for each particle.

- **Hyperflux Velocimeter**

The following description of the instrument is adapted from the IKOTECH website. The HyperFlux system, developed by IKOTECH, is a particle analyzer and velocimeter that is used for high definition magnetic particle tracking. The system utilizes Point Grey's Grasshopper camera and a patented magnetic cell sorting solution called Quadrasep that can sort at speeds up

to 10,000,000 cells per second in a closed system making it 144 times faster than existing systems on the market. Many analysis technologies today can measure fluorescence intensity of cells and analyze individual images of cells. However, HyperFlux is the only system that is able to provide quantitative video analysis of cells or particles and their motion as part of a fast and automated turnkey system. It combines fast images and morphology analysis with time-lapse velocimetry measurements to provide new ways for cell researchers, pharmaceutical manufacturers, magnetic particle manufacturers, environmental biologists, and many other to improve their research and quality control data.

Figure 2-7 illustrates the Hyperflux. Hyperflux analysis can provide detailed data of sample cells by using a microscope that observes cells and particles in a micro capillary glass tube that is mechanically aligned within a custom magnet assembly, recording the particle movement to a hard drive as image files. The magnet induces lateral motion ('mobility') for objects that contain magnetically responsive materials

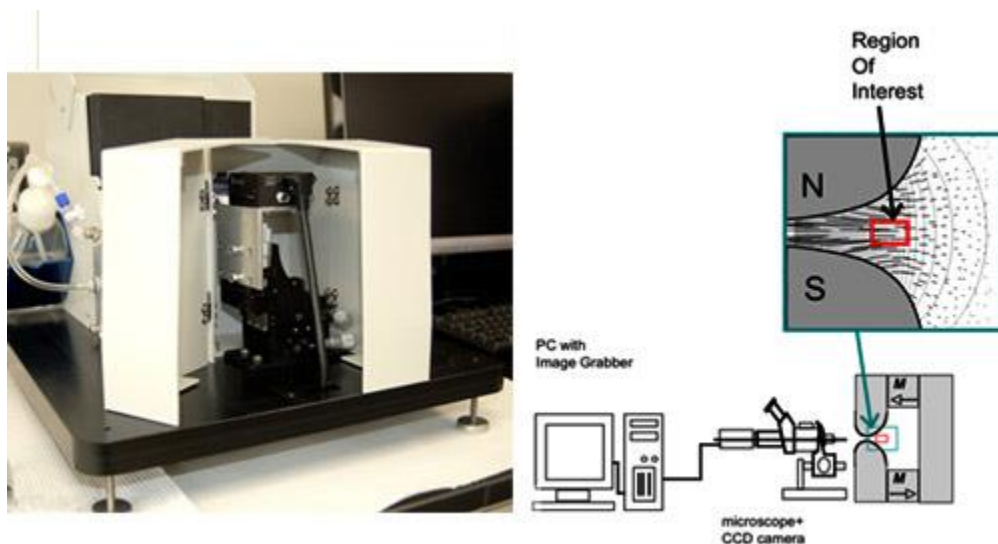


Figure 2.7 - Diagram of the Hyperflux Velocimeter (Camera focused on region of interest)

such as iron oxide, while gravity induces vertical motion that is related to the mass density and the size of the object (either downward sedimentation or upward buoyancy). The horizontal microscope consists of a darkfield LED ring that illuminates the capillary tube and a high definition Grasshopper 2.0 MP monochrome FireWire camera that captures the images paired to a long working distance telecentric lens (typically either 4 or 6x magnification). The camera and lens are mounted to a tri-axial micrometer stage, allowing for vertical and horizontal alignment of the camera to the capillary as well as adjustment of the focal plane. Images are captured at high definition, 30 frames per second and are recorded to a computer. The computer runs custom software that automates the image capture and analysis written using Point Grey's FlyCapture library. Image samples are taken in 'sets', with each set representing a fresh fluid sample in the field of view.

A typical field of view will contain anywhere from ten to ten thousand cells or particles depending on the concentration of the sample. In order to obtain a statistically significant data set for the sample, it is a necessity that the Hyperflux analyze from 10,000 to 100,000 or more cells or particles, and therefore anywhere from ten to one hundred sets or more may be taken. The HyperFlux refreshes the sample automatically using a pump and pinch valves that are actuated between each set that is captured. A Dell computer running Ubuntu Linux contains a dual quad core CPU design and the software leverages this computational capacity by multithreading the analysis to analyze multiple sets at once. Each image is analyzed to identify each particle or cell as an 'object'. The objects are identified in subsequent frames and linked together as a single 'track' via a database.

Characteristics for each object are measured in each frame, such as the size of the object, the brightness of the object, and morphology parameters such as surface roughness and

elongation. These parameters are then averaged and the standard deviation for each object is calculated over the "track". Additionally, the motion of the centroid position of each object is used to calculate track linearity and vertical/horizontal velocities. Open source data presentation tools integrated into the software allow the user to visualize the data using single parameter histograms, dual parameter scatter plots, and three dimensional dot plots.

2.3.2.2 - Separation Technology

- **Commercial magnetic cell separation technology**

Currently, a large number of cell separation devices are available in the market. Thus, it's convenient for users to select a device based on their purpose and the price. Table 2-2 lists the company and brand name of the products:

**Table 2.2 - Commercial magnetic cell separation products and devices
(BDBiosciences , JanssenDiagnostics , LifeTechnologiesCorporation , MiltenyiBiotec , R&D , StemCellTechnologies)**

Company	Product	Description	Application
Life Technologies Corp.	Dynabeads®	Dynabeads are superparamagnetic, mono-sized polymer beads. When Dynabeads are mixed with sample and bind to target cells, it's easy to isolate the target cells from the rest of sample with the help of a Dynal magnet.	1. Positive isolation 2. In depletion unwanted cell 3. Negative isolation
R&D Systems, Inc.	MagCelect cell selection/detection kits, Flow Cytometry, Cell Enrichment Column Kits	Magcellect technology is based on the use of Ferrofluids which are superparamagnetic particles with diameter up to 150 nm. Small and uniform size results in rapid binding rate and higher biding capacity.	Selective isolation; Rare cell detection
Janssen	CellSearch®	The CellSearch® System is the only	identify, count, and

<p>Diagnostics, LLC</p>	<p>Circulating Tumor Cell (CTC) Kit, CellSearch® CTC Control Kit, CellSave Preservative Tube, CellTracks® AutoPrep® System, CellTracks Analyzer II®</p>	<p>laboratory platform that standardizes sample collection, cell capture, staining, enumeration, and characterization of CTCs</p>	<p>characterize tumor cells</p>
<p>Miltenyi Biotec</p>	<p>MACS Microbeads, Cell Separator, Buffer, Flow Cytometry, Etc.</p>	<p>MACS MicroBeads are superparamagnetic particles, about 50- nm in diameter. They are too small to activate cells or saturate cell surface epitopes. The labeled cells binding with colloidal MACS Microbeads will be retained within the MACS Columns placed in MACS separator</p>	<p>Positive selection, Depletion, Untouched isolation, Sequential sorting</p>
<p>StemCell Technologies, Inc.</p>	<p>EasySep</p>	<p>EasySep is a fast, easy and column – free cell selection system with open-gradient magnetic field configuration. The design is based on quadrupole field. Target cell bounded to magnetic nanoparticles after incubation will be retained in the tube while untouched cells can be poured off into a new tube. The EasySep nanoparticles don't interfere with downstream application thus do not need to remove.</p>	<p>Positive selection Depletion</p>
<p>BD Biosciences</p>	<p>BD IMagnet cell separation system</p>	<p>BD IMagnet is a direct magnet. Economical option for cell pre-</p>	<p>Enrichment or depletion of leukocyte</p>

		enrichment.	subpopulations.
--	--	-------------	-----------------

- **Quadrupole field and quadrupole magnetic sorter (QMS)**

Magnetic quadrupole fields can be made by placing four identical magnet poles perpendicular to each other. The south pole of one piece is next to the north pole of the other, as shown in Figure 2.9. This configuration will produce a high field gradient as the field grows rapidly along with the radial distance from the center where the field is zero. In an ideal quadrupole magnetic field, the field gradient (B_0/r_0) is constant and high field strength is reached near the magnet tip.

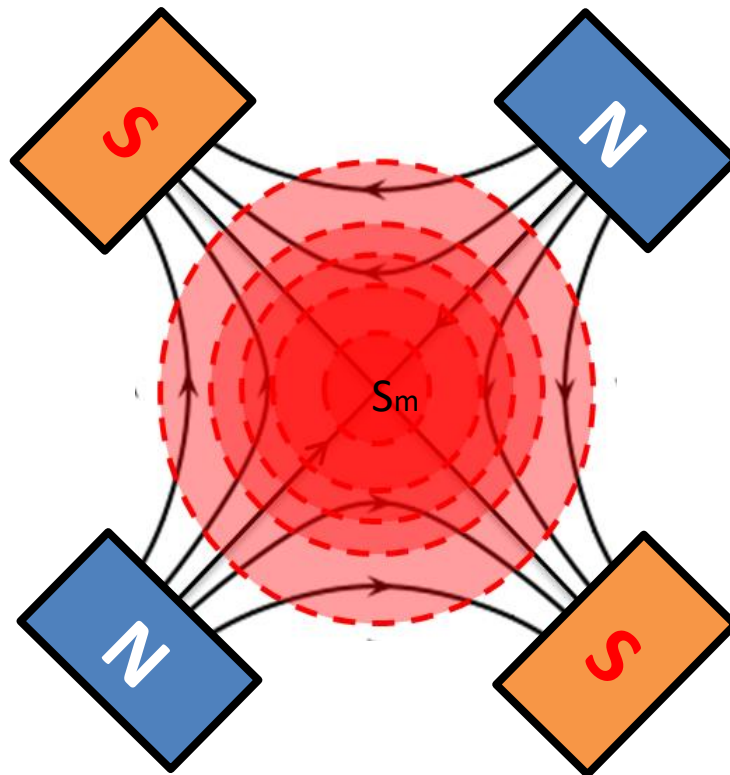


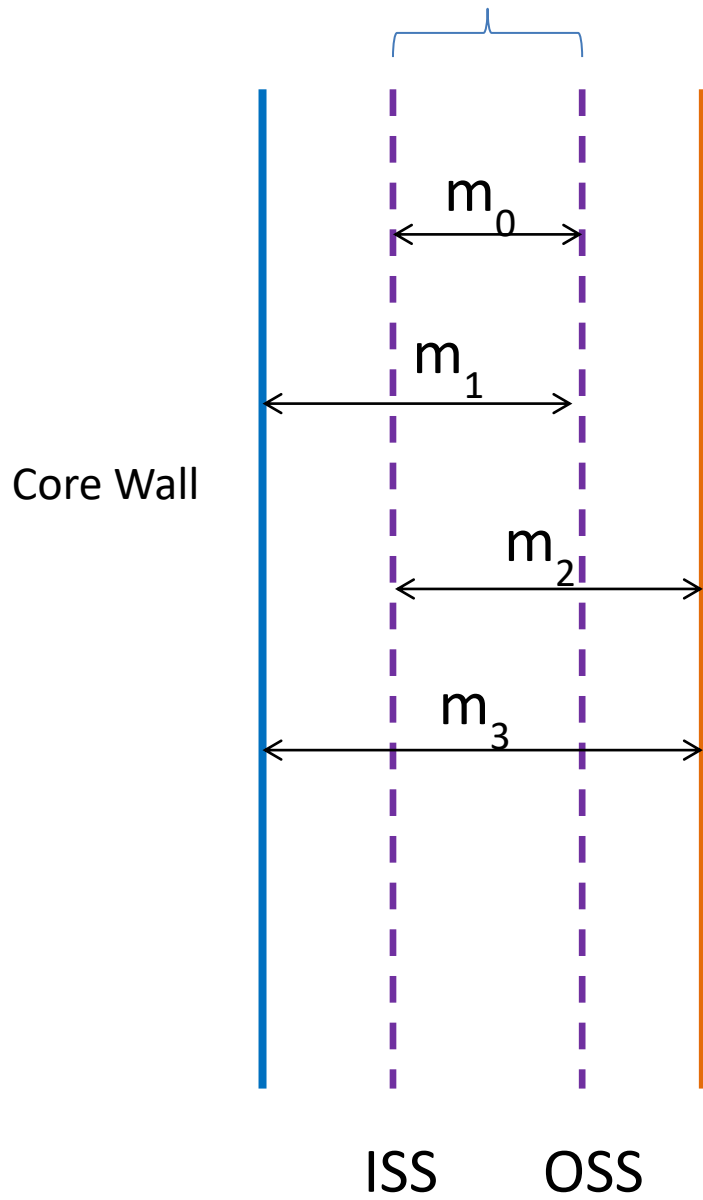
Figure 2.8 - Quadrupole field. The black lines with arrow are the field lines. The red dashed lines represent the magnetic field contour (dark red-low field; light red-high field)

The quadrupole magnetic sorter (QMS) is a continuous, efficient, split-flow magnetic cell separation system. It is based on Split-Flow Lateral-Transport Thin (SPLITT) separation technology (Giddings 1985), which is developed from Field Flow Fractionation (FFF) method (Giddings 1966, Giddings 1968, Thompson, Myers et al. 1969, Giddings, Hovingh et al. 1970). QMS was designed to separate labeled cells from nonmagnetic cells. The target products could be collected by positive isolation or depletion. Three key portions are employed by QMS: a thin split-flow channel with inlet and outlet flow splitters, quadruple magnetic field produced by four pieces of permanent magnets and pump. Fig. 2.9 describes the mechanism of QMS. The sample with labeled cells was pumped into flow channel at inlet a' while the buffer carrier enter at outlet b'. The magnetic particle will move centrifugally in the quadrupole field during precipitation. There are four critical motilities which could help to predict the behavior of particles in the channel and analyze the fraction of effluent liquid (Jing, Moore et al. 2007, Sajja, Hanley et al. 2011). They are listed as follow:

m_0 , mobility whereby a particle entering the flow channel at the ISS and will reach the OSS and exit at b; m_1 , mobility whereby a particle entering at the wall of the core reaches the OSS and can flow out at b; m_2 , mobility whereby a particle entering at ISS reaches the outer wall of the channel and will stay in the channel; m_3 , mobility whereby a particle entering at the core wall reaches the outer wall. $m_0 < m_1 < m_2 < m_3$. Particles with $m < m_0$ exit at outlet a; those with $m_0 \leq m \leq m_1$ will exit either in a or b fraction; those having $m_1 \leq m \leq m_2$ will flow out at b; those with $m_2 \leq m \leq m_3$ will exit in b or become trapped on the shell wall; those with mobility $m \geq m_0$ will be retain on the shell wall.

(a)

Transport Lamina



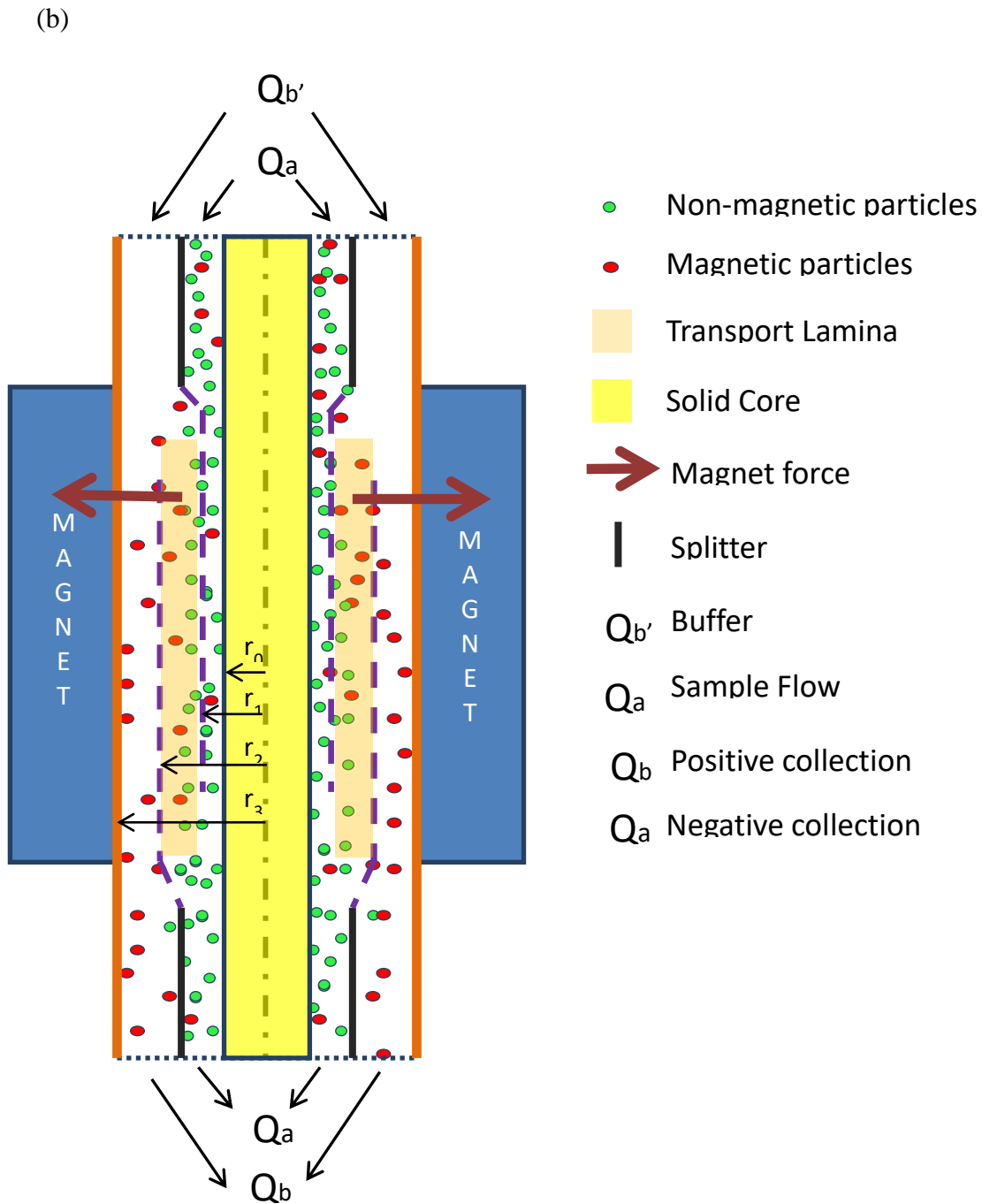


Figure 2.9 - QMS: (a) transport lamina; (b) schematic of quadrupole flow sorter: r_1 refers to the distance between inner splitting surface (ISS) and the core; r_2 is the distance from core to outer splitting surface (OSS). The space between ISS and OSS is called the transport lamina.

2.4 Label Cell

Mammalian Cells labeled with various superparamagnetic iron oxide nanoparticles (SPION) are studied to investigate the efficiency and toxicity of labeling cells and the application potential on clinic, say biological detection and imaging(Kircher, Allport et al. 2003, Daldrup-Link, Rudelius et al. 2005, Maxwell, Bonde et al. 2008), cell labeling/targeting (Hideyuki Terazono 2010, Tseng, Shih et al. 2010, Ruan, Shen et al. 2011), cell separation (Odette, McCloskey et al. 1984, Bieva, Vander Brugghen et al. 1989, Kuhara, Takeyama et al. 2004). There are many advantages to use the technology of magnetic cell labeling to in target cell detection and separation: minimizing manual labor, more precise results, rapid, sensitive and simple(Stampfli, Miescher et al. 1994, Parra, Wingren et al. 1997, Schratzberger, Reinisch et al. 1997, Sawakami-Kobayashi, Segawa et al. 2003). To establish a method to characterize magnetic label cell, we not only need to understand how to choose the magnetic particles/cells combination, but also culture conditions and uptake chemistry.

2.4.1 Cytotoxicity

Cytotoxicity is the priority issue to be considered in application of magnetic particles both in vivo and in vitro. Sometimes we hope to kill target cells, say tumor, the cytotoxic particles might also attacks normal cells which lead to serious side-effects. In other cases, cell sorting/separation as a goal, product cells are expected to be healthy or easy to recover after MNPs label/combination. If we could suppress the cytotoxicity or design a more suitable particles/target cells system, the major disadvantage of the uses of magnetic particles in biomedical applications could be overcome.

It's reported that the carboxyl groups on the surface of DMSA-coated Fe_2O_3 produce low cytotoxicity (C. Wilhelm and F. Gazeau 2008) . As a surface protector, PEG is widely used in

biological research to improve biocompatibility and increase blood circulation time, (G Storm 1995) reduce particle toxic and prevent interacting from cells or proteins (CG Gölönder 1992). Other than PEGylation, surface protection such as poloxamers and poloxamines are also investigated (Moghimi and Hunter 2000, Mayol, Quaglia et al. 2008).

The MTT assay (Tetrazolium dye assays) for cell viability is of great value to detect biomaterial toxicity (loss of viable cells). (Mosmann 1993)

2.4.2 Cell uptake

(Wilhelm and Gazeau 2008) revealed two types of cell uptake mechanism, electrostatic adsorptive endocytosis for anionic magnetic nanoparticles (AMNPs) and fluid-phase endocytosis for dextran or BSA-coated nanoparticles. The AMNP shows non-specific affinity for cell membrane which lead to high labelling efficiency.

A mass action kinetics model was developed to explain the AMNP uptake mechanism (C Wilhelm 2002) as a two-step process: biding of AMNP on reactive sites on cell surface (Langmuir adsorption) and cell internalization of the reactive sites by endocytosis pathway (saturation mechanism). The Langmuir adsorption rate, based on electrostatic interactions between charged particles and cell surface, is a mass change function proportional to particles concentration (C) in the medium. Desorbing process is related to the mass of adsorbed nanoparticles. The absorbed rate expression is as follow:

$$\frac{dm}{dt} = k_a C(m_0 - m) - k_d m$$

$m(t)=0$ @ $t=0$, so

$$m_{ext}(t, C) = \frac{k_a C}{k_a C + k_d} m_0 (1 - \exp[-(k_a C + k_d)t])$$

where k_a ($M^{-1}s^{-1}$) is and k_d (s^{-1}) are for adsorption and desorption, separately.

The internalization process occurs subsequently. Some particles adsorb on the surface pass through the membrane to create intracellular endosomes.

The internalization rate could be expressed:

$$\frac{dm_{int}(t)}{dt} = \frac{d\phi_{int}(t)}{dt} m_{ext}(t) = k_1(\phi_0 - \phi_{int}(t))m_{ext}(t)$$

Where ϕ is the fraction of the reactive surface that can be internalized and k_1 is the internalization rate constant (s^{-1}).

There are many reports that electrostatic interaction between a charged particles and the membrane could enhance cell uptake. The cell surface contains large domains of anionic sites which could attract the cationized particles more than native and anionized adsorbate. The cationic sites also exist but relatively with smaller domain which could assist the binding of anionized particles (Farquhar 1978, Mutsaers and Papadimitriou 1988, Lee, Nir et al. 1993, Miller, Bondurant et al. 1998, Chenevier, Veyret et al. 2000).

2.4.3 Culture Condition

For different study objectives, labeling conditions such as iron concentration, exposure time and temperature might vary. To evaluate the effect of ferumoxides–poly-l-lysine (PLL) complex for magnetic cell labeling on the long-term viability, function etc, more than 44 days labeling experiment are conducted (Arbab, Bashaw et al. 2003). To analyze uptake model and compare internalization and external absorption, two temperature 4 and 37 °C were chosen (C Wilhelm 2002).

References

- Abracado, L. G., D. M. S. Esquivel and E. Wajnberg (2012). "ZFC/FC of oriented magnetic material in the *Solenopsis interrupta* head with antennae: Characterization by FMR and SQUID." Journal of Biological Physics **38**(4): 607-621.
- Agnoli, F., W. L. Zhou and C. J. O'Connor (2001). "Synthesis of cubic antiferromagnetic KMnF₃ nanoparticles using reverse micelles and their self-assembly." Advanced Materials **13**(22): 1697-1699.
- Anirudhan, T. S., S. S. Gopal and S. Sandeep (2014). "Synthesis and characterization of montmorillonite/N-(carboxyacyl) chitosan coated magnetic particle nanocomposites for controlled delivery of paracetamol." Applied Clay Science **88-89**: 151-158.
- Arbab, A. S., L. A. Bashaw, B. R. Miller, E. K. Jordan, B. K. Lewis, H. Kalish and J. A. Frank (2003). "Characterization of biophysical and metabolic properties of cells labeled with superparamagnetic iron oxide nanoparticles and transfection agent for cellular MR imaging." Radiology **229**(3): 838-846.
- BDBiosciences, retrieved Jan 1, 2013, product details,
"http://www.bdbiosciences.com/us/reagents/research/magnetic-cell-separation/other-species-cell-separation-reagents/cell-separation-magnet/p/552311."
- Bhukal, S., S. Bansal and S. Singhal (2014). "Co_{0.6}Zn_{0.4}Cu_{0.2}Cd_xFe_{1.8-x}O₄ (0.2 ≤ x ≤ 0.8) magnetic ferrite nano-particle: Synthesis, characterization and photo-catalytic degradation of methyl orange." Journal of Molecular Structure **1059**: 150-158.
- Bieva, C. J., F. J. Vander Bruggen and P. A. Stryckmans (1989). "Malignant leukemic cell separation by iron colloid immunomagnetic adsorption." Exp Hematol **17**(8): 914-920.
- Binns, C., P. Prieto, S. Baker, P. Howes, R. Dondi, G. Burley, L. Lari, R. Kroger, A. Pratt, S. Aktas and J. K. Mellon (2012). "Preparation of hydrosol suspensions of elemental and core-shell

nanoparticles by co-deposition with water vapour from the gas-phase in ultra-high vacuum conditions." Journal of Nanoparticle Research **14**(9).

Branquinho, L. C., M. S. Carriao, A. S. Costa, N. Zufelato, M. H. Sousa, R. Miotto, R. Ivkov and A. F. Bakuzis (2013). "Effect of magnetic dipolar interactions on nanoparticle heating efficiency: Implications for cancer hyperthermia." Scientific Reports **3**.

Brittenham, G. M., D. E. Farrell, J. W. Harris, E. S. Feldman, E. H. Danish, W. A. Muir, J. H. Tripp and E. M. Bellon (1982). "Magnetic-Susceptibility Measurement of Human Iron Stores." New England Journal of Medicine **307**(27): 1671-1675.

Bulte, J. W. M. and D. L. Kraitchman (2004). "Iron oxide MR contrast agents for molecular and cellular imaging." Nmr in Biomedicine **17**(7): 484-499.

Burke, N. A. D., H. D. H. Stover, F. P. Dawson, J. D. Lavers, P. K. Jain and H. Oka (2001). "Preparation and characterization of polymer-coated magnetic nanoparticles." Ieee Transactions on Magnetism **37**(4): 2660-2662.

C Wilhelm, F. G., J Roger, JN Pons, JC Bacri (2002). "Interaction of anionic superparamagnetic nanoparticles with cells: kinetic analyses of membrane adsorption and subsequent internalization." langmuir **18**(21): 8148–8155.

C. Wilhelm and F. Gazeau (2008). "Universal cell labelling with anionic magnetic nanoparticles." Biomaterials **29**(3161).

Carpenter, E. E., C. J. O'Connor and V. G. Harris (1999). "Atomic structure and magnetic properties of MnFe₂O₄ nanoparticles produced by reverse micelle synthesis." Journal of Applied Physics **85**(8): 5175-5177.

CG Gölander, J. H., K Lim, P Claesson (1992). "Properties of immobilized PEG films and the interaction with proteins." Chapter Poly(Ethylene Glycol) Chemistry Part of the series Topics in Applied Chemistry 221-245.

Chalmers, J. J., Y. Zhao, M. Nakamura, K. Melnik, L. Lasky, L. Moore and M. Zborowski (1999). "An instrument to determine the magnetophoretic mobility of labeled, biological cells and paramagnetic particles." Journal of Magnetism and Magnetic Materials **194**(1-3): 231-241.

Chenevier, P., B. Veyret, D. Roux and N. Henry-Toulme (2000). "Interaction of cationic colloids at the surface of J774 cells: a kinetic analysis." Biophys J **79**(3): 1298-1309.

Clarke, J. (1994). "Squids." Scientific American **271**(2): 46-53.

Cole, A. J., A. E. David, J. X. Wang, C. J. Galban, H. L. Hill and V. C. Yang (2011). "Polyethylene glycol modified, cross-linked starch-coated iron oxide nanoparticles for enhanced magnetic tumor targeting." Biomaterials **32**(8): 2183-2193.

Cole, A. J., A. E. David, J. X. Wang, C. J. Galban and V. C. Yang (2011). "Magnetic brain tumor targeting and biodistribution of long-circulating PEG-modified, cross-linked starch-coated iron oxide nanoparticles." Biomaterials **32**(26): 6291-6301.

Daldrup-Link, H. E., M. Rudelius, G. Piontek, S. Metz, R. Brauer, G. Debus, C. Corot, J. Schlegel, T. M. Link, C. Peschel, E. J. Rummeny and R. A. Oostendorp (2005). "Migration of iron oxide-labeled human hematopoietic progenitor cells in a mouse model: in vivo monitoring with 1.5-T MR imaging equipment." Radiology **234**(1): 197-205.

Dearing, J. A. (1994). Environmental magnetic susceptibility : using the Bartington MS2 system. Kenilworth, Chi Publishing.

Deng, J. G., C. L. He, X. P. Long, Y. X. Peng, P. Li and A. S. C. Chan (2003). "Preparation and characterization of magnetic Fe₃O₄- polypyrrole nanoparticles." Acta Polymerica Sinica(3): 393-397.

Dvorak, H. F., J. A. Nagy, J. T. Dvorak and A. M. Dvorak (1988). "Identification and Characterization of the Blood-Vessels of Solid Tumors That Are Leaky to Circulating Macromolecules." American Journal of Pathology **133**(1): 95-109.

Edelman, R. R. and S. Warach (1993). "Medical Progress .1. Magnetic-Resonance-Imaging." New England Journal of Medicine **328**(10): 708-716.

Edelman, R. R. and S. Warach (1993). "Medical Progress .2. Magnetic-Resonance-Imaging." New England Journal of Medicine **328**(11): 785-791.

Farquhar, M. G. (1978). "Recovery of surface membrane in anterior pituitary cells. Variations in traffic detected with anionic and cationic ferritin." J Cell Biol **77**(3): R35-42.

Filippoussi, M., T. Altantzis, G. Stefanou, M. Betsiou, D. N. Bikiaris, M. Angelakeris, E. Pavlidou, D. Zamboulis and G. Van Tendeloo (2013). "Polyhedral iron oxide core-shell nanoparticles in a biodegradable polymeric matrix: preparation, characterization and application in magnetic particle hyperthermia and drug delivery." Rsc Advances **3**(46): 24367-24377.

Foner, S. (1959). "Versatile and Sensitive Vibrating-Sample Magnetometer." Review of Scientific Instruments **30**(7): 548-557.

Freeman, M. W., A. Arrott and J. H. L. Watson (1960). "Magnetism in Medicine." Journal of Applied Physics **31**(5): S404-S405.

Fung, K. K., B. X. Qin and X. X. Zhang (2000). "Passivation of alpha-Fe nanoparticle by epitaxial gamma-Fe₂O₃ shell." Materials Science and Engineering a-Structural Materials Properties Microstructure and Processing **286**(1): 135-138.

G Storm, S. B., T Daemen, DD Lasic (1995). "Surface modification of nanoparticles to oppose uptake by the mononuclear phagocyte system." Advanced drug delivery reviews **17**(1).

Gazeau, F., M. Levy and C. Wilhelm (2008). "Optimizing magnetic nanoparticle design for nanothermotherapy." Nanomedicine **3**(6): 831-844.

Gherca, D., A. Pui, N. Cornei, A. Cojocariu, V. Nica and O. Caltun (2012). "Synthesis, characterization and magnetic properties of MFe₂O₄ (M = Co, Mg, Mn, Ni) nanoparticles using ricin oil as capping agent." Journal of Magnetism and Magnetic Materials **324**(22): 3906-3911.

Giddings, J. C. (1966). "A New Separation Concept Based on a Coupling of Concentration and Flow Nonuniformities." Separation Science **1**(1): 123-125.

Giddings, J. C. (1968). "Nonequilibrium Theory of Field-Flow Fractionation." Journal of Chemical Physics **49**(1): 81-&.

Giddings, J. C. (1985). "A System Based on Split-Flow Lateral-Transport Thin (Splitt) Separation Cells for Rapid and Continuous Particle Fractionation." Separation Science and Technology **20**(9-10): 749-768.

Giddings, J. C. (1992). "Optimization of Transport-Driven Continuous Splitt Fractionation." Separation Science and Technology **27**(11): 1489-1504.

Giddings, J. C. (1993). "Field-flow fractionation: analysis of macromolecular, colloidal, and particulate materials." Science **260**(5113): 1456-1465.

Giddings, J. C., M. E. Hovingh and G. H. Thompson (1970). "Measurement of Thermal Diffusion Factors by Thermal Field-Flow Fractionation." Journal of Physical Chemistry **74**(24): 4291-&.

Gong, J., Y. Liu and J. H. Yang (2010). "Influence of Co-Doping on Synthesis, Structure and Magnetic Properties of Ni Nanoparticles." Rare Metal Materials and Engineering **39**: 328-331.

Gul, I. H., W. Ahmed and A. Maqsood (2008). "Electrical and magnetic characterization of nanocrystalline Ni-Zn ferrite synthesis by co-precipitation route." Journal of Magnetism and Magnetic Materials **320**(3-4): 270-275.

Gul, I. H. and A. Maqsood (2007). "Influence of Zn-Zr ions on physical and magnetic properties of co-precipitated cobalt ferrite nanoparticles." Journal of Magnetism and Magnetic Materials **316**(1): 13-18.

Gupta, A. K. and M. Gupta (2005). "Synthesis and surface engineering of iron oxide nanoparticles for biomedical applications." Biomaterials **26**(18): 3995-4021.

Gutierrez, J. M., C. Gonzalez, A. Maestro, I. Sole, C. M. Pey and J. Nolla (2008). "Nano-emulsions: New applications and optimization of their preparation." Current Opinion in Colloid & Interface Science **13**(4): 245-251.

Heel, A., P. Holtappels and T. Graule (2010). "On the synthesis and performance of flame-made nanoscale $\text{La}_{0.6}\text{Sr}_{0.4}\text{CoO}_3$ -delta and its influence on the application as an intermediate temperature solid oxide fuel cell cathode." Journal of Power Sources **195**(19): 6709-6718.

Hideyuki Terazono, Y. A., Mikhail Soloviev and Kenji Yasuda (2010). "Labelling of live cells using fluorescent aptamers: binding reversal with DNA nucleases." Journal of Nanobiotechnology **8**(8).

Hrouda, F. (1994). "A Technique for the Measurement of Thermal-Changes of Magnetic-Susceptibility of Weakly Magnetic Rocks by the Cs-2 Apparatus and Kly-2 Kappabridge." Geophysical Journal International **118**(3): 604-612.

Huang, H., B. Lu, J. P. Lei and X. L. Dong (2009). "Low-Temperature Nitridation of Fe Nanoparticles Precursor." Journal of Nanoscience and Nanotechnology **9**(12): 7383-7387.

Huang, S. H. and R. S. Juang (2011). "Biochemical and biomedical applications of multifunctional magnetic nanoparticles: a review." Journal of Nanoparticle Research **13**(10): 4411-4430.

Hurt, D., S. Li and A. Amann (2013). "Versatile SQUID Susceptometer With Multiple Measurement Modes." Ieee Transactions on Magnetics **49**(7): 3541-3544.

Inouye, K., R. Endo, Y. Otsuka, K. Miyashiro, K. Kaneko and T. Ishikawa (1982). "Oxygenation of Ferrous-Ions in Reversed Micelle and Reversed Micro-Emulsion." Journal of Physical Chemistry **86**(8): 1465-1469.

Jain, R. K. (1987). "Transport of Molecules across Tumor Vasculature." Cancer and Metastasis Reviews **6**(4): 559-593.

JanssenDiagnostics, retrived Jan, 2013, CELLSEARCH® System Overview,

" <https://www.cellsearchctc.com/product-systems-overview/cellsearch-system-overview>."

Jing, Y., L. R. Moore, T. Schneider, P. S. Williams, J. J. Chalmers, S. S. Farag, B. Bolwell and M. Zborowski (2007). "Negative selection of hematopoietic progenitor cells by continuous magnetophoresis." Experimental Hematology **35**(4): 662-672.

Jing, Y., L. R. Moore, P. S. Williams, J. J. Chalmers, S. S. Farag, B. Bolwell and M. Zborowski (2007). "Blood progenitor cell separation from clinical leukapheresis product by magnetic nanoparticle binding and magnetophoresis." Biotechnology and Bioengineering **96**(6): 1139-1154.

Jones, T. B. (1995). Electromechanics of particles. Cambridge ; New York, Cambridge University Press.

Jonsson, P. E., H. Mamiya and H. Takayama (2004). "Glassy dynamics of an interacting Fe-N nanoparticle system." Journal of Magnetism and Magnetic Materials **272**: 1290-1291.

Katepetch, C. and R. Rujiravanit (2011). "Synthesis of magnetic nanoparticle into bacterial cellulose matrix by ammonia gas-enhancing in situ co-precipitation method." Carbohydrate Polymers **86**(1): 162-170.

Keng, P. Y., I. Shim, B. D. Korth, J. F. Douglas and J. Pyun (2007). "Synthesis and self-assembly of polymer-coated ferromagnetic nanoparticles." Acs Nano **1**(4): 279-292.

Kim, J. E., J. Y. Shin and M. H. Cho (2012). "Magnetic nanoparticles: an update of application for drug delivery and possible toxic effects." Archives of Toxicology **86**(5): 685-700.

Kim, Y. H., B. J. Park, H. J. Choi and Y. Seo (2007). "Coating of magnetic particle with polystyrene and its magnetorheological characterization." Physica Status Solidi a-Applications and Materials Science **204**(12): 4178-4181.

Kircher, M. F., J. R. Allport, E. E. Graves, V. Love, L. Josephson, A. H. Lichtman and R. Weissleder (2003). "In vivo high resolution three-dimensional imaging of antigen-specific cytotoxic T-lymphocyte trafficking to tumors." Cancer Res **63**(20): 6838-6846.

Kligfield, R., W. H. Owens and W. Lowrie (1981). "Magnetic-Susceptibility Anisotropy, Strain, and Progressive Deformation in Permian Sediments from the Maritime Alps (France)." Earth and Planetary Science Letters **55**(1): 181-189.

Kobayashi, Y., H. Kakinuma, D. Nagao, Y. Ando, T. Miyazaki and M. Konno (2009). "Silica coating of Co-Pt alloy nanoparticles prepared in the presence of poly(vinylpyrrolidone)." Journal of Nanoparticle Research **11**(7): 1787-1794.

Kuhara, M., H. Takeyama, T. Tanaka and T. Matsunaga (2004). "Magnetic cell separation using antibody binding with protein expressed on bacterial magnetic particles." Anal Chem **76**(21): 6207-6213.

Laachir, A., V. Perrichon, A. Badri, J. Lamotte, E. Catherine, J. C. Lavalley, J. Elfallah, L. Hilaire, F. Lenormand, E. Quemere, G. N. Sauvion and O. Touret (1991). "Reduction of CeO₂ by Hydrogen - Magnetic-Susceptibility and Fourier-Transform Infrared, Ultraviolet and X-Ray Photoelectron-Spectroscopy Measurements." Journal of the Chemical Society-Faraday Transactions **87**(10): 1601-1609.

Lange, J., R. Kotitz, A. Haller, L. Trahms, W. Semmler and W. Weitschies (2002). "Magnetorelaxometry - a new binding specific detection method based on magnetic nanoparticles." Journal of Magnetism and Magnetic Materials **252**(1-3): 381-383.

Lee, K. D., S. Nir and D. Papahadjopoulos (1993). "Quantitative analysis of liposome-cell interactions in vitro: rate constants of binding and endocytosis with suspension and adherent J774 cells and human monocytes." Biochemistry **32**(3): 889-899.

Li, C. Y., C. Ma, F. Wang, Z. J. Xi, Z. F. Wang, Y. Deng and N. Y. He (2012). "Preparation and Biomedical Applications of Core-Shell Silica/Magnetic Nanoparticle Composites." Journal of Nanoscience and Nanotechnology **12**(4): 2964-2972.

Li, L., P. S. Greenberg, K. W. Street and D. R. Chen (2011). "Study of a Magnetic Filter System for the Characterization of Particle Magnetic Property." Aerosol Science and Technology **45**(3): 327-335.

Li, S. Q., Z. Chen, Y. D. Jin, S. H. Chen, H. Wang, J. X. Geng, Q. Song, X. D. Yang, L. J. Ma, S. J. Li, Z. Qin and C. Zheng (2011). "A new approach for preparation of magnetite-graphite composite: Intercalation of polyhydroxy iron cation into graphite oxide in L-arginine medium." Solid State Sciences **13**(5): 862-866.

Li, Z. X., M. Kawashita, T. Kudo and H. Kanetaka (2012). "Sol-gel synthesis, characterization, and in vitro compatibility of iron nanoparticle-encapsulating silica microspheres for

hyperthermia in cancer therapy." Journal of Materials Science-Materials in Medicine **23**(10): 2461-2469.

LifeTechnologiesCorporation, retrived Jan 2013, Dynabeads® Products & Technology, <http://www.lifetechnologies.com/us/en/home/brands/product-brand/dynal/dynabeads-technology.html?icid=fr-dynabeads-main> ".

Ludwig, F., E. Heim and M. Schilling (2004). "Magnetorelaxometry of magnetic nanoparticles-a new method for the quantitative and specific analysis of biomolecules." Nanotechnology **4th**: 245 - 248.

Ma, Z. Y., D. Dosev, M. Nichkova, R. K. Dumas, S. J. Gee, B. D. Hammock, K. Liu and I. M. Kennedy (2009). "Synthesis and characterization of multifunctional silica core-shell nanocomposites with magnetic and fluorescent functionalities." Journal of Magnetism and Magnetic Materials **321**(10): 1368-1371.

Marek, R., M. Caruso, A. Rostami, J. B. Grinspan and J. D. Sarma (2008). "Magnetic cell sorting: A fast and effective method of concurrent isolation of high purity viable astrocytes and microglia from neonatal mouse brain tissue." Journal of Neuroscience Methods **175**(1): 108-118.

Masoudi, A., H. R. M. Hosseini, M. A. Shokrgozar, R. Ahmadi and M. A. Oghabian (2012). "The effect of poly(ethylene glycol) coating on colloidal stability of superparamagnetic iron oxide nanoparticles as potential MRI contrast agent." International Journal of Pharmaceutics **433**(1-2): 129-141.

Masubuchi, Y., S. Yamashita, T. Motohashi, S. Kikkawa and M. Niederberger (2011). "Magnetite/maghemite mixture prepared in benzyl alcohol for the preparation of alpha ⁻Fe₁₆N₂ with alpha-Fe." Journal of the European Ceramic Society **31**(14): 2471-2474.

Maxwell, D. J., J. Bonde, D. A. Hess, S. A. Hohm, R. Lahey, P. Zhou, M. H. Creer, D. Piwnica-Worms and J. A. Nolta (2008). "Fluorophore-conjugated iron oxide nanoparticle labeling and analysis of engrafting human hematopoietic stem cells." Stem Cells **26**(2): 517-524.

Mayol, L., F. Quaglia, A. Borzacchiello, L. Ambrosio and M. I. La Rotonda (2008). "A novel poloxamers/hyaluronic acid in situ forming hydrogel for drug delivery: rheological, mucoadhesive and in vitro release properties." Eur J Pharm Biopharm **70**(1): 199-206.

McCloskey, K. E., J. J. Chalmers and M. Zborowski (2003). "Magnetic cell separation: Characterization of magnetophoretic mobility." Analytical Chemistry **75**(24): 6868-6874.

Meyers, P. H., C. M. Nice and F. Cronic (1963). "Experimental Approach in Use and Magnetic Control of Metallic Iron Particles in Lymphatic and Vascular System of Dogs as a Contrast and Isotopic Agent." American Journal of Roentgenology Radium Therapy and Nuclear Medicine **90**(5): 1068-&.

Miller, C. R., B. Bondurant, S. D. McLean, K. A. McGovern and D. F. O'Brien (1998). "Liposome-cell interactions in vitro: effect of liposome surface charge on the binding and endocytosis of conventional and sterically stabilized liposomes." Biochemistry **37**(37): 12875-12883.

MiltenyiBiotec, retrieved Jan 2013, MACS[®] MicroBeads - the most trusted and proven "https://www.miltenyibiotec.com/en/products-and-services/macscellseparation/macstechnology/microbeads_dp.aspx."

Moghimi, S. M. and A. C. Hunter (2000). "Poloxamers and poloxamines in nanoparticle engineering and experimental medicine." Trends Biotechnol **18**(10): 412-420.

Moore, L. R., S. Milliron, P. S. Williams, J. J. Chalmers, S. Margel and M. Zborowski (2004). "Control of magnetophoretic mobility by susceptibility-modified solutions as evaluated by cell tracking velocimetry and continuous magnetic sorting." Analytical Chemistry **76**(14): 3899-3907.

Mosmann, T. (1993). "Rapid colorimetric assay for cellular growth and survival: Application to proliferation and cytotoxic assay." J. Immunol. Methods **95**: 55-63.

Mutsaers, S. E. and J. M. Papadimitriou (1988). "Surface charge of macrophages and their interaction with charged particles." J Leukoc Biol **44**(1): 17-26.

Odette, L. L., M. A. McCloskey and S. H. Young (1984). "Ferritin conjugates as specific magnetic labels. Implications for cell separation." Biophys J **45**(6): 1219-1222.

Osborne, E. A., T. M. Atkins, D. A. Gilbert, S. M. Kauzlarich, K. Liu and A. Y. Louie (2012). "Rapid microwave-assisted synthesis of dextran-coated iron oxide nanoparticles for magnetic resonance imaging." Nanotechnology **23**(21).

Park, J. W., I. S. Yoo, W. S. Chang, E. C. Lee, H. Ju, B. H. Chung and B. S. Kim (2008). "Magnetic moment measurement of magnetic nanoparticles using atomic force microscopy." Measurement Science & Technology **19**(1).

Parra, E., A. G. Wingren, G. Hedlund, T. Kalland and M. Dohlsten (1997). "The role of B7-1 and LFA-3 in costimulation of CD8+ T cells." J Immunol **158**(2): 637-642.

Popa, M., L. Van Hong and M. Kakihana (2003). "Particle morphology characterization and magnetic properties of LaMnO₃+d perovskites." Physica B-Condensed Matter **327**(2-4): 237-240.

Prabhakar, P. K., S. Vijayaraghavan, J. Philip and M. Doble (2011). "Biocompatibility Studies of Functionalized CoFe₂O₄ Magnetic Nanoparticles." Current Nanoscience **7**(3): 371-376.

R&D "System, Retrived Jan 2013, MagCollect Cell Selection Kits,

http://www.rndsystems.com/product_detail_objectname_cell_selection_kits_product.aspx."

Raj, P. M., H. Sharma, S. Samtani, D. Mishra, V. Nair and R. Tummala (2013). "Magnetic losses in metal nanoparticle-insulator nanocomposites." Journal of Materials Science-Materials in Electronics **24**(9): 3448-3455.

Ranganathan, R. and A. Ray (2002). "Ferrites - what is new?" Pramana-Journal of Physics **58**(5-6): 995-1002.

Reece, L. M., L. Sanders, D. Kennedy, B. Guernsey, P. Todd and J. F. Leary (2010). "High-throughput magnetic flow sorting of human cells selected on the basis of magnetophoretic mobility " Proc. SPIE 7568, Imaging, Manipulation, and Analysis of Biomolecules, Cells, and Tissues VIII, 75680P **7568**.

Riskin, M., B. Basnar, Y. Huang and I. Willner (2007). "Magnetoswitchable charge transport and bioelectrocatalysis using maghemite-Au core-shell nanoparticle/polyaniline composites." Advanced Materials **19**(18): 2691-+.

Rosicka, D. and J. Sembera (2011). "Influence of structure of iron nanoparticles in aggregates on their magnetic properties." Nanoscale Research Letters **6**.

Ruan, J., J. Shen, Z. Wang, J. Ji, H. Song, K. Wang, B. Liu, J. Li and D. Cui (2011). "Efficient preparation and labeling of human induced pluripotent stem cells by nanotechnology." Int J Nanomedicine **6**: 425-435.

Sadjadi, M. S., F. Fathi, N. Farhadyar and K. Zare (2011). "Synthesis and characterization of PVP coated ultra-small Fe₃O₄ nanowires." Research Journal of Chemistry and Environment **15**(2): 873-875.

Saenz, J. J., N. Garcia, P. Grutter, E. Meyer, H. Heinzelmann, R. Wiesendanger, L. Rosenthaler, H. R. Hidber and H. J. Gunterodt (1987). "Observation of Magnetic Forces by the Atomic Force Microscope." Journal of Applied Physics **62**(10): 4293-4295.

Sajja, V. S. K., T. R. Hanley, H. Gapsis, B. Guernsey, D. J. Kennedy, M. J. Taylor, K. K. Papas and P. W. Todd (2011). "Application of Magnetic Particle Tracking Velocimetry to Quadrupole Magnetic Sorting of Porcine Pancreatic Islets." Biotechnology and Bioengineering **108**(9): 2107-2117.

Sawakami-Kobayashi, K., O. Segawa, K. Obata, E. Hornes, M. Yohda, H. Tajima and M. Machida (2003). "Multipurpose robot for automated cycle sequencing." Biotechniques **34**(3): 634-637.

Schimpf, M. E., K. Caldwell and J. C. Giddings (2000). Field flow fractionation handbook. New York, Wiley-Interscience.

Schmidl, F., P. Weber, T. Koettig, M. Buttner, S. Prass, C. Becker, M. Mans, J. Heinrich, M. Roder, K. Wagner, D. V. Berkov, P. Gornert, G. Glockl, W. Weitschies and P. Seidel (2007). "Characterization of energy barrier and particle size distribution of lyophilized ferrofluids by magnetic relaxation measurements." Journal of Magnetism and Magnetic Materials **311**(1): 171-175.

Schratzberger, P., N. Reinisch, W. M. Prodingler, C. M. Kahler, B. A. Sitte, R. Bellmann, R. Fischer-Colbrie, H. Winkler and C. J. Wiedermann (1997). "Differential chemotactic activities of sensory neuropeptides for human peripheral blood mononuclear cells." J Immunol **158**(8): 3895-3901.

Seemann, K., H. Leiste and K. Kruger (2013). "Ferromagnetic resonance frequency increase and resonance line broadening of a ferromagnetic Fe-Co-Hf-N film with in-plane uniaxial anisotropy by high-frequency field perturbation." Journal of Magnetism and Magnetic Materials **345**: 36-40.

Seto, T., K. Koga, F. Takano, H. Akinaga, T. Orii, M. Hirasawa and M. Murayama (2006). "Synthesis of magnetic COPt/SiO₂ nano-composite by pulsed laser ablation." Journal of Photochemistry and Photobiology a-Chemistry **182**(3): 342-345.

Sherlock, S. P. and H. J. Dai (2011). "Multifunctional FeCo-graphitic carbon nanocrystals for combined imaging, drug delivery and tumor-specific photothermal therapy in mice." Nano Research **4**(12): 1248-1260.

Silva, A. K. A., E. L. Silva, A. S. Carrico and E. S. T. Egito (2007). "Magnetic carriers: A promising device for targeting drugs into the human body." Current Pharmaceutical Design **13**(11): 1179-1185.

Silva, A. K. A., C. Wilhelm, J. Kolosnjaj-Tabi, N. Luciani and F. Gazeau (2012). "Cellular Transfer of Magnetic Nanoparticles Via Cell Microvesicles: Impact on Cell Tracking by Magnetic Resonance Imaging." Pharmaceutical Research **29**(5): 1392-1403.

Stampfli, M. R., S. Miescher, I. Aebischer, A. W. Zurcher and B. M. Stadler (1994). "Inhibition of human IgE synthesis by anti-IgE antibodies requires divalent recognition." Eur J Immunol **24**(9): 2161-2167.

StemCellTechnologies, retrived Jan 2013, Easysep,
"<http://www.stemcell.com/en/Products/Popular-Product-Lines/EasySep.aspx>."

Tang, Z. X., G. C. Hadjipanayis, S. I. Shah, V. Papaefthymiou and K. J. Klabunde (1993). "Preparation of Fe₄N from Nd-Containing Precursors." Journal of Magnetism and Magnetic Materials **119**(1-2): 49-53.

Tangsali, R. B., J. S. Budkuley, S. H. Keluskar, G. K. Naik and S. C. Watave (2011). "High density nanoparticle Mn-Zn ferrite synthesis, characterisation and magnetic properties." International Journal of Nanotechnology **8**(10-12): 948-962.

Tarasov, K. A., V. P. Isupov, B. B. Bokhonov, Y. A. Gaponov, B. P. Tolochko, M. M. Yulikov, V. F. Yudanov, A. Davidson, P. Beaunier, E. Marceau and M. Che (2008). "Control of particle size via chemical composition: Structural and magnetic characterization of Ni-Co alloy nanoparticles encapsulated in lamellar mixed oxides." Microporous and Mesoporous Materials **107**(1-2): 202-211.

Thompson, G. H., M. N. Myers and J. C. Giddings (1969). "Thermal Field-Flow Fractionation of Polystyrene Samples." Analytical Chemistry **41**(10): 1219-&.

Todd, P., R. P. Cooper, J. F. Doyle, S. Dunn, J. Vellinger and M. S. Deuser (2001). "Multistage magnetic particle separator." Journal of Magnetism and Magnetic Materials **225**(1-2): 294-300.

Tomitaka, A., T. Yamada and Y. Takemura (2012). "Magnetic Nanoparticle Hyperthermia Using Pluronic-Coated Fe₃O₄ Nanoparticles: An In Vitro Study." Journal of Nanomaterials.

Tomlinson, M. J., S. Tomlinson, X. B. Yang and J. Kirkham (2013). "Cell separation: Terminology and practical considerations." J Tissue Eng **4**: 2041731412472690.

Tresilwised, N., P. Pithayanukul, O. Mykhaylyk, P. S. Holm, R. Holzmuller, M. Anton, S. Thalhammer, D. Adiguzel, M. Doblinger and C. Plank (2010). "Boosting Oncolytic Adenovirus Potency with Magnetic Nanoparticles and Magnetic Force." Molecular Pharmaceutics **7**(4): 1069-1089.

Tseng, C. L., I. L. Shih, L. Stobinski and F. H. Lin (2010). "Gadolinium hexanedione nanoparticles for stem cell labeling and tracking via magnetic resonance imaging." Biomaterials **31**(20): 5427-5435.

Usselman, R. J., S. E. Russek, M. T. Klem, M. A. Allen, T. Douglas, M. Young, Y. U. Idzerda and D. J. Singel (2012). "Temperature dependence of electron magnetic resonance spectra of iron oxide nanoparticles mineralized in *Listeria innocua* protein cages." Journal of Applied Physics **112**(8).

Wang, H. W., T. B. Shrestha, M. T. Basel, R. K. Dani, G. M. Seo, S. Balivada, M. M. Pyle, H. Prock, O. B. Koper, P. S. Thapa, D. Moore, P. Li, V. Chikan, D. L. Troyer and S. H. Bossmann (2012). "Magnetic-Fe/Fe₃O₄-nanoparticle-bound SN38 as carboxylesterase-cleavable prodrug for the delivery to tumors within monocytes/macrophages." Beilstein Journal of Nanotechnology **3**: 444-455.

Wardal, K., J. Typek, G. Zolnierkiewicz, N. Guskos, U. Narkiewicz and D. Sibera (2013). "FMR study of 0.30(Fe₂O₃)/0.70(ZnO) nanocomposite." European Physical Journal-Applied Physics **62**(1).

Wilhelm, C. and F. Gazeau (2008). "Universal cell labelling with anionic magnetic nanoparticles." Biomaterials **29**(22): 3161-3174.

Wilhelm, C. and F. Gazeau (2008). "Universal cell labelling with anionic magnetic nanoparticles." Biomaterials **29**(22): 3161-3174.

Xu, H. Y., Z. P. Aguilar, L. Yang, M. Kuang, H. W. Duan, Y. H. Xiong, H. Wei and A. Wang (2011). "Antibody conjugated magnetic iron oxide nanoparticles for cancer cell separation in fresh whole blood." Biomaterials **32**(36): 9758-9765.

Xu, J., K. Mahajan, W. Xue, J. O. Winter, M. Zborowski and J. J. Chalmers (2012). "Simultaneous, single particle, magnetization and size measurements of micron sized, magnetic particles." Journal of Magnetism and Magnetic Materials **324**(24): 4189-4199.

Ye, F., S. Laurent, A. Fornara, L. Astolfi, J. Qin, A. Roch, A. Martini, M. S. Toprak, R. N. Muller and M. Muhammed (2012). "Uniform mesoporous silica coated iron oxide nanoparticles as a highly efficient, nontoxic MRI T2 contrast agent with tunable proton relaxivities." Contrast Media & Molecular Imaging **7**(5): 460-468.

Yoo, M. K., I. Y. Park, I. Y. Kim, I. K. Park, J. S. Kwon, H. J. Jeong, Y. Y. Jeong and C. S. Cho (2008). "Superparamagnetic Iron Oxide Nanoparticles Coated with Mannan for Macrophage Targeting." Journal of Nanoscience and Nanotechnology **8**(10): 5196-5202.

You, B., D. J. Zhou, S. L. Zhang, F. Yang and X. C. Ren (2012). "Preparation of core-shell nanoparticle-based hindered amine stabilizer and its application in polyoxymethylene." Journal of Applied Polymer Science **126**(4): 1291-1299.

Zborowski, M. and J. J. Chalmers (2008). Magnetic cell separation. Amsterdam ; Boston, Elsevier.

Chapter 3 - Magnetic Particle Characterization – Magnetophoretic Mobility and Particle Size

Abstract

Quantitative characterization of magnetic particles is useful for analysis and separation of labeled cells and magnetic particles. A particle velocimeter is utilized to directly measure the magnetophoretic mobility, size and other parameters of magnetic particle suspensions. The instrument provides quantitative video analysis of particles and their motion. The trajectories of magnetic particles in an isodynamic magnetic field are recorded using a high-definition camera/microscope system for image collection. Image analysis software then converts the image data to the parameters of interest. The distribution of magnetophoretic mobility is determined by combining fast image analysis with velocimetry measurements. Particle size distributions have been characterized to provide a better understanding of sample quality. The results have been utilized in the development and operation of analyzer protocols for counting particle concentrations accurately and measuring magnetic susceptibility and size for simultaneous display for routine application to particle suspensions and magnetically labeled biological cells.

Keywords: image cytometry, magnetic carriers, magnetic particles, magnetophoretic mobility, particle size distribution

3.1 INTRODUCTION

Since magnetism and magnetic particles are used widely in many bioengineering and medical applications, characterization of magnetic particle properties is required both in research and production. Specific cytometry-relevant applications include the analysis and/or separation of biological cells labeled with magnetic particles. Various methods and instruments have been developed for magnetic particle characterization. Dynamic light scattering or laser diffraction determine the particle size, scanning electron microscopy (SEM) (Popa M 2003, Gherca D 2012) or transmission electron microscopy (TEM) (Li ZX 2012) observe the microstructure of the particle, energy dispersive X-ray spectrometer (EDX) (Tarasov KA 2008) determines the element composition and x-ray diffraction (XRD) (Li and Takahashi 2000, Zhao, Wan et al. 2000) provides information about the crystalline phase. Methods to determine magnetic properties include the vibrating sample magnetometer (Foner 1959, Fønnum G 2005, Kim, Park et al. 2007, Bhukal, Bansal et al. 2014), the superconducting quantum interference device (SQUID) (Clarke 1994, Hurt, Li et al. 2013) and giant magnetic magnetoresistance sensors (Little CAE 2013). These methods provide only bulk average magnetization/susceptibility of a sample. For many applications, including applications to biological cells, a bulk value is not sufficient for analysis and experiment design. More information concerning homogeneity of magnetic susceptibility among particles in a population is needed by both researchers and manufacturers. Moreover, susceptibility of the particle cannot comprehensively describe the motion of the particle in a defined magnetic field. The particle size and the interaction between particle and medium also impact the behavior of magnetic particles. Individual particles can be characterized by measuring their *magnetophoretic mobility*. Magnetophoretic mobility not only contains information on susceptibility of the individual particle but also reflects the particle size and viscosity of fluid medium (Chalmers JJ 1999, Zborowski M 1999, Zborowski M 2008).

Non-commercial instrumentation has been applied by specific investigators to the measurement of magnetophoretic mobility of individual particles and magnetically labeled cells by particle tracking velocimetry (Reddy S 1996, Moore LR 2000, Suwa M 2001, Xu J 2012). In certain cases these measurements are applied directly to the establishment of parameters for the enrichment of magnetically labeled cells in flowing devices (Williams PS 1999, Watarai H 2002, McCloskey KE 2003, Sajja VSK 2011) or to the quantification of cell surface markers (McCloskey KE 2000, McCloskey KE 2001).

This study develops a method to characterize the properties of magnetic particles by particle tracking velocimetry using a commercial HyperfluxTM velocimeter (IKOTECH Inc., Greenville, Indiana, USA). This velocimeter tracks the motion of each particle in the magnetic field and describes the particle size distribution and magnetophoretic mobility. The particle-by-particle analysis provides statistically useful and meaningful data to allow researchers and manufacturers to understand the distribution of properties and to control the quality of the product. The main scope of this study was to demonstrate procedures in which the Hyperflux Velocimeter may accurately describe the properties of a magnetic particle suspension. In this study we tested the effects of image analysis parameters on magnetophoretic mobility measurement, compared the particle concentration counts with corresponding hemacytometer counts, then a means of particle size measurement was developed based on reported standard particle size. In all cases the impact of instrument optical threshold settings was analyzed.

3.2 Theory

In an isodynamic magnetic field (Frantz SG 1936, Chalmers JJ 1999, Zborowski M 1999, Zborowski M 2008), assuming a micro-sized magnetic particle is in a viscous creeping diamagnetic fluid medium, the magnetic force acting on the particle can be expressed as

$$F_m = \Delta\chi V \nabla \left(\frac{B_0^2}{2\mu_0} \right)$$

where $\Delta\chi = \chi_p - \chi_f$, the difference between the magnetic susceptibility of particle and fluid; V is the volume of the particle; B_0 and μ_0 are magnetic induction and magnetic permeability of free space, respectively. $\Delta\chi = \chi_p$ in most practical cases, but deliberate exceptions exist (Moore LR 2004, Zhang HD 2005).

At the same time, the drag force on the particle in the direction opposite to that of the magnetic force, according to Stokes' law, should be

$$F_d = 6\pi\eta R v$$

where η is the viscosity of fluid, R is the radius of the particle, and v is the terminal velocity of the particle.

When the particle reaches a terminal velocity in the system the drag force will balance the magnetic force, $F_m = F_d$. One obtains the terminal velocity of the particle:

$$v = \frac{\Delta\chi V}{6\pi\eta R} \nabla \left(\frac{B_0^2}{2\mu_0} \right) \quad (1)$$

The left term, $\frac{\Delta\chi V}{6\pi\eta R}$, describes the properties of the particle and fluid medium and is defined as *magnetophoretic mobility*, U_m . Rearranging the above expression we find that magnetophoretic

mobility is the ratio of the terminal velocity of the particle, v_m , to the gradient of the magnetic energy, $\frac{\nabla B_0^2}{2\mu_0}$,

$$U_m = v_m / \frac{\nabla B_0^2}{2\mu_0} \quad (2)$$

The units of U_m are $\text{m s}^{-1}/\text{T A m}^{-2}$ or $\text{m}^3\text{T}^{-1} \text{A}^{-1} \text{s}^{-1}$ (meters cubed per Tesla-Ampere-second), expressed in this work as $\text{m}^3/\text{T}\cdot\text{A}\cdot\text{s}$.

Thus by measuring the terminal velocity of the particle the magnetophoretic mobility of the particle may be calculated, as the magnetic pressure in the isodynamic magnetic field is constant. The Hyperflux Velocimeter uses this feature to track the mobility information of each particle.

From the definition of magnetophoretic mobility, $U_m = \frac{2}{9\eta} R^2 \Delta\chi$, we find that it is a function of effective magnetic particle size and magnetic susceptibility and medium viscosity. These three parameters are independent and could all influence the motion of the particle. This means that the magnetic susceptibility of each single particle can be calculated when these variables are measured simultaneously for a single particle (Frantz SG 1936, Reddy S 1996, Chalmers JJ 1999, Zborowski M 2008, Xu J 2012).

3.3 Materials and Methods

3.3.1 Non-magnetic Particles and Magnetic Particles

Three types of calibration beads were used: medium mobility calibration beads ($U_m = 6.61 \pm 2.58 \times 10^{-12} \text{ m}^3/\text{T}\cdot\text{A}\cdot\text{s}$), large size non-magnetic calibration beads (diameter, $D = 4.993 \pm$

0.040 μm), medium size non-magnetic calibration beads ($D = 1.999 \pm 0.020 \mu\text{m}$). Their characteristics are summarized in Table 1. The reference mobility of the medium mobility calibration beads was determined by the vendor using a measured and mapped magnetic field and gradient. Several de-identified commercial product beads were studied to demonstrate the range of measurements possible and the variation that exists within the commercial bead market, keeping in mind that such beads are used in magnetic cell sorting. The bead samples were designated as follows (with the diameters, D , provided by the vendors): B_1 ($D = \sim 3\text{-}12 \mu\text{m}$), B_2 ($D = \sim 1.5 \mu\text{m}$), B_3 ($D = \sim 1.5 \mu\text{m}$), P_1 ($D = 0.88 \mu\text{m}$, uniform microspheres), P_2 ($D = 3.13 \mu\text{m}$, uniform microspheres), P_3 ($D = 3.16 \mu\text{m}$, uniform microspheres). B and P series particles are provided by Bangs Labs. Inc; L_1 (bead content $\sim 10 \text{ mg/ml}$, $D \approx 2.7 \mu\text{m}$); L_2 (bead content $\sim 28 \text{ mg/ml}$, $D \approx 2.7 \mu\text{m}$); L_3 (bead content $\sim 28 \text{ mg/ml}$, $D \approx 2.7 \mu\text{m}$). L type magnetic beads are provided by Agilent Technologies. All the size and other information was obtained from vendors' label and catalogue data.

3.3.2 Hyperflux Velocimeter

The Hyperflux Velocimeter (Figure 3.1(A)) includes a channel cell, a magnet assembly providing an isodynamic magnetic field and gradient (Frantz SG 1936, Chalmers JJ 1999, Zborowski M 1999, Little CAE 2013), an automated pump for sample changing, a high-sensitivity and high-resolution (4.4 μm) Grasshopper[®] monochrome 2.0 MP Fire-Wire CCD camera (Point Grey) combined with a 2X to 8X telecentric lens (Edmund Optics) to capture dark-field images of the moving particles at 30 frames/s as part of a fully automated process. The 6X telecentric lens used in this study results in a 0.733 μm point-to-point resolution in the object plane within the 400 μm -thick liquid sample cell. This lens is positioned to view the mapped isodynamic zone between two Frantz-type polepieces (Frantz SG 1936) as described for earlier instrumentation for magnetic particle velocimetry (Chalmers JJ 1999, Zborowski M 1999).

A Linux system computer with software (“IKOvisonTM” and “Cytotest”, IKOTECH, LLC) is capable of capturing and analyzing the video images for particle characteristics and trajectory. Every frame is permanently recorded and available to the operator as well as for repeated image analysis (replay of experiment). After the operator has set intensity and size thresholds and limits, the image data are sent to software (“MagexTM”) that can generate up to 23 characteristics of particles including magnetophoretic mobility, size, sedimentation rate, shape and intensity. A particle “diameter” is provided in the display based on the pixel count for each object, the camera resolution and the lens magnification. This method systematically overestimates particle diameter because it is based on a dark-field image. Correct diameter displays must be based on a calibration factor for this variable, the determination of which is a component of the present study.

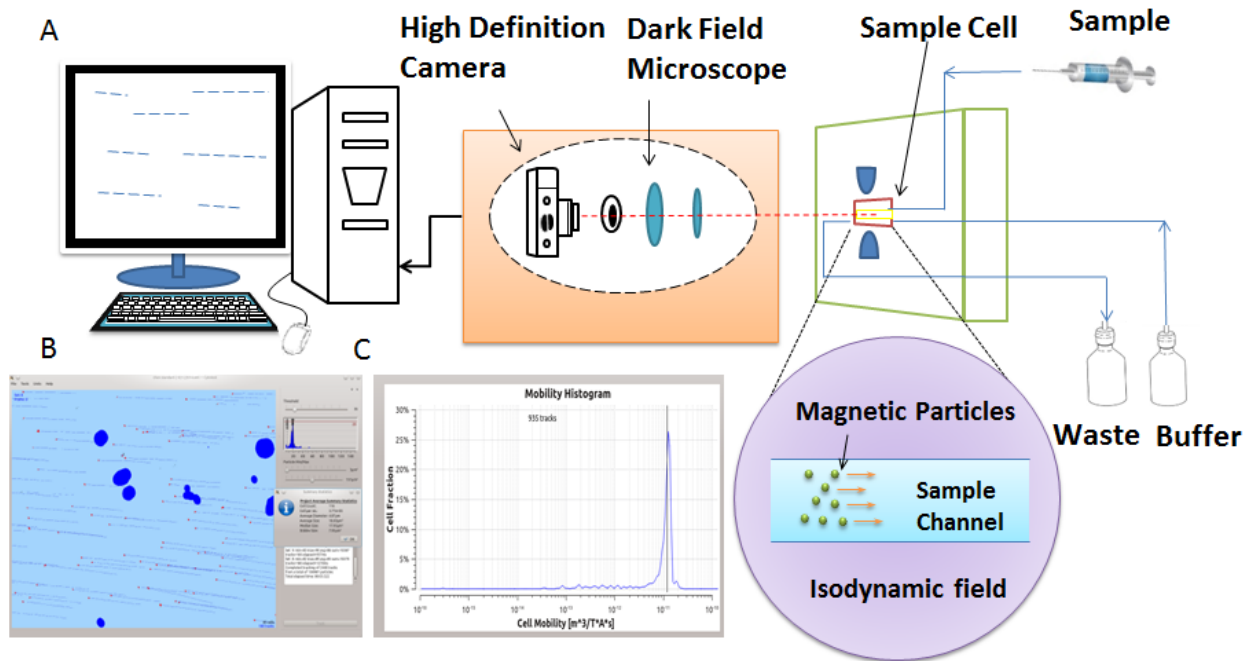


Figure 3.1 - Hyperflux™ Velocimeter instrument layout, image data analysis processing and mobility distribution display. (A) Velocimeter Layout. Three major parts are included: microscope and camera system, stopped-flow channel cell positioned in the isodynamic magnetic field, image analysis software. (B) Working window of Cytotest™ Image Analysis Software Display: The trajectory of each particle can be observed, and artefacts can be excluded (blue disks). Threshold and size gates are set before automatic track calculation. Size distribution and statistical summary are listed on the right. (C) Graphical Display: Magnetophoretic mobility histogram of medium-mobility calibration beads.

3.3.3 Procedure

A Z359629-1EA Bright-Line™ Hemacytometer is used for particle counting. The particle concentration was obtained by counting in five large squares, which typically provided $\pm 10\%$ precision. Hemacytometer counts were used to adjust particle concentrations to approximately $5 \times 10^4/\text{mL}$ for velocimetry and as “ground truth” for direct comparison with particle concentrations displayed by the velocimeter software.

3.4 Results and Discussion

3.4.1 Magnetophoretic Mobility Measurements

The velocimeter was tested by using standard medium mobility calibration beads (Table 3.1) to evaluate its capability of measuring magnetophoretic mobility and other characteristics. At an intensity threshold setting of 35 (arbitrary units between 0 and 255, see below), the particle trajectories (blue dashed lines shown in Figure 3.1(B)) are displayed, and interactive distributions for setting thresholds are displayed on the right-hand side of the working window. Figure 3.1(C) illustrates a magnetophoretic mobility histogram displayed on a log scale by the “Cytotest” analysis software package. The distribution in Figure 3.2(A) for these beads is based on >2200 tracks detected in a suspension of particles at $4 \times 10^5/\text{mL}$ and is displayed on a linear scale of mobility in Figure 3.2(A). The averaged mobility of the tracked particles is $6.86 \pm 1.95 \times 10^{-12} \text{ m}^3/\text{T}\cdot\text{A}\cdot\text{s}$, near the calibration value provided with the sample (Table 3.1). Triplicate tests were made to measure the medium mobility calibration beads to prove the repeatability of the instrument. The three mobility distributions are shown in Figure 3.2(A) and indicate $\pm 0.6\%$ repeatability and a consistent coefficient of variation, $\text{CV} = 28\%$, for this sample. The mean mobility is within 3.5% of the catalogue value (Table 3.1). The distribution and average result are essentially the same which suggests the stability of Hyperflux Velocimeter measurements.

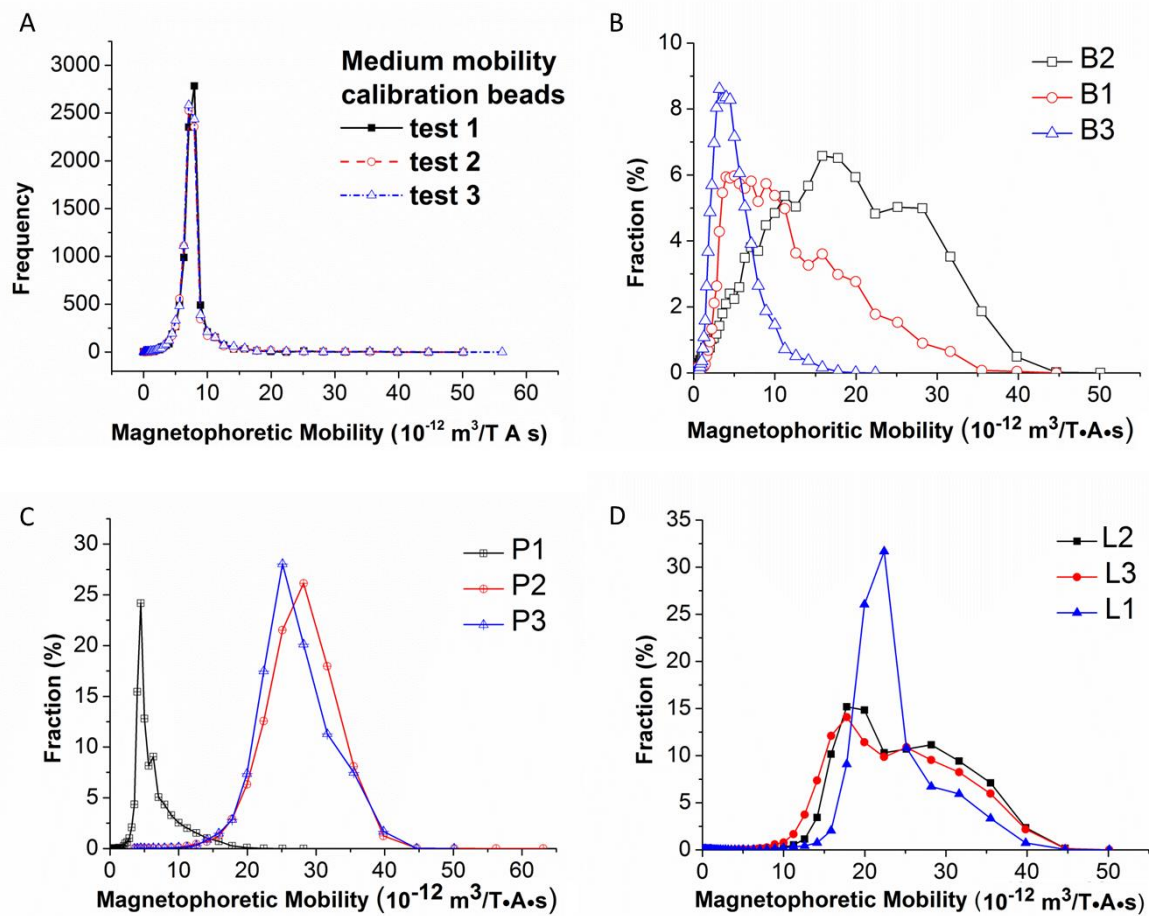


Figure 3.2 - Mobility Distribution Results displayed on a linear scale. (A) Mobility distribution for Standard Medium Mobility Calibration Beads, results of triplicate tests: average mobilities of tests 1, 2 and 3 are 6.87 ± 1.85 , 6.80 ± 1.89 , 6.89 ± 2.05 . (B) Magnetophoretic Mobility Distributions of B Magnetic Particles. (C) Magnetophoretic Mobility Distributions of P Magnetic Particles. (D) Magnetophoretic Mobility distributions of L Samples.

Table 3.1. Summary characteristics of beads used for calibrations and supplied by vendor, IKOTECH, LLC.

Hyperflux Bead Name	Part No.	Diameter	Mobility	Manufacturer	Traceability
Large Calibration Beads	220-006	4.99 ± 0.04	0.00	Duke Standards	NIST
Medium Size Calibration Beads	220-007	2.00 ± 0.02	0.00	Duke Standards	NIST
Medium Mobility Calibration Beads	220-002	1.0	6.61 ± 2.58	Dynal	IKOTECH
Units		μm	10^{-12} m^3/TAs		

3.4.2 Characterization of Paramagnetic Particles

De-identified commercial magnetic particles were tested. One magnetophoretic mobility distribution is shown for each (at least three repetitions of each distribution were determined). B1, B2, and B3 are non-spherical particles. They are irregular-shaped clusters of iron oxide with a broad size distribution. Three varieties, B1, B2 and B3, contain high percentages of iron oxide which could result in a fast magnetic separation of cells labeled with these particles, and a coating which provides surface primary carboxyl groups for the attachment of proteins or antibodies and/or for colloid stability. Their magnetophoretic mobility distributions are shown in Figure 3.2(B). The average magnetophoretic mobilities of B1, B2 and B3 are 4.04, 13.5 and $8.31 \times 10^{-12} \text{ m}^3/\text{T}\cdot\text{A}\cdot\text{s}$, respectively; average diameters calculated from dark-field images are 4.99, 7.5 and 6 μm respectively – larger than actual size due to dark-field optics. Diameter measurement in dark field is considered further, below.

Superparamagnetic particles P1, P2 and P3 are highly uniform polymer-based magnetite spheres in diameters of 1 μm and 3 μm . Figure 3.2(C) shows the distribution of the three types

with average magnetophoretic mobilities of P1, P2 and P3 being 5.65 , 25.96 and 26.84×10^{-12} $\text{m}^3/\text{T}\cdot\text{A}\cdot\text{s}$, respectively. The P2 and P3 types possess much higher mobility than that of P1 due to the particle size. The calculated particle diameters of the three P samples were 5.2 , 8.31 and 11.3 μm , respectively. The P2 has a smaller average size than that of P3 but similar mobility.

L1, L 2 and L3 are all superparamagnetic microbeads with a microcrystalline ferric oxide component uniformly dispersed throughout the bead. The mobility distributions of the three particles are shown in Figure 3.3(D). With similar reported particle size, the commercial product L1 has higher peak mobility $22.75 \times 10^{-12} \text{m}^3/\text{T}\cdot\text{A}\cdot\text{s}$ and a narrow distribution. The other two samples show two peak mobilities around 18.87 and $29.90 \times 10^{-12} \text{m}^3/\text{T}\cdot\text{A}\cdot\text{s}$. In this case the velocimeter shows that the three particle distributions are not the same, whereas measurements by SQUID, VSM or giant magnetoresistance resonance would be expected to indicate similar results.

The particle magnetophoretic mobilities and distributions reported here were measured at a fixed single value of magnetic induction, $B_o = 0.56$ Tesla (equation (2)). The magnetization curves of specific commercial beads having the same composition as the commercial standard used in this study have been determined (Fonnum G 2005), and $B_o > 0.10$ mT is within the region of saturation magnetization (Xu J 2012). Thus, χ_p , the slope of the magnetization curve, is not constant but diminishes with increasing applied magnetic induction B_o until the particle magnetization becomes constant meaning no further increases in v_m . Magnetic velocimetry is a robust measurement of particle quality; however, different laboratories using different values of applied magnetic induction could find different mobilities for the same particles. Meanwhile, vendor-supplied calibration beads may be used as a basis for measuring the mobility distribution of labeled cell populations and other velocity-derived properties.

The magnetophoretic mobility of microparticles generally increases with particle diameter, as expected. The commercial products tested have coefficients of variation ranging from 20% to 75% of mean mobility, consistent with other published values (Xu J 2012). These results suggest that commercial products should be evaluated for magnetic uniformity by manufacturers, and reporting magnetophoretic mobility should be treated with similar status to reporting uniform particle diameter.

3.4.3 Particle counting

A comparison was made between the Hyperflux Velocimeter and a hemacytometer by counting particles of standard calibration beads (Table [3.1](#)) to test the capability of the velocimeter in measuring the particle concentration. In velocimeter operations the operator selects an intensity threshold for identifying particles using a scale of 0-255 and feedback from the interactive image display on which the selected particles are highlighted in color. An acceptable size range for counting is selected in the same manner. (An option exists to set default values when several similar samples are being tested.) Table [3.2](#) summarizes the results of an example of such a comparison, in which the effects of the above-mentioned threshold settings are explored. Two sets of settings were used for each particle type, as shown in the table. The data in the table were obtained from a single image file in each of the three cases. The operator is able to “re-play” every stored experiment by opening the stored semi-raw image files to make a new set of counts, sizes, tracks, and other parameters. When the higher intensity threshold was used in each case the Hyperflux count agreed with the hemacytometer count within counting precision. A lower threshold setting led to overestimations of particle concentration. This finding is consistent with the science of dark-field illumination, in which low-intensity light scattered at the detection angle can arise from objects other than the target objects (see below). In this instrument these are apparent below intensity threshold setting = 35.

Based on the first entry in Table 3.2, if one particle is detected in the Hyperflux image field the concentration of particles in the sample syringe is 3.23×10^3 particles/ml. If N particles are detected, then the concentration should be $N \times 2.23 \times 10^3$ p/mL.

Table 3.2 – Particle Concentration Measurement by Hyperflux Imaging Compared to Hemacytometer Counts

Standard Sample	Hyperflux Velocimeter			Hemacytometer (p/mL)
	Intensity Threshold	Size Range*	Count (p/mL)	
Medium mobility	20	2-186	5.77×10^5	3.72×10^5
	25	13-152	3.21×10^5	
Large size	20	2-304	2.65×10^5	1.3×10^5
	55	0-311	1.22×10^5	
Medium size	22	2-304	9.77×10^5	12.7×10^5
	63	6-112	11.6×10^5	

*Numerical values are velocimeter settings displayed in μm^2 (translated algorithmically from pixel counts)

A statistical analysis further demonstrates the agreement of particle count results. Using the samples L₁, L₂ and L₃ three different concentrations were chosen for each comparison between velocimeter statistics and hemacytometer counts. Threshold setting was held at 35 and all size gating was $1 \mu\text{m}^2$ and $1521 \mu\text{m}^2$ in the “Cytotest” selection pane. Data are summarized in Table 3.3, where “DIFF” column is a tabulation of the differences between counts (in 10^5 p/mL) to see if the difference between manual counts and Hyperflux counts differed by more than one standard deviation of the hemacytometer count. A “Y” in the last column means this difference was less than the standard deviation of the hemacytometer count. The result reveals that the two methods of particle counting do not result in significant differences in each case, and instrument data can be used to determine absolute particle (or cell) concentration.

Table 3.3 – Statistical Analysis of the Agreement between Hyperflux Velocimeter and Hemacytometer Particle Counts

	Hyperflux Velocimeter			Hemacytometer				
	$C_1(\times 10^5 \text{ p/ml})$	SD_1	T_1	$C_2(\times 10^5 \text{ p/ml})$	SD_2	T_2	$DIFF(C_2-C_1)$	$DIFF \leq S_{D_2}$
L_2	2.54	0.09	786	2.68	0.23	134	0.14	Y
	1.06	0.06	328	1.14	0.15	57	0.08	Y
	0.51	0.04	158	0.48	0.1	24	-0.03	Y
L_1	1.76	0.08	545	1.82	0.19	91	0.06	Y
	0.97	0.06	300	1.12	0.15	56	0.15	Y
	0.49	0.04	152	0.44	0.09	22	-0.05	Y
L_3	2.79	0.09	864	2.88	0.24	144	0.09	Y
	0.93	0.05	288	1.02	0.14	51	0.09	Y
	0.51	0.04	158	0.52	0.1	26	0.01	Y

Note: C_1 and C_2 are concentrations determined from velocimeter and hemacytometer counts, respectively. T_1 and T_2 are particle-number total counts by velocimeter and hemacytometer, respectively. SD of concentration is calculated by equation $SD = \text{concentration} * (\frac{SD \text{ of particle total count}}{\text{particle total count}})$

3.4.4 Threshold Settings

The science of the method is dependent on the detection of objects of interest in dark field illumination. Therefore the velocimeter allows the operator to select particles to be analyzed by setting an intensity threshold and upper and lower size limits interactively with the image display. This is useful for heterogeneous and debris-containing specimens. An image intensity threshold must be established before tracking particles, as just discussed. Multiple trials with a single data set are possible, because all original image frames are permanently stored, and they are not modified by any settings related to data analysis. All images are available for “replay”. To identify each particle, the software converts each gray scale image into a black and

white image. Each pixel in a gray scale image represents an intensity value from 0 to 255, with 0 being a black pixel and 255 being white. All pixels with intensity below the threshold setting will be displayed as white, whereas above the setting value all pixels are displayed as black. Threshold points from 0 to 255 are selectable and should be chosen carefully; if the value is too low, neighboring particles will combine into single points which will result in a high number of tracking errors; if threshold value is set too high, the particle concentration will drop below the actual value. A study was done to reveal the influence of threshold setting on particle counting, size and magnetophoretic mobility measurement. The tested samples were the three types of calibration beads (Table 3.1). Threshold settings in the value range from 15 to 100 were studied.

Figure 3.3(A) indicates that the particle count is almost the same when the intensity threshold setting is between 30 and 70. When this is below 30 (especially below 20), the particle count decreases sharply to the true value as threshold increases.

Figure 3.3(B) demonstrates that a threshold setting below 30 impacts the diameter reading, particularly for larger size particles. Also at settings above 30, the diameter decreases for all particle sizes and is always larger than the true value owing to the fact that a dark-field image is being analyzed (see below). When the intensity threshold setting is low (below about 35) numerous small particle dots appear on the fringe of particles, and higher particle numbers will be calculated while bringing down the level of average diameter. From observation of Fig 3.3 (A)(B) we learn that at intensity threshold settings above about 35 the diameter displayed is a monotonic function of actual particle size, and the particle count is constant and in agreement with the true value. In studies of magnetic and other synthetic particles it is therefore generally advised to analyze data using intensity threshold settings around 35 or slightly greater.

Figure 3.3(C) indicates that intensity threshold setting has little influence on mobility distribution (except threshold 15, not shown) but only affects the particle fraction tracked. The reason is simple: mobility is calculated by the trajectory (terminal velocity) of the particle which is measured independently of particle size. Therefore magnetophoretic mobility is a robust measurement. In summary, intensity threshold settings have significant influence on displayed size distribution, negligible effect on particle count when set >30 , and only slightly impacts mobility distribution. As a result, threshold settings should be chosen carefully and, in the case of synthetic particles should always be 35 or above. Further study is needed to determine optimal settings for labeled living biological cells.

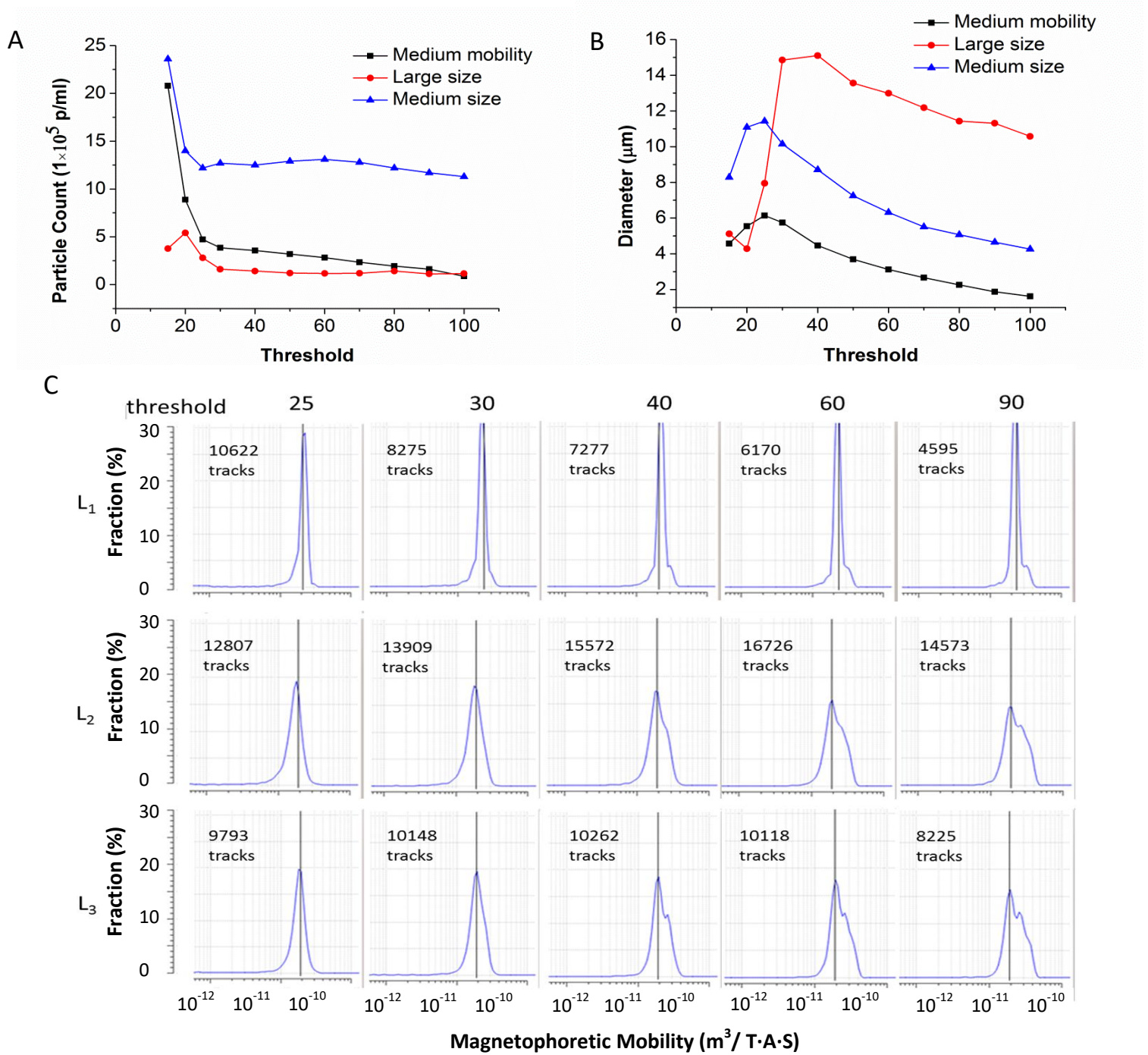


Figure 3.3 - Influence of Threshold Setting Value on Analysis Results. (A) Particle Count versus intensity threshold. (B) Diameter versus intensity threshold. (C) Magnetophoretic Mobility Distributions of L1, L2 and L3 beads with different intensity threshold values 25, 30, 40, 60 and 90, respectively.

3.4.5 Size Calibration

Because dark field images of particles are larger than the actual particle size, consistent with the data presented above, a size calibration procedure is needed in order to develop 2-parameter displays of magnetophoretic mobility vs. size. A series of particles with reported diameter range from 0.7 μm to 4.99 μm was chosen to investigate the effect of threshold on size calibration. Three threshold values were initially selected: 25, 50 and 90. The Hyperflux Velocimeter Min and Max size range gate was set between 1 and 450 pixels (nominally [0 and 250 μm^2]). The larger the threshold value, the better the linear relation between the reported actual diameter and the displayed calculated average diameter (data not shown). Threshold settings that provide a combination of accurate particle count, correct magnetophoretic mobility and useful size calibration need to be applied. If an optimal spot is discovered between threshold settings of 25 and 50, a conversion method for size (diameter) can be developed. Thus, similar analysis was performed using the same particle series and intensity thresholds of 30, 35, 40, 45 and 50 with size range 1- 450 pixels (Figure 3.4(A)).

Two solutions for the threshold could be chosen. First, one may set the value 40 as a reference threshold no matter what size the magnetic particle is. Second, if the particle size is less than 1 micrometer, set threshold at 30; otherwise, set threshold at 50. For submicron particles:

$$D = \frac{d-5.2315}{1.793} \quad (3)$$

and for particles with size $> 1 \mu\text{m}$:

$$D = \frac{d-2.518}{2.3027} \quad (4)$$

where d = calculated diameter displayed by Hyperflux velocimeter, and D = correct particle diameter (in this case provided by vendors). Applying equation (4) to a complete list-mode data set obtained for bead sample L_1 (for example) results in a diameter estimate for every particle, which can be displayed as a two-parameter scatter diagram as shown in Figure [3.4\(B\)](#), where it is also seen that the faster objects detected in Figure [3.2\(D\)](#) are the larger objects revealed in two-parameter space.

The dark-field particle velocimeter, while robust for determining particle count and velocity, only measures and reports particle size through an algorithm requiring calibration, which has here been demonstrated to be feasible. It should be added that particle velocimetry can also measure sedimentation velocity, from which the square of the particle diameter can be determined but only if also viscosity and particle and medium density are known. A particle velocimeter does not measure these values independently.

3.5 Conclusion

In conclusion, a method has been researched for the simultaneous determination of particle count, particle diameter and magnetophoretic mobility using dark-field video-microscope velocimetry with image storage, processing and analysis software using the commercial Hyperflux particle-tracking Velocimeter (Zhou C 2014). This study has demonstrated an available capability to analyze magnetic particles and cells that has been heretofore limited to only a handful of laboratories (Gill SJ 1960, Molday RS 1977, Chalmers JJ 1999, Suwa M 2001, Häfeli UO 2002, Wilhelm C 2002, Sajja VSK 2011) with one-of-a-kind instruments. With correct operator-based settings measurements of magnetophoretic mobility and particle count are robust, and diameter can be determined on the basis of calibration. The

application of this commercial technology to the characterization of magnetically labeled biological cells is ongoing, and further developments are expected.

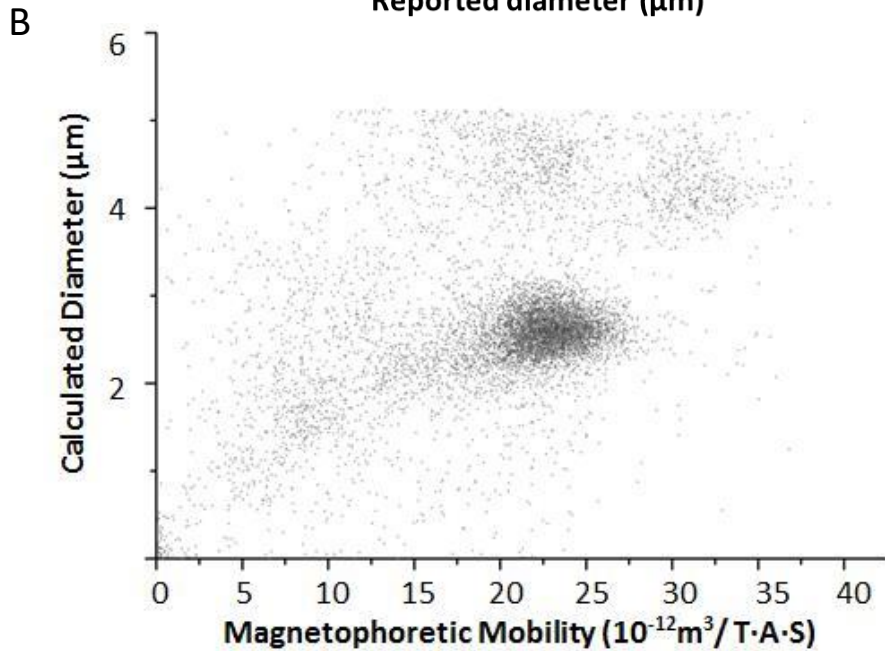
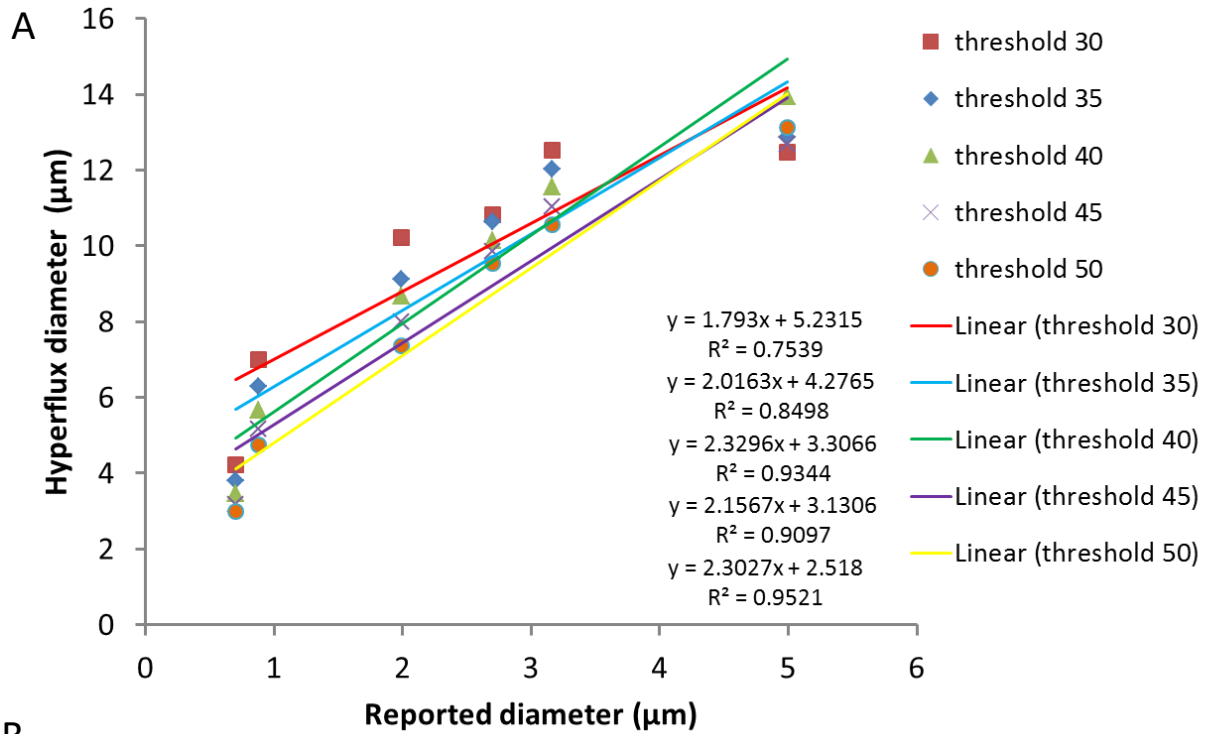


Figure 3.4 – (A) Particle size calibration plots showing average calculated (Hyperflux Velocimeter) diameter versus vendor reported diameter with intensity threshold values from 30 to 50. The fitted linear equations apply to the intensity threshold values shown to the right of each of the equations. (B) Two-parameter scatter plot of calculated diameter using equation (4) vs. measured magnetophoretic mobility for magnetic beads designated L1.

References

- Bhukal, S., S. Bansal and S. Singhal (2014). "Co_{0.6}Zn_{0.4}Cu_{0.2}Cd_xFe_{1.8-x}O₄ (0.2 ≤ x ≤ 0.8) magnetic ferrite nano-particle: Synthesis, characterization and photo-catalytic degradation of methyl orange." Journal of Molecular Structure **1059**: 150-158.
- Chalmers JJ, Z. Y., Nakamura M, Melnik K, Lasky L, Moore L, Zborowski M (1999). "An instrument to determine the magnetophoretic mobility of labeled, biological cells and paramagnetic particles." Journal of Magnetism and Magnetic Materials **194**: 231-241.
- Clarke, J. (1994). "Squids." Scientific American **271**(2): 46-53.
- Foner, S. (1959). "Versatile and Sensitive Vibrating-Sample Magnetometer." Review of Scientific Instruments **30**(7): 548-557.
- Fonnum G, J. C., Molteberg A, Morup S, Asknes E. (2005). "Characterisation of Dynabeads by magnetization measurements and Mössbauer spectroscopy." Journal of Magnetism and Magnetic Materials **293**(1): 41-47.
- Frantz SG (1936). "Magnetic separation method and means." US Patent No. 2,056,426A.
- Gherca D, P. A., Cornei N, Cojocariu A, Nica V, Caltun O (2012). "Synthesis, characterization and magnetic properties of MFe₂O₄ (M = Co, Mg, Mn, Ni) nanoparticles using ricin oil as capping agent." Journal of Magnetism and Magnetic Materials **324**(22): 3906-3911.
- Gill SJ, M. C., Downing M (1960). "Magnetic susceptibility of single small particles." Review of Scientific Instruments **31**(12): 1299-1303.
- Häfeli UO, C. R., Dailey JP (2002). "Characterization of magnetic particles and microspheres and their magnetophoretic mobility using a digital microscopy method." European Cells and Materials **3**(2): 24-27.
- Hurt, D., S. Li and A. Amann (2013). "Versatile SQUID Susceptometer With Multiple Measurement Modes." Ieee Transactions on Magnetics **49**(7): 3541-3544.

Kim, Y. H., B. J. Park, H. J. Choi and Y. Seo (2007). "Coating of magnetic particle with polystyrene and its magnetorheological characterization." Physica Status Solidi a-Applications and Materials Science **204**(12): 4178-4181.

Li, X. G. and S. Takahashi (2000). "Synthesis and magnetic properties of Fe-Co-Ni nanoparticles by hydrogen plasma-metal reaction." Journal of Magnetism and Magnetic Materials **214**(3): 195-203.

Li ZX, K. M., Kudo T, Kanetaka H (2012). "Sol-gel synthesis, characterization, and in vitro compatibility of iron nanoparticle-encapsulating silica microspheres for hyperthermia in cancer therapy." Journal of Materials Science **23**(10): 2461-2469.

Little CAE, P. J., Russek SE (2013). "Microfluidic platform for magnetic nanoparticle trapping and detection." IEEE Transactions on Magnetics **49**(7): 3402-3405.

McCloskey KE, C. J., Zborowski M (2000). "Magnetophoretic mobilities correlate to antibody binding capacity." Cytometry **40**(4): 307-315.

McCloskey KE, C. J., Zborowski M (2003). "Magnetic cell separation: Characterization of magnetophoretic mobility." Analytical chemistry **75**(24): 6868-6874.

McCloskey KE, C. K., Chalmers JJ, Margel S, Zborowski M (2001). "Mobility measurements of immunomagnetically labeled cells allow quantitation of secondary antibody binding amplification." Biotechnology and Bioengineering **75**(6): 642-655.

Molday RS, Y. S., Rembaum A (1977). "Applications of magnetic microspheres in labeling and separation of cells." Nature **268**: 437-438.

Moore LR, M. S., Williams PS, Chalmers JJ, Margel S, Zborowski M (2004). "Control of Magnetophoretic Mobility by Susceptibility-Modified Solutions as Evaluated by Cell Tracking Velocimetry and Continuous Magnetic Sorting. ." Analytical Chemistry **76**(14): 3899-3907.

Moore LR, S. L., Zborowski M, Nakamura M, Chalmers JJ, McCloskey K, Gura S, Burdygin I, Margel S (2000). "The use of magnetite-doped polymeric microspheres in calibrating cell tracking velocimetry." Journal of Biochemical and Biophysical Methods **44**(1-2): 115-130.

Popa M, V. H. L., Kakihana M (2003). "Particle morphology characterization and magnetic properties of LaMnO₃+d perovskites." Physica B **327**: 237-240.

Reddy S, M. L., Sun L, Zborowski M, Chalmers JJ (1996). "Determination of the magnetic susceptibility of labeled particles by video imaging." Chemical Engineering Science **51**(6): 947-956.

Sajja VSK, H. T., Gapsis H, Guernsey B, Taylor M, Kennedy DJ, Taylor MJ, Papas KK, Todd PW (2011). "Application of magnetic particle tracking velocimetry to quadrupole magnetic sorting of porcine pancreatic islets." Biotechnology and Bioengineering **108**(9): 2107-2117.

Suwa M, W. H. (2001). "Magnetophoretic velocimetry of manganese(II) in a single emulsion droplet at the femtomole level." Analytical chemistry **73**(21): 5214-5219.

Tarasov KA, I. V., Bokhonov BB, Gaponov YA, Tolochko BP, Yulikov MM, et al (2008). "Control of particle size via chemical composition: Structural and magnetic characterization of Ni-Co alloy nanoparticles encapsulated in lamellar mixed oxides." Microporous and Mesoporous Materials **107**(1-2): 202-211.

Watarai H, N. M. (2002). "Capillary magnetophoresis of human blood cells and their magnetophoretic trapping in a flow system." Journal of chromatography A **961**(1): 3-8.

Wilhelm C, G. F., Bacri JC (2002). "Magnetophoresis and ferromagnetic resonance of magnetically labeled cells." European Biophysics Journal **31**(2): 118-125.

Williams PS, Z. M., Chalmers JJ (1999). "Flow rate optimization for the quadrupole magnetic cell sorter." Analytical chemistry **71**(17): 3799-3807.

Xu J, M. K., Xue W, Winter JO, Zborowski M, Chalmers, JJ (2012). "Simultaneous, single particle, magnetization and size measurements of micron sized, magnetic particles." Journal of Magnetism and Magnetic Materials **324**(24): 4189-4199.

Zborowski M, C. J. (2008). "Magnetic Cell Separation. 1st ed. Amsterdam." Boston: Elsevier **xviii**: 454 p., 414 p. of plates p.

Zborowski M , C. J., Moore LR (1999). "Method for determining particle characteristics." US patent 5974901 A.

Zhang HD, M. L., Zborowski M, Williams PS, Margel S, Chalmers JJ (2005). "Establishment and implications of a characterization method for magnetic nanoparticle using cell tracking velocimetry and magnetic susceptibility modified solutions." Analyst **130**(4): 514-527.

Zhao, B., X. G. Wan, W. H. Song, Y. P. Sun and J. J. Du (2000). "Nano-MgO particle addition in silver-sheathed (Bi,Pb)(2)Sr2Ca2Cu3Ox tapes." Physica C **337**(1-4): 138-144.

Zhou C, B. E., Todd PW, Hanley TR (2014). "Magnetic Particles Characterization Magnetophoretic Mobility and Particle Size."

<http://www3.aiche.org/proceedings/Abstract.aspx?ConfID=Annual-2014&GroupID=1884&SessionID=27158&PaperID=386362>.

Chapter 4 - Application of Magnetic Carriers to Two Examples of Quantitative Cell Analysis

Abstract

The use of magnetophoretic mobility as a surrogate for fluorescence intensity in quantitative cell analysis was investigated. The objectives of quantitative fluorescence flow cytometry include establishing a level of labeling for the setting of parameters in fluorescence activated cell sorters (FACS) and the determination of levels of uptake of fluorescently labeled substrates by living cells. Likewise, the objectives of quantitative magnetic cytometry include establishing a level of labeling for the setting of parameters in flowing magnetic cell sorters and the determination of levels of uptake of magnetically labeled substrates by living cells. The magnetic counterpart to fluorescence intensity is *magnetophoretic mobility*, defined as the velocity imparted to a suspended cell per unit of magnetic ponderomotive force. A commercial velocimeter available for making this measurement was used to demonstrate both applications. Cultured *Gallus* lymphoma cells were immunolabeled with commercial magnetic beads and shown to have adequate magnetophoretic mobility to be separated by a novel flowing magnetic separator. Phagocytosis of starch nanoparticles having magnetic cores by cultured Chinese hamster ovary cells, a CHO line, was quantified on the basis of magnetophoretic mobility.

Keywords: magnetophoretic mobility; nanoparticle uptake; cell separation; cell Velocimeter

4.1 Introduction

When cells are to be separated by fluorescence activated cell sorters (FACS) it is customary to determine the distribution of fluorescence intensity in a fluorophore-labeled population of cells and to set flow parameters that select the desired cell population (Shapiro 2003). Likewise the measurement of magnetophoretic mobility has been used historically to set flow parameters in a quadrupole magnetic cell sorter (K. E. McCloskey 2003, David J. Kennedy 2007, L.M. Reece 2010, V. S. K. Sajja 2011) and a very early version of a magnetic flow sorter (RS Molday 1977, SPS Yen 1980). This approach does not appear to have been applied to a wider variety of magnetic cell sorters. The magnetophoretic mobility requirements for almost any magnetic separation can be determined by computational fluid dynamic analysis (Zhang 2005, V. S. K. Sajja 2011). In a separation with flow-rate requirements, for example, a minimum required mobility can be calculated. Tumor cells were chosen as an example of cells to be labeled for magnetic separation owing to interest in magnetically separating tumor cells from circulating blood (M Nakamura 2001, DF Hayea 2006).

Fluorescence flow cytometry is also used to determine levels of uptake of fluorescently labeled substrates by living cells. Fluorescent substrates are usually antibodies identifying cell surface markers and may or may not be internalized by receptor-mediated endocytosis and/or due to cell-membrane regeneration. The determination of levels of uptake of magnetically labeled substrates by living cells can be assessed by the measurement of magnetophoretic mobility (KE McCloskey 2000). There is considerable interest in the phagocytosis of nanomaterials (A. J. Cole 2011), and nanomaterials used in MRI have magnetic cores (A. Lindemann 2014). Micro- and nanoparticles are ingested by cells by mechanisms dependent on particle size and surface composition including targeting moieties such as antibody labels

(Rosales 2005) and can be ingested by a plethora of cell uptake mechanisms (phagocytosis, pinocytosis, receptor and non-receptor mediated endocytosis). Fluorescent labels modify the surface properties of most types of particles (with the possible exception of particles coated with fluorescent antibodies), whereas magnetic cores do not necessarily modify particle surface chemistry. One unintended consequence of labeling of blood and bone marrow with beads is the non-specific ingestion of labeling particles by phagocytic cells in the environment either by direct uptake or by released endocytotic vesicles (AK Andriola Silva 2012). In this study a commercial velocimeter was used to measure magnetophoretic mobility distributions in two example applications: flowing magnetic cell separation and nanoparticle phagocytosis. The adequacy of tumor cell labeling to meet the requirements of a particular flowing separator was established, and the kinetics of starch-particle phagocytosis was characterized.

4.2 Experimental

4.2.1 Cells

The tumor cell line used in all tests is CRL-211, DT40, obtained from ATCC, a chicken B-cell lymphoma cell line. These cells were maintained in suspension culture by twice-weekly passage in culture medium consisting of 69% (v/v) Dulbecco's modified eagle's medium (DMEM), 10% (v/v) tryptose phosphate broth solution, 5% (v/v) chicken serum, and 1% (v/v) ABAM (Antibiotic-Antimycotic mixture, all supplied by SIGMA™, St. Louis, MO, USA, plus 10% (v/v) fetal bovine serum (FBS) produced by ATCC. Cells were counted manually using hemacytometer and diluted in Dulbecco's phosphate-buffered saline (PBS) to about 5×10^4 cells/mL for reaction with bead reagent and evaluation in the Hyperflux™ velocimeter.

CHO Cells (Chinese Hamster Ovary cells, line CHO-K1) were maintained in monolayer culture in T-75 flasks at a passage ratio of about 1:8 every two days. For endocytosis experiments cells were trypsinized and counted for plating at about 1×10^6 cells per well in 6-

well plates and incubated at 37 °C for one day. They were then switched to complete medium containing various concentrations of magnetic nanoparticles for various times from 1 to 24 hours. They were then trypsinized and suspended in Hanks' Balanced Salts Solution for analysis using materials and protocols as previously described (Camille C. Hanot 2016).

4.2.2 Particles

Medium to high mobility particles were required for tumor cell labeling for the separator proposed for use. Beads were magnetically selected according to manufacturer's instructions before and after antibody labeling. The antibody used is Mouse monoclonal M-1 Anti-Chicken IgM mu chain (Biotin), Abcam[™] product id ab99719. Labeling of beads with this antibody was achieved before mixing particles with cells following manufacturers' instructions. Magnetic beads used in the testing are 2.8 µm diameter Dynabeads® Biotin Binder (Invitrogen/Dynal) with measured magnetophoretic mobility range of 1.3--2.0 x 10⁻¹¹ m³/TAS, the concentration of beads is 4 x 10⁸ beads/mL. Nonspecific particle internalization was avoided by reacting label with cells at 8 °C or 23 °C. Phagocytosis (deliberate internalization) studies utilized 50 and 100 nm superparamagnetic iron-oxide nanoparticles with magnetite core and starch matrix and coating (Chemicell FluidMAG-D, Berlin, Germany, Article Number: 4101-1 (1 ml)) (Camille C. Hanot 2016). The concentration of nanoparticles is expressed as µg/mL of iron.

4.2.3 Magnetophoretic mobility measurement

Magnetophoretic mobility is the ratio of the terminal velocity of the particle, v_m , to the gradient of the magnetic energy, $\frac{\nabla B_0^2}{2\mu_0}$, with B being the local magnetic flux density at the point of the particle or cell:

$$U_m = v_m / \frac{\sqrt{B_0^2}}{2\mu_0} \quad (1)$$

The units of U_m are $\text{m s}^{-1}/\text{T A m}^{-2}$ or $\text{m}^3\text{T}^{-1} \text{A}^{-1} \text{s}^{-1}$ (meters cubed per Tesla-Ampere-second), expressed in this work as m^3/TAs . The HyperfluxTM velocimeter (IKOTECH, LLC, New Albany IN, USA) measures v_m by image velocimetry and divides it by the denominator in equation (1), which is an adjustable constant in the velocimeter software. The HyperfluxTM image velocimeter, in brief, consists of a stopped-flow sample cell connected to sample, supply and waste fluid reservoirs and served by an automated pump, which transfers a fresh volume of sample into the optical cell after each “set” of a specified number of video frames has been recorded by a high-resolution camera. Raw video frames are maintained in a file that can then be analyzed using operator-selected parameters, especially including an intensity threshold setting that is adjusted interactively on the basis of simultaneous image and graphical display. For every recorded event at least 20 parameters are calculated and stored including velocity, magnetophoretic mobility, size, shape and image processing parameters. Additional details are given in (C. Zhou 2016), and a view of the HyperfluxTM velocimeter is given in Figure 4.1. An example of a data display screen is shown in Figure 4.2.

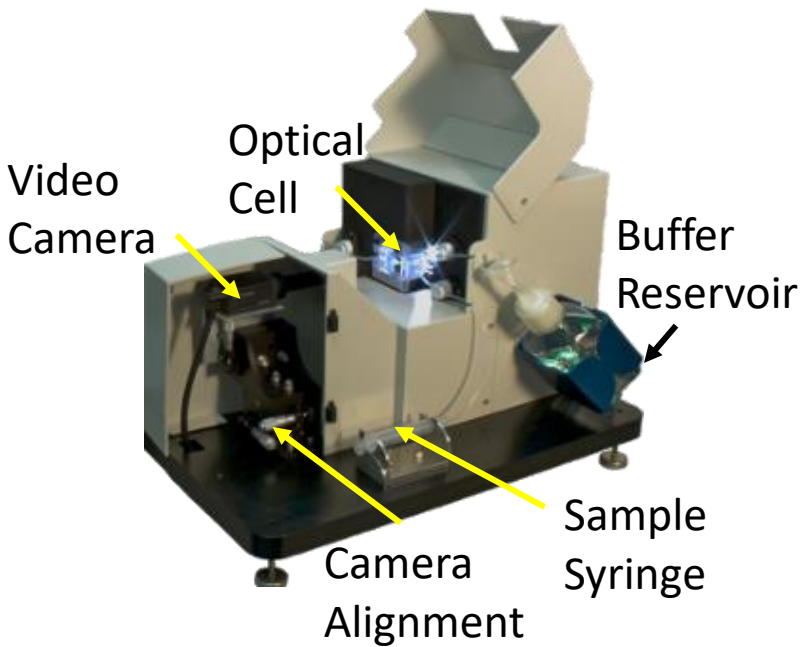


Figure 4.1. Labeled photograph of the Hyperflux™ magnetic velocimeter demonstrated in this study.

4.3 Results and Discussion

4.3.1 Magnetophoretic mobility of tumor cells labeled for flowing separation

Magnetophoretic mobility distributions were determined on the basis of several thousand analyzed cell tracks, and an example is given in Figure 4.2, a screen shot of the Hyperflux™ velocimeter output. For the flowing magnetic separator in question, a compact multistage capture device with a desired flow rate of 1.0 mL/min, the minimum required magnetophoretic mobility for 100% cell capture was calculated to be $1.3 \times 10^{-12} \text{ m}^3/\text{TAs}$. This is marked as a dashed vertical line in Figure 4.2. From the mobility data set it may be calculated that the separator in question would capture about 90% of the labeled cells.

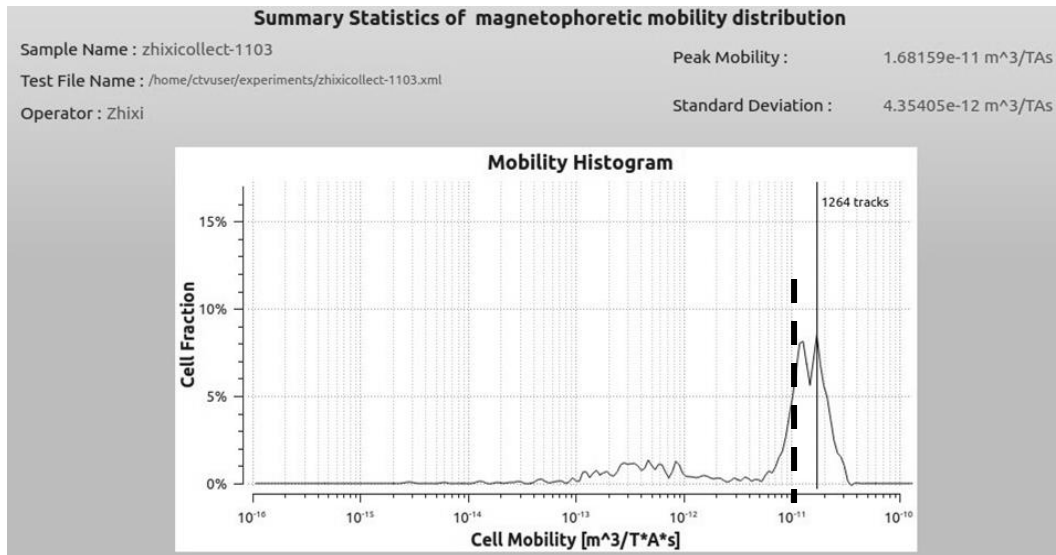


Figure 4.2. Screen shot of mobility histogram generated automatically by the HyperfluxTM velocimeter for magnetically labeled chicken lymphoma cells. Vertical solid line indicates peak mobility. Vertical dashed line indicates minimum magnetophoretic mobility ($1.3 \times 10^{-12} \text{ m}^3/\text{TAs}$) for 100% capture of cells in a modeled cell separator flowing at 1.0 mL/min.

4.3.2 Magnetophoretic mobility and nanoparticle phagocytosis

In order to use magnetophoretic mobility as a robust indicator of particle ingestion, instrument settings that provide reproducible results were established. The most significant operator-controlled setting is a threshold intensity value used by the HyperfluxTM image analysis package to accept or reject imaged objects for calculation of their average magnetophoretic mobilities. The range of intensity values is 0-255. In Figure 4.3 it is seen that mid-range values, 130 and 190 for example, provide essentially reproducible mobility distributions for magnetically labeled CHO cells.

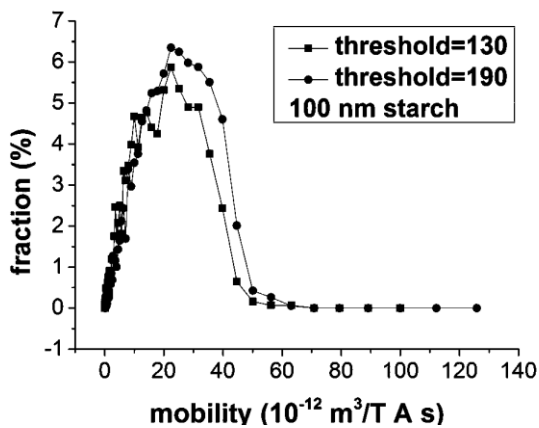
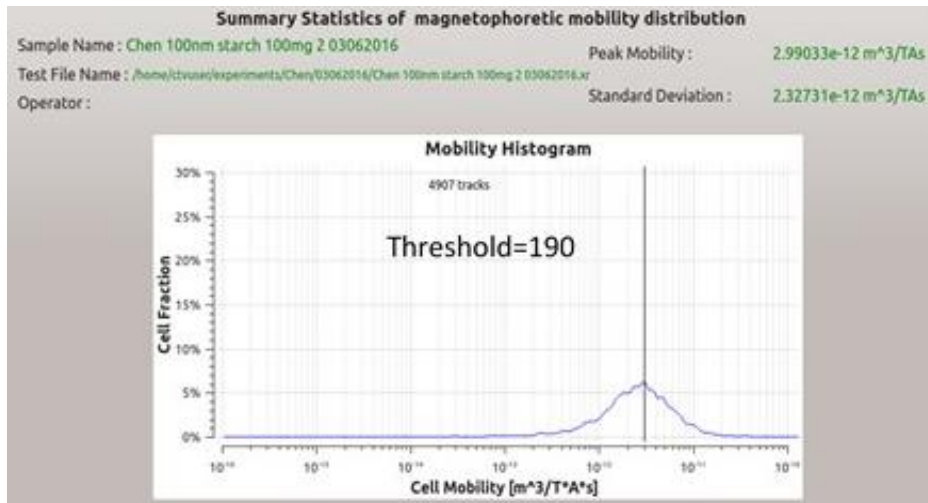


Figure 4.3. Magnetophoretic mobility distributions of CHO cells labeled for 24 h with 100 nm starch-coated Chemicell Fluid MAG-D magnetic particles measured using two intensity threshold settings of the HyperfluxTM velocimeter. Top: Screen shot of image analysis data at Threshold= 190. Lower: Mobility distributions at threshold = 130 and 190 on a linear mobility scale.

Cells were fed several concentrations (based on $\mu\text{g/mL Fe}$) of 100 nm starch-coated Chemicell Fluid MAG-D magnetic particles for 24 hours in kinetic studies, and mobility histograms were determined on the basis of velocities calculated from several thousand tracks. Histograms of cells' magnetophoretic mobilities are given in Figure 4.4. The clear trend to higher mobility is seen by visual comparison of the five histograms, and peak mobilities plotted

vs. particle concentration in Figure 4.5 follow a monotonic trend up to 200 $\mu\text{g/mL}$ Fe. These observations using magnetophoretic mobility as a measurement of phagocytosis are consistent with quantifications using other, traditional chemical and cytological methods (C.C. Hanot 2016).

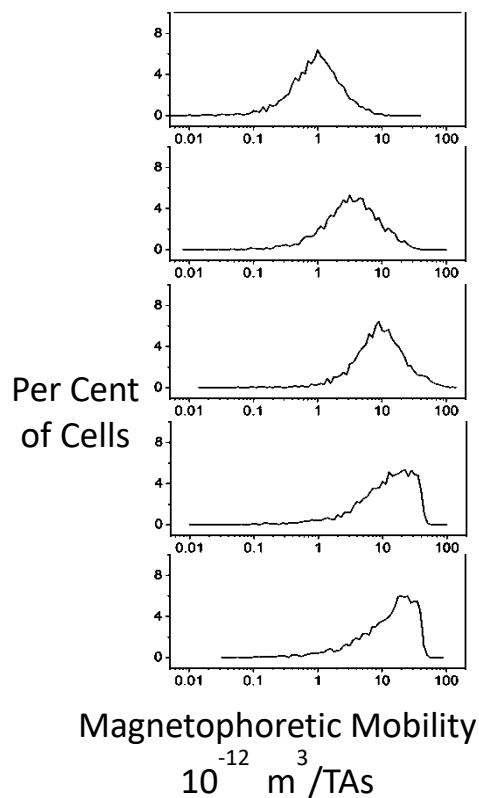


Figure 4.4. Magnetophoretic mobility distributions of CHO cells labeled for 24 hours with five concentrations of 100 nm starch-coated beads. There is a 15-fold increase in beads/cell over this concentration range. Unlabeled cells have no magnetophoretic mobility.

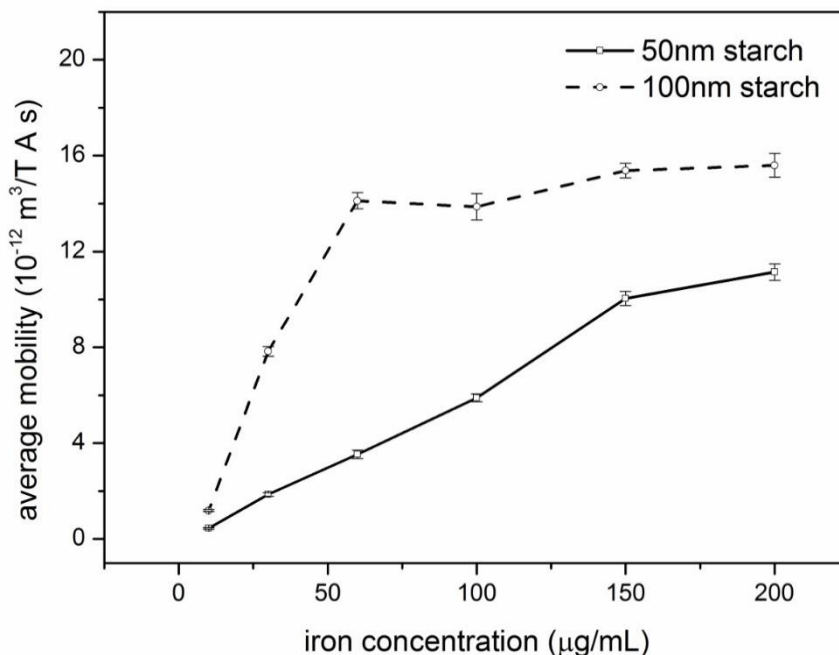


Figure 4.5. Average magnetophoretic mobility of CHO cells that ingested five concentrations of 50 nm or 100 nm starch-coated beads vs. concentration of beads as measured by iron content.

4.4. Conclusions

Labeled tumor cells have been characterized magnetically, and phagocytosis kinetics studies have been performed in a user laboratory by measuring magnetophoretic mobility distributions using the HyperfluxTM magnetic Velocimeter. The ability of labeled tumor cells to be captured by a flowing cell separator was predicted. The kinetics of starch nanoparticle phagocytosis was characterized quantitatively, providing data suitable for theoretical model fitting. Such measurements can now be achieved on a rapid, convenient and routine basis using commercial instrumentation.

Acknowledgments

We thank Dr. Eugene Boland for setting up tumor cell culture and particle labeling protocols. Research support was provided by graduate research assistantships from Auburn University, and Dr. Y.S. Choi has been partially funded by a Department of Defense FY2012 Prostate Cancer Research Program (PCRP) Idea Development Award (Award #W81XWH-13-1-0288) and by a grant from the Auburn University Research Initiative in Cancer (AURIC).
Statement of Interest: Dr. Hanley and Dr. Todd are former shareholders in IKOTECH, LLC.

References

- A. J. Cole, A. E. David, J. X. Wang, C. J. Galban, H. L. Hill, V. C. Yang, *Biomaterials* 32 (2011) 2183-2193.
- A. K. Andriola Silva, C. Wilhelm, J. Kolosnjaj Tabi, F. Gazeau, *Pharmaceutical Research* 29(2012) 1392-1403.
- A. Lindemann, K. Ludtke-Buzug, B. M. Fraderich, K. Grafe, R. Pries, B. Wollenberg, *Int. J. Nanomed.* 9 (2014) 5025-5040.
- C. C. Hanot, Y. S. Choi, T. B. Anani, D. Soundarrajan, A. E. David, *International Journal of Molecular Sciences* 17 (2016) 15-27.
- C. Rosales, *Molecular Mechanisms of Phagocytosis*. Chapter 2, Steven Greenberg, Springer, 2005.
- C. Zhou, E. D. Boland, P. W. Todd, T. R. Hanley, *Cytometry Part A*, 89A (2016) 589-593.
- D. J. Kennedy, P. Todd, S. Logan, M. Becker, K.K. Papas, and L. R. Moore, *J. Magnetism Mag. Materials* 311 (2007) 388-395.
- D. F. Hayes, et al., *Clin Cancer Res* 12 (2006) 4218-4224.
- H. M. Shapiro, *Practical Flow Cytometry*, 4th Edition, Wiley, New York, 2003.
- K. E. McKloskey, M. Zborowski, *Cytometry* 40 (2000) 307-315.

K. E. McCloskey, L. R. Moore, M. Hoyos, A. Rodrigues, J. J. Chalmers, M. Zborowski, Biotechnol. Progress 19 (2003) 899-907.

L.M. Reece, L. Sanders, D. Kennedy, B. Guernsey, P. Todd and J. F. Leary. Proc. of SPIE Vol. 7568 (2010) 75680P.

M. Nakamura, K. Decker, J. Chosy, K. Comella, K. Melnick, L. Moore, L. C. Lasky, M. Zborowski, J. J. Chalmers, Biotechnol. Progr.17 (2001) 1145-1155.

R. S. Molday, S. P. S. Yen, and A. Rembaum, Nature 268 (1977) 437-438.

S-P. S. Yen, A. Rembaum, R. S. Molday, Cell sorting apparatus, US PATENT 4,219,411 (1980).

V. S. K. Sajja, D. J. Kennedy, P. W. Todd, T. R. Hanley, Canad. J. Chem. Engin. 89 (2011) 1068-1075.

V. S. K. Sajja, T. R. Hanley, H. Gapsis, B. Guernsey, M. Taylor, D. J. Kennedy, M. J. Taylor, K. K. Papas and P. W. Todd. Biotechnol. Bioeng. 108 (2011) 2107-2117.

Y. Zhang, R. W. Barber, D. R. Emerson, Curr. Anal. Chem. 1(3) (2004) 345-354.

Chapter 5 - Magnetically Labeled Cell Characterization and Quantification

Abstract

Labeled cell characterization is of importance and in high demand in medical biology research and clinical application. A Hyperflux™ Velocimeter is utilized to directly measure the magnetophoretic mobility, size and other morphology parameters of labeled cells. The magnetophoretic mobility is a key parameter to describe the cell motion behavior in a defined magnetic field and is used in this study as a quantitative indicator of number of paramagnetic particles ingested per cell. The CHO cell capture of approximately 50 and 100 nm diameter iron oxide particles coated with starch, aminated starch and PEG (2k, 5k and 20k Daltons) was studied to reveal the chemistry of phagocytosis. By quantitatively characterizing and determining the cell uptake kinetics as a function of particle size and surface chemistry, we have been able to reveal the dependencies of phagocytosis on particle concentration, incubation time, particle composition, particle size and particle toxicity. We found that surface aminated particles, which are highly positively charged, are more effectively taken up by CHO cells than starch-coated particles. The PEG content in coating, though bio-friendly, will prevent the penetration of MNPs into CHO cells. In addition, the velocimeter analysis provides a better understanding of cell labeling and serves as a tool to optimize selecting of MNPs type and incubation conditions. Fluorescence-activated cell sorting (FACS) assays and ferrozine assays were done as comparison analysis methods to magnetophoresis to measure the labeled cell and uptake ratio. The strength and weakness of each method are examined and discussed.

5.1 - Introduction

When magnetic particles are introduced into cell labeling, many methods could not thoroughly characterize the properties of labeled cells in a suspension system, such as vibration sample magnetometer and SQUID. Flow cytometry might do this task as it could monitor each

cell entering the instrument. However, particles without fluorescence properties could not be detected in this analysis. Modification of particles by fluorescence dye might cause the surface chemistry of the particle to change after the modification, limiting FACS analysis applications to measuring particle uptake by cells. A magnetophoretic velocimeter can provide direct, undisturbed analysis. The instrument, based on cell-by-cell analysis, describes the behavior of each labeled cell in a defined magnetic field and quantitatively reveals magnetophoretic mobility distribution of the cells in samples.

In our work, a magnetophoretic velocimeter was employed to measure the magnetic properties of Chinese hamster ovary (CHO) cells labeled by ten types of unmodified/modified particles (50 and 100 nm diameter paramagnetic-core beads coated with starch, primary amine groups or 2k/5k/20k Da polyethylene glycol (PEG)). Cell uptake of each type of particle could be revealed after data analysis. The measured results are also compared with that gained from flow cytometry and Ferrozine assay.

5.2 - Theory

In an isodynamic magnetic field, assuming a micro-sized magnetic particle is in a viscous creeping diamagnetic fluid medium, the magnetic force acting on the particle can be expressed as

$$F_m = \Delta\chi V \nabla \left(\frac{B_0^2}{2\mu_0} \right) \quad (5-1)$$

where $\Delta\chi = \chi_p - \chi_f$, the difference between the magnetic susceptibility of the particle and that of the fluid; V is the volume of the particle; B_0 and μ_0 are magnetic induction and magnetic permeability of free space, respectively. $\Delta\chi = \chi_p$ in most practical cases, but deliberate exceptions exist.

At the same time, the drag force on the particle in the direction opposite to that of the magnetic force, according to Stokes' law, should be

$$F_d = 6\pi\eta Rv \quad (5-2)$$

where η is the viscosity of fluid, R is the radius of the particle, and v is the terminal velocity of the particle.

When the particle reaches a terminal velocity in the system, the drag force will balance the magnetic force, $\mathbf{F}_m = \mathbf{F}_d$. One obtains the terminal velocity of the particle.

$$v = \frac{\Delta\chi V}{6\pi\eta R} \nabla \left(\frac{B_0^2}{2\mu_0} \right) \quad (5-3)$$

The left term, $\frac{\Delta\chi V}{6\pi\eta R}$, describes the properties of the particle and fluid medium and is defined as magnetophoretic mobility, U_m . Rearranging the above expression we find that magnetophoretic mobility is the ratio of the terminal velocity of the particle, v_m , to the gradient of the magnetic energy, $\frac{\nabla B_0^2}{2\mu_0}$,

$$U_m = \frac{v_m}{\frac{\nabla B_0^2}{2\mu_0}} \quad (5-4)$$

The units of U_m are $\text{m s}^{-1}/\text{T A m}^{-2}$ or $\text{m}^3\text{T}^{-1} \text{A}^{-1} \text{s}^{-1}$ (meters cubed per Tesla-ampere-second), expressed in this work as $\text{m}^3/\text{T}\cdot\text{A}\cdot\text{s}$.

5.3 - Experimental

5.3.1 - SPIONs Surface Modifications

50 and 100 nm superparamagnetic iron-oxide nanoparticles (SPIONs) with magnetite core and starch matrix and coating (Chemicell FluidMAG-D, Chemicell, Berlin, Germany) are suspended, then aminated and then PEGylated. As shown in Figure 5.1, amino groups are introduced to the particles' coating during amination treatment. Some of the amino groups are replaced by PEG groups during the PEGylation process (Dissolve 6 mg m-PEG_NES in 120 μL

3×PBS and 120 μL DMSO; add 1mL concentrated aminated NP; Incubate at room temperature for 4hrs with shaking; Add 2mL water and magnetically separate 4 times; retain the concentrated product at the last step of purification).

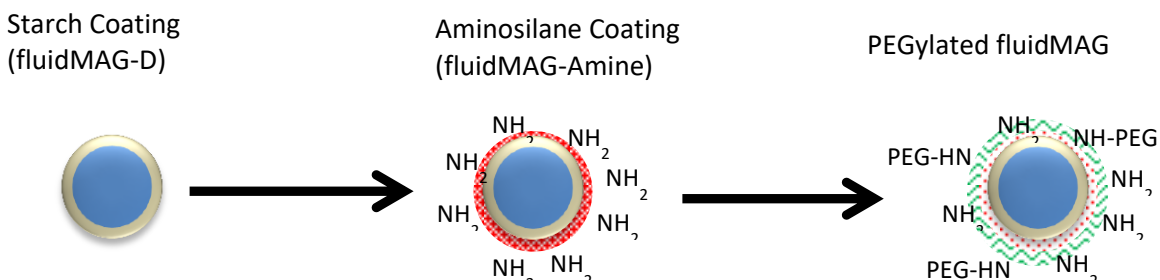


Figure 5.1 - Approximately 50 and 100 nm superparamagnetic iron-oxide nanoparticles with various coatings after surface treatment. Starch coating supplied by Chemicell (fluidMAG-D), aminated-starch, 2k-PEG, 5k-PEG, 20k-PEG

5.3.2 - Stained SPIONs

The unmodified/modified SPIONs could not be detected by FACS as they do not produce a fluorescence signal. Thus, a fluorescent dye was chosen to further stain the particles. Alexa Fluor® 488 dye (AF488 NHS) was employed in our work. The Alexa Fluor® 488 dye (AF488 NHS) was dissolved in DMSO at 10 mg/mL, then stored under $-5\text{ }^\circ\text{C}$ and protected from light. 10 μL dye solution (0.1 mg) was slowly added into a particle suspension (100 nm aminated or 2k, 5k, 20k PEGylated fluidMAG) containing 1 mg iron and then incubated for reaction for 1 hour at room temperature with continuous stirring. Particles were washed using DI water and separated 4 times by magnetic separator, then stored below $5\text{ }^\circ\text{C}$ and protected from light.

5.3.3 – CHO-K1 cell subculture (every 48 hours)

The following procedure was used. Discard the cell culture medium (89% (v/v) F-K12 + 10% (v/v) FBS + 1% (v/v) Antibiotics) from 75mL flask. Rinse the cell monolayer with 10 mL HBSS and remove. Add 1 mL TripLE (ThermoFisher Scientific) and incubate 5 minutes at $37\text{ }^\circ\text{C}$ to detach the cells. Add 10 mL HBSS and transfer the cell suspension from flask to 50 mL tube.

Centrifuge at 1500 rpm for 5 minutes. Discard the supernatant. Add 5 ml new culture medium. Pipette to resuspend the cells. Collect some cell solution to a new flask with 14 mL culture medium (subcultivation ratio is about 1:8). Incubate the cells at 37 °C.

5.3.4 - Labeling of cells

Seed about 1×10^6 cells into each well of a six-well plate; add the culture medium to 2 mL; incubate at 37 °C for one day; change culture media and add unstained/stained SPIONs to cell solution to link the magnetic particles to cells (varying iron concentration from 10 µg/mL to 200 µg/mL). The final iron concentration should be between 5 to 200 µg/mL. Incubate at 37 °C for 1 to 24 hours.

5.3.5 - Preparing test samples for Hyperflux analysis

Discard the culture media. Wash the cell monolayer using 2 mL HBSS and incubate three minutes (repeat five times). Add 0.5 ml TripLE (ThermoFisher Scientific) and incubate 5 to 10 minutes. Collect cell suspension into a 50 mL tube. Centrifuge at 1500 rpm for 5 minutes. Discard supernatant and resuspend the cell with 4 mL PBS. Collect the cell suspension (CS) for later testing.

5.3.6 - Further treatment for flow cytometry test

CS needs to be resuspended at a concentration of 1 to 10 million cells per ml in the plain PBS in a tube. Add 1 µL of Ghost Dye™ Red 780 (Tonbo Biosciences, Tucson, AZ) for each 1 ml of cell suspension. Make sure your pipets are giving you an accurate volume (just 1 µL per mL of cell suspension). Incubate in the tube for 30 minutes on ice protected from light (wrap the tube in aluminum foil). Wash the cells at least twice with staining buffer, centrifuge the cells, discard supernatant and resuspend in staining buffer, 98% PBS + 2% FBS). The FBS (VWR Life Science Seradigm, Radnor, PA) is used as a protein source in the PBS to remove the unreacted dye.

5.3.7 - Flow Cytometry Test

An Accuri C6 Flow cytometer analyzer (BD Biosciences, San Jose, CA) with 488 nm laser was utilized to detect and quantify the fluorescent signal of the label cells. The results were used to confirm the velocimetry analysis on cell uptake.

5.3.8 - Ferrozine assay

5.3.8.1 *The bicinchoninic acid assay (BCA assay) to generate standard curve for CHO Cells*

Start with cells suspended in 1X PBS (cell count number approximately 6.5×10^6 cells/mL). Place different amounts of cells in 18 wells of a new 24-well plate according to Table 5-1, making three samples for each cell number.

Table 5.1 – Concentrations for BCA Analysis

Tube	μL cell suspension (650×10^4 cells/mL)	μL 1X PBS
A	100	0
B	70	30
C	45	55
D	25	75
E	15	85
F	0	100

Add 200 μ L 50 mM NaOH to all wells and incubate for 2 hours at 37 $^{\circ}$ C. Transfer three 25 μ L samples into 96 well plate for BCA assay. Add 200 μ L of the WR reagent (ThermoFisher Scientific) (BCA reagent A:B = 50:1) to each well and mix plate thoroughly on a plate shaker for 30 seconds. Cover plate and incubate at 60 $^{\circ}$ C for 30 minutes. Cool plate to room temperature for five minutes at room temperature. Mix in plate reader for 20 seconds at medium setting and measure absorbance at 562 nm.

5.3.8.2 - Cell uptake studies

Cells were seeded in 24 well plates at 2.6×10^4 cells/mL) and allowed to grow in 2 mL complete medium for 48 hours. The following procedure was then implemented. Prepare SPIONs (0.1 mg Fe/mL) in culture medium (Ham's F-12K culture media using SPIONs with different sizes and coatings as designated in Table 5-2.

Table 5.2 – SPION and Coatings for Cell Uptake Testing

Tube	100 μ g Fe/mL SPIONs
1	100 nm starch
2	100 nm aminated
3	100 nm 2k PEGylated
4	100 nm 5k PEGylated
5	100 nm 20k PEGylated
6	50 nm starch
7	50 nm aminated
8	50 nm 2k PEGylated
9	50 nm 5k PEGylated
10	50 nm 20k PEGylated

Wash wells once with sterilized 1X PBS. Add 1 mL of tubes (contents listed on above table) 3 times (n=3). Incubate for 24 hours at 37 °C, then wash with 1X PBS 5 times.

5.3.8.3 - Ferrozine and BCA assay to quantify iron uptake and cell number

After completely washing the wells twice with 1X PBS, and ensuring no solution is left, add 100 µL 1X PBS to all the wells. Add 200 µL 50 mM NaOH to all wells and incubate for 2 hours at 37°C. Transfer two 25 µL samples for BCA assay (in 96 well plate) and one 200 µL sample for ferrozine assay (in 24 well plate). For the ferrozine assay, add 200 µL iron-releasing reagent consisting of equal volumes of 4.5% KMnO₄ and 1.4 M HCl. Incubate for 2 hours at 60 C. Cool for 10 minutes. Mix. Add 50 µL ferrozine, then mix. For ferrozine reagent, combine ferrozine (510.48 g/mol * 3 mL * 6.5 mmol/L * 1mol/1000mmol * 1 L/1000mL * 1000 mg/1g = 9.95 mg), neocuproine (5.12 mg), ammonium acetate (578 mg) and ascorbic acid (528 mg). Mix all components with 3 mL water. Incubate for 30 minutes at room temperature. Transfer 250 µL to 96 well plate. Measure absorbance at 550 nm. For the BCA analysis, in addition to cell samples, include a control (8.34 µL 1X PBS and 16.66 µL 50 mM NaOH). Add 200 µL of the WR reagent (50:1, reagent A:B) to each well and mix plate thoroughly on a plate shaker for 30 seconds. Cover plate and incubate at 60 C for 30 minutes. Cool plate at room temperature for 5 minutes. Mix in plate reader for 20 seconds at medium setting, and measure absorbance at 562 nm.

5.4 - Results and Discussion

5.4.1 - Chemistry of Phagocytosis

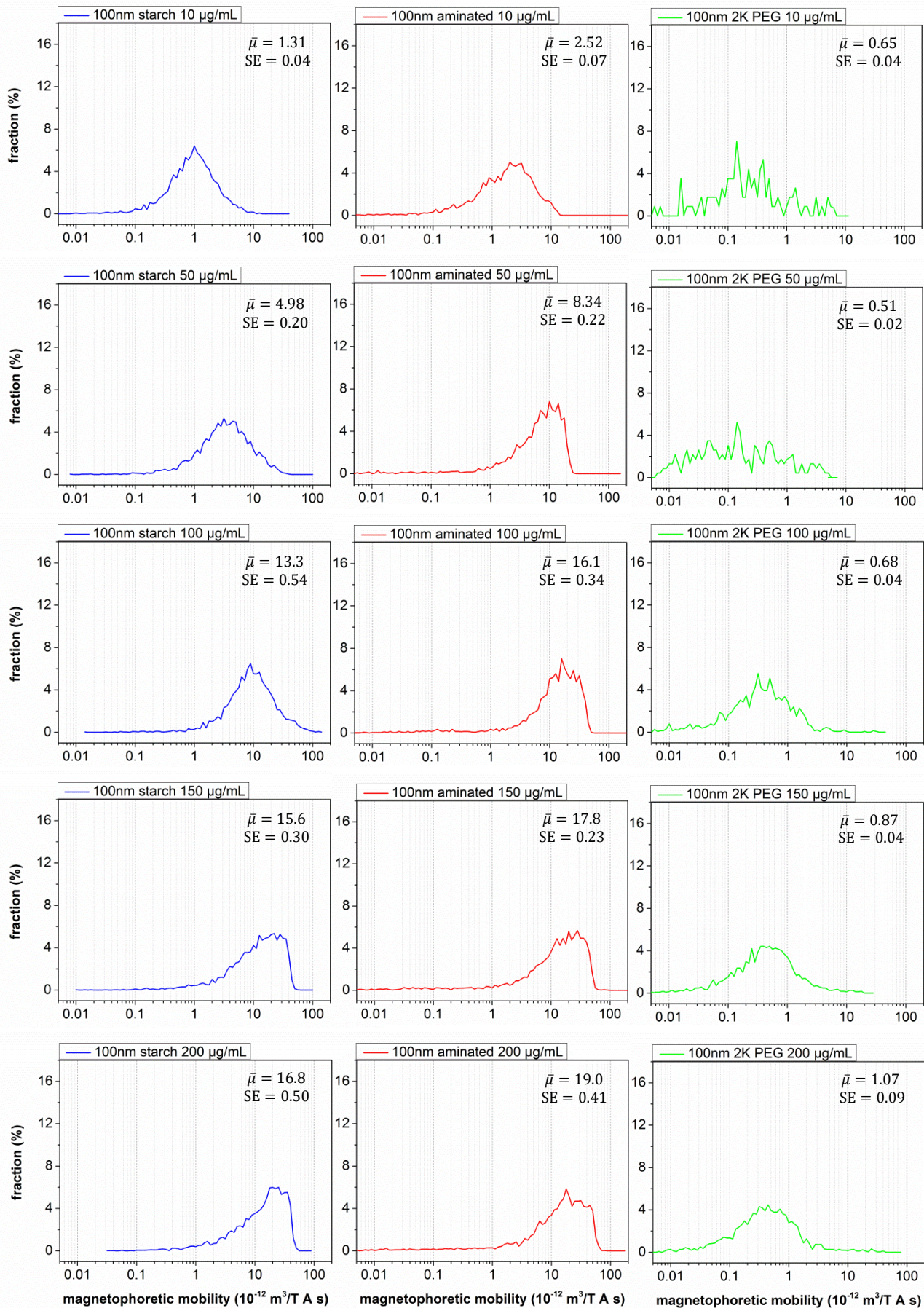
Chinese hamster ovary (CHO) cells were chosen to investigate the phagocytosis mechanisms. The cells were cultured with 10 types of unmodified or modified particles: 50 and 100 nm diameter paramagnetic-core beads coated with starch, starch aminated by primary amine groups or 2k/5k/20k Da polyethylene glycol (PEG) attached to the primary amine groups. It was

found that the cell labeling degree is highly dependent on particle type, incubation concentration and time. Thus, two series of experiments were designed to study the nanoparticle uptake by measuring the magnetophoretic mobility of the cells as a function of three variables: particle size/surface composition, incubation time (for rate data) and incubation concentration (for equilibrium data).

Figure 5.2 summarizes raw data sets showing the impact of incubation conditions on cell uptake of the nanoparticles. Quantification is achieved using the velocimeter to measure the magnetophoretic mobility distribution by determining the velocity of magnetically labeled cells in a defined magnetic field. From Figures 5.2a and 5.2b, we find that the amination treatment, which produces a large amount of primary amino groups on the particle surface, could highly increase the uptake rates. On the other hand, the PEGylating process, which will replace the ammonia group by PEG group, reduces the degree of labeling. There is higher content of 2k and 5k PEG in the coating than in the case of 20k PEG, (the coating content of 2k, 5k and 20k PEG is 72.5%, 29.6% and 1.5%) which results in lower cell uptake rate of particles in the former two types of particles. The uptake rate increases dramatically when the particle concentration increases from 10 to 100 $\mu\text{g/mL}$, but the increasing trend is less above 150 $\mu\text{g/mL}$ which suggests reaching a saturation limit.

The incubation time study shown in Figures 5.2 c and d further reveals the uptake mode of particles. The 20k PEG SPIONs have a much lower PEG content than 2k and 5k PEG SPIONs. The uptake pattern is similar to aminated SPIONs. The uptake of aminated and 20k PEG MNPs begins within 4 hours. The particles with 2k and 5k PEG in coating produce a low cell uptake rate, but the uptake trend lies between those of the aminated SPIONs and unmodified starch SPIONs. The most interesting finding is that there is not much uptake of 100 nm starch

MNPs within 8 hours, even when increasing the iron concentration from 100 $\mu\text{g/ml}$ to 200 $\mu\text{g/ml}$. The labeling process appears during the 8 to 24 hour stage. By contrast, almost 90% of intercellular process finishes within 4 hours for the aminated and PEGylated SPIONs.



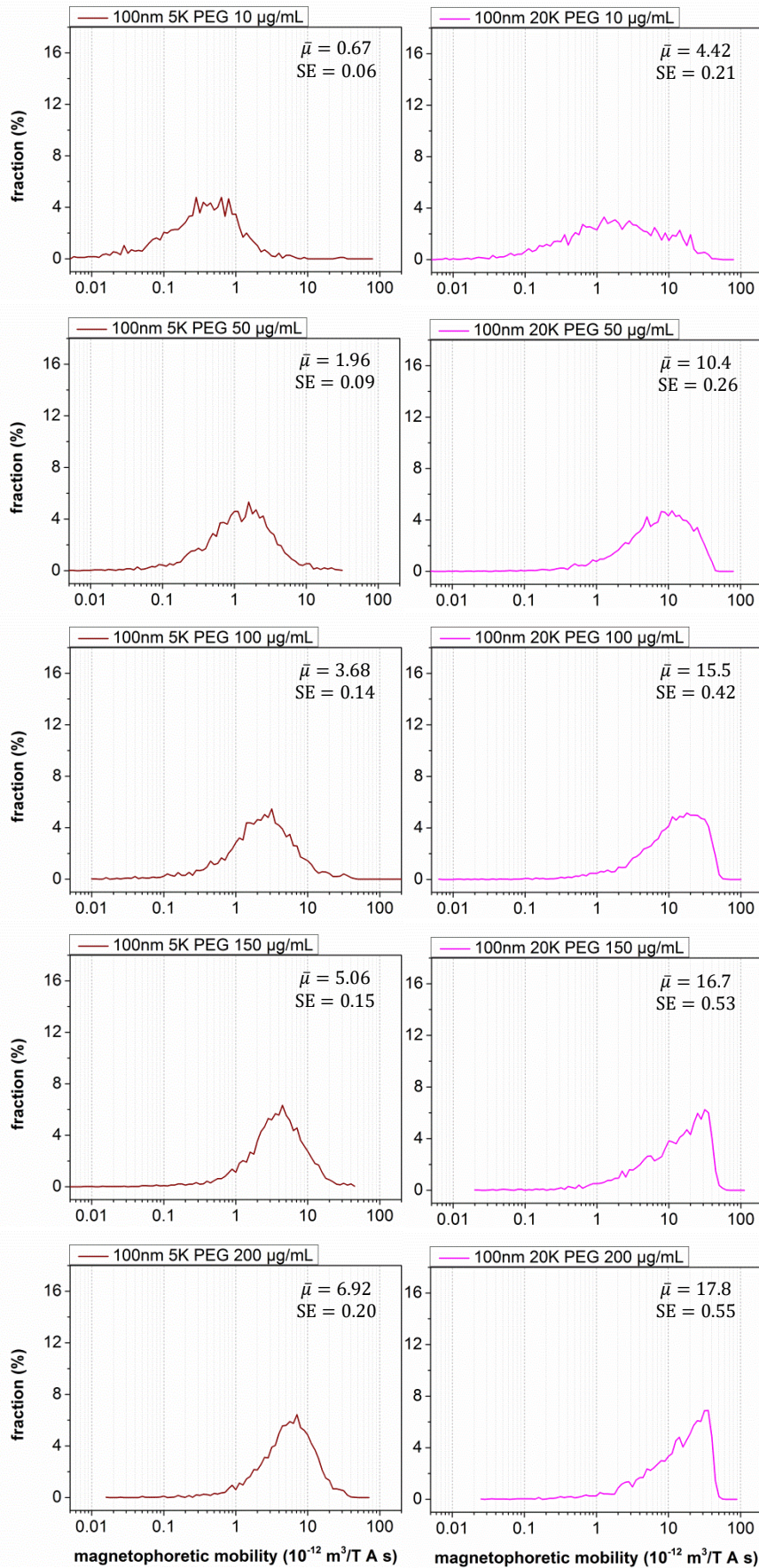
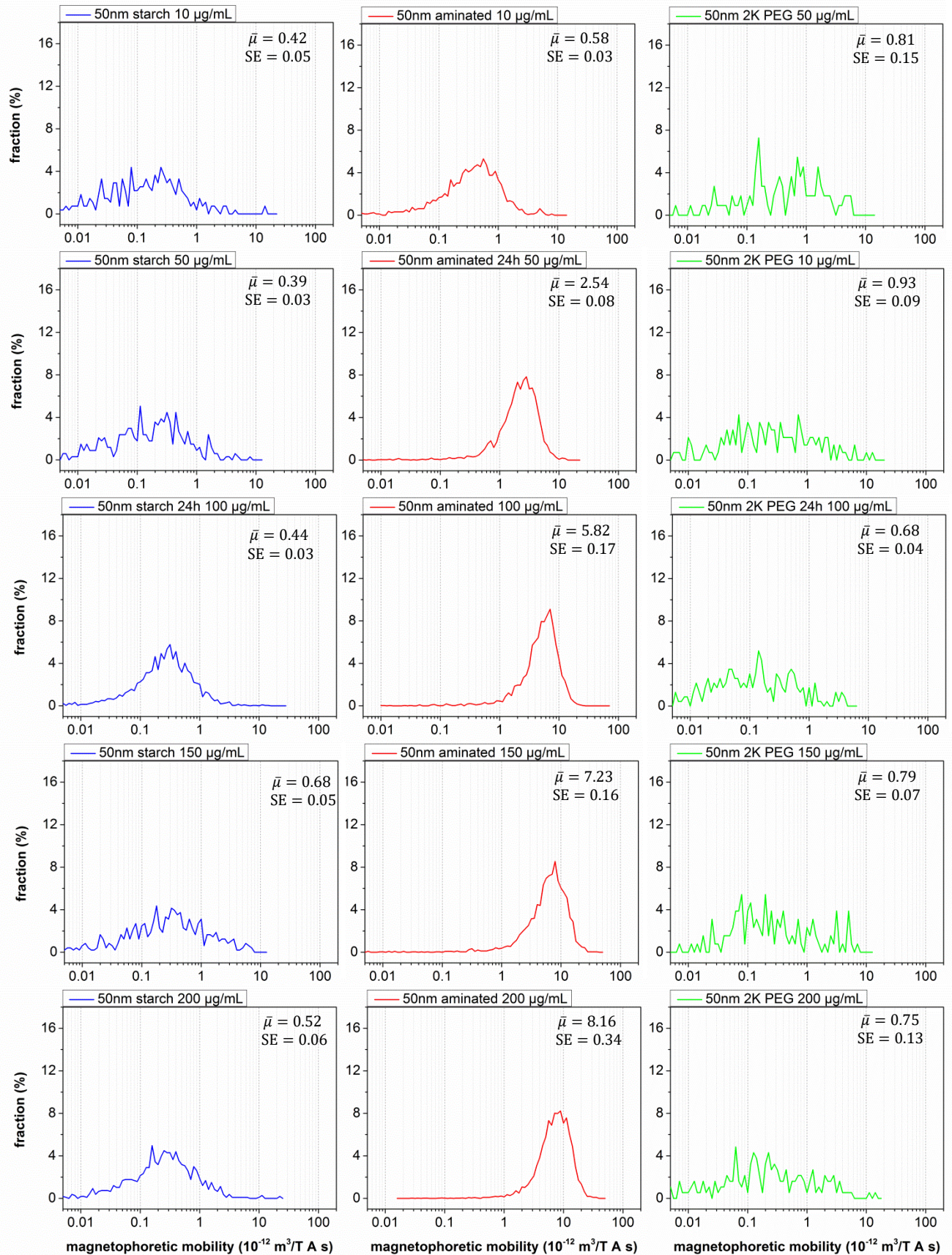


Figure 5.2a.
Magnetophoretic
mobility
distributions of CHO
cells labeled by
100nm SPIONs coated
with starch, primary
amine groups or
2k/5k/20k Da
polyethylene glycol
(PEG), incubation
time = 24h,
incubation
concentration= 10,
50, 100, 150,
200µg/mL of iron.



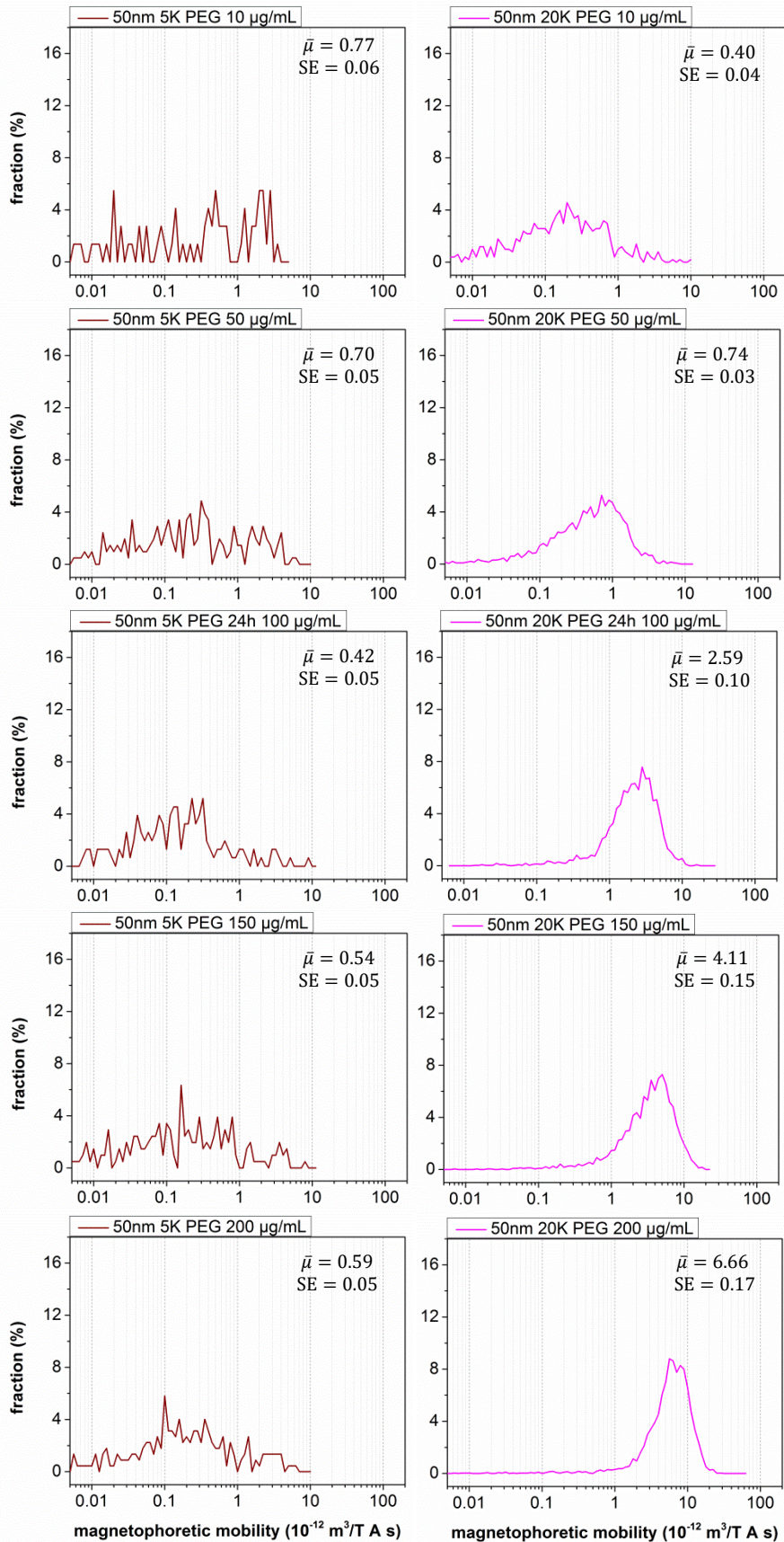
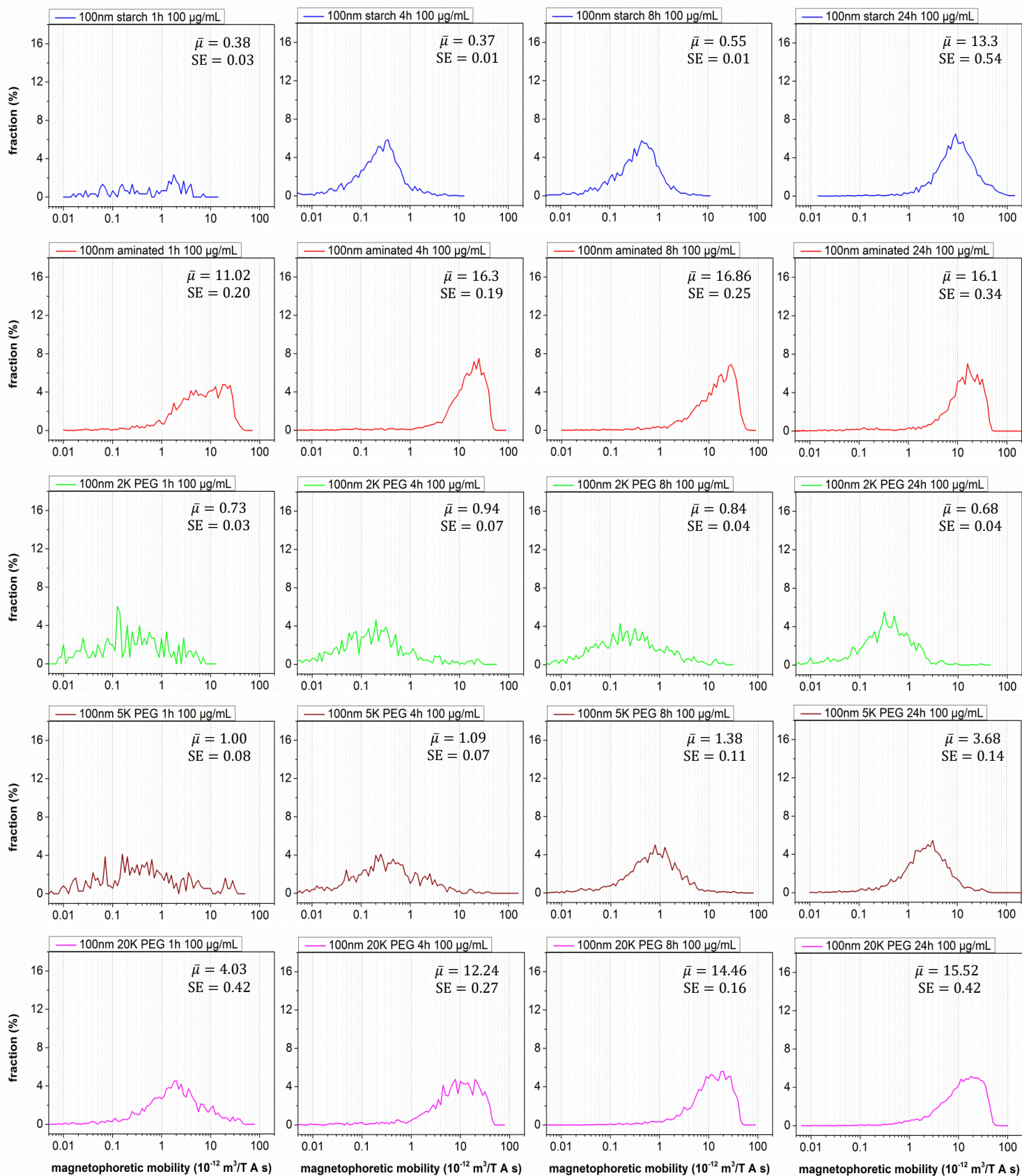


Figure 5.2b.
Magnetophoretic mobility distribution of CHO cells labeled by 50nm SPIONs coated with starch, primary amine groups or 2k/5k/20k Da poly(ethylene glycol) (PEG). Incubation time = 24h, incubation concentration= 10, 50, 100, 150, 200µg/mL.
 *SE, standard error= $SD/(\text{track number})^{0.5}$



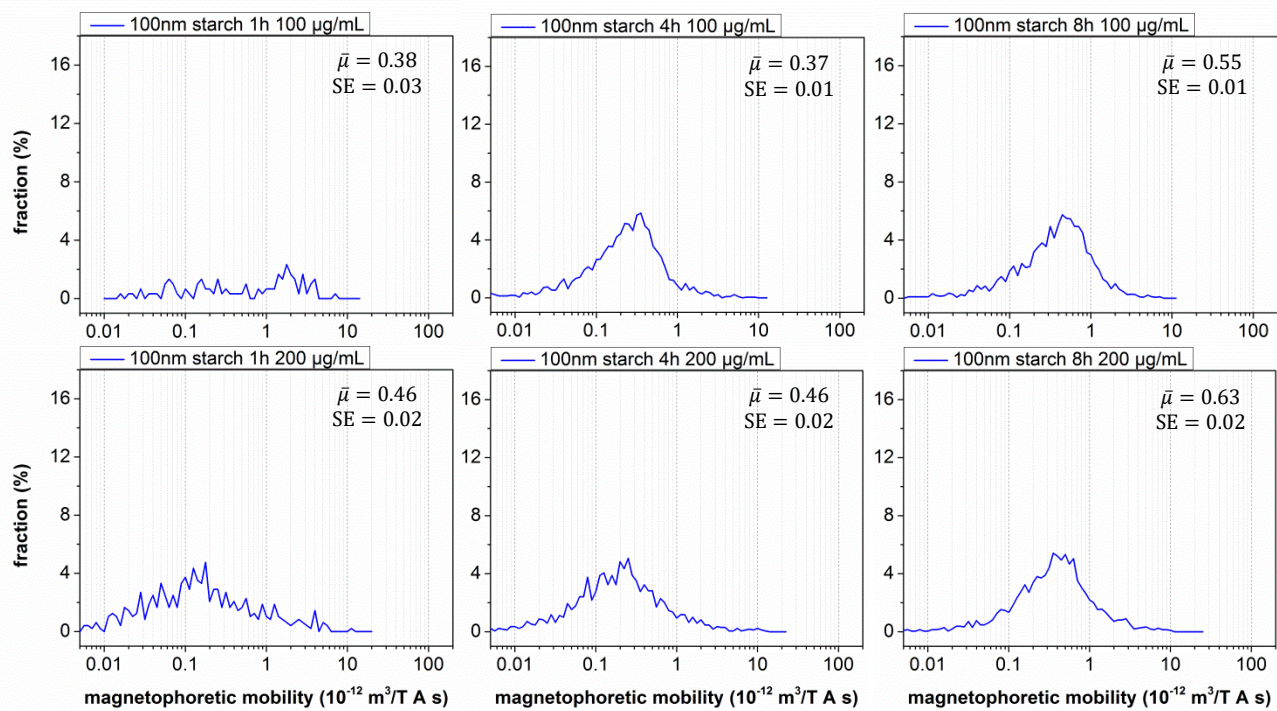


Figure 5.2c. Magnetophoretic mobility distributions of CHO cells labeled by 100nm SPIONs coated with starch, primary amine groups or 2k/5k/20k Da polyethylene glycol (PEG). incubation time = 1, 4, 8, 24 h, incubation concentration= 100, 200 $\mu\text{g/mL}$ iron.

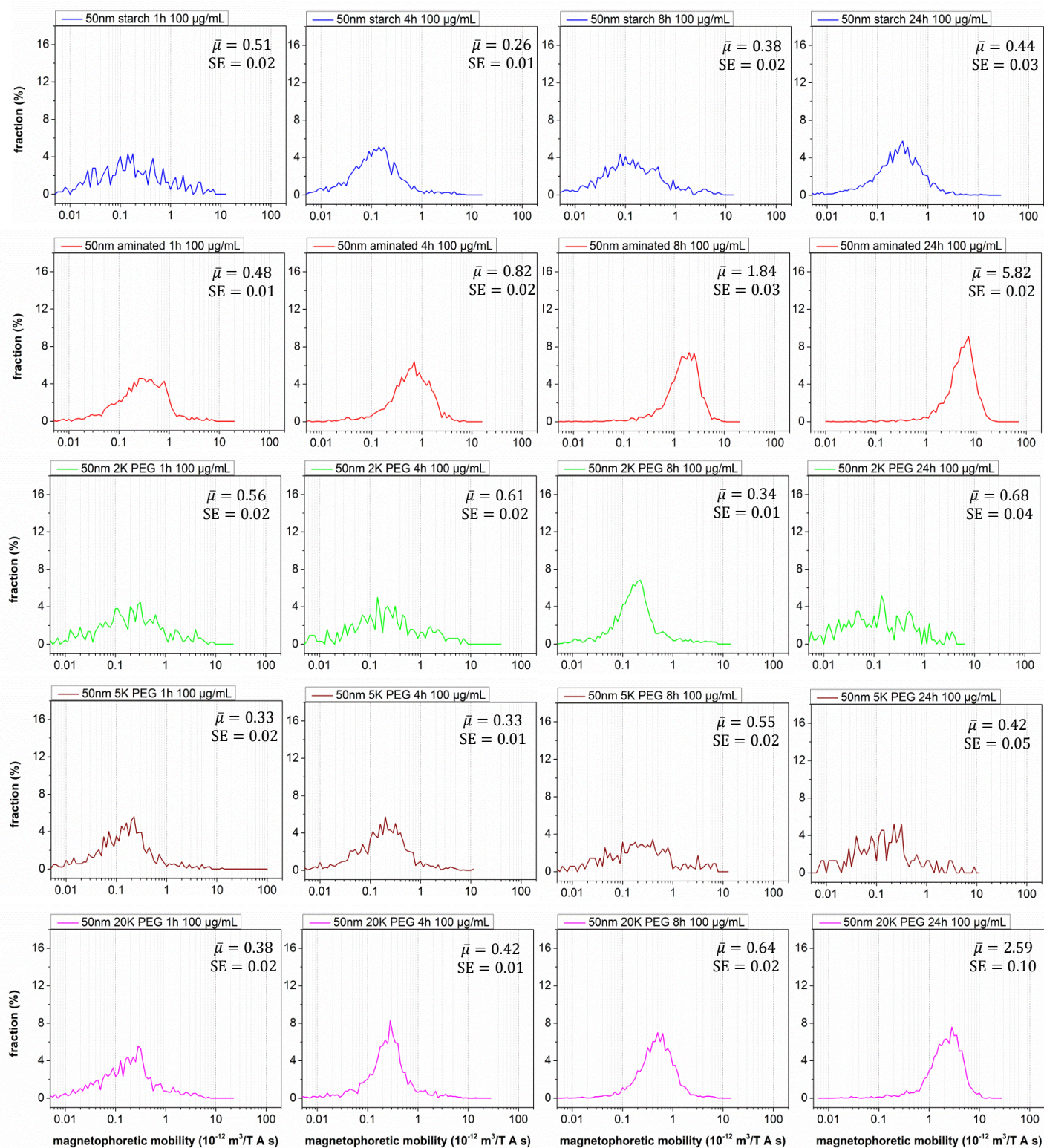


Figure 5.2d. Magnetophoretic mobility distributions of CHO cells labeled by 50 nm SPIONs coated with starch, primary amine groups or 2k/5k/20k Da polyethylene glycol (PEG). Incubation time = 1, 4, 8, 24 hours, incubation concentration = 100, 200 $\mu\text{g/mL}$.

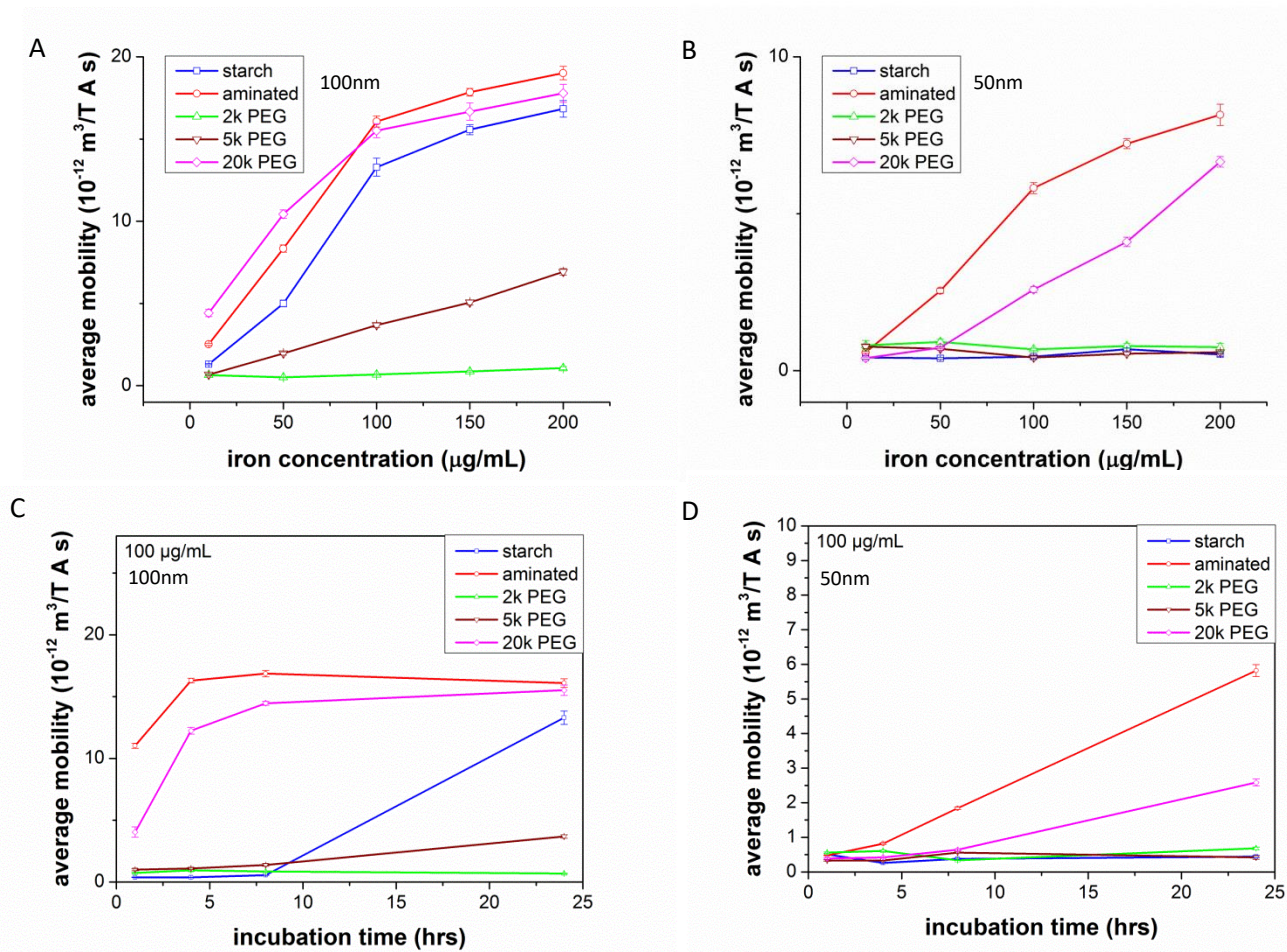


Figure 5.3. Average mobility after 24 h vs iron concentration. A: 100nm, B: 50nm diameter Average mobility vs. incubation time at 100 $\mu\text{g/mL}$ C: 100nm, D: 50nm.

Figure 5.3 summarizes the study of iron concentration and time dependence of SPION uptake. Micro- and nanoparticles are ingested by cells by mechanisms dependent on particle size and surface composition including targeting moieties such as antibody labels and can be ingested by a plethora of cell uptake mechanisms (phagocytosis, pinocytosis, receptor and non-receptor mediated endocytosis). The cell uptake could be considered as a two-step process: binding of AMNP on reactive sites on cell surface (Langmuir adsorption) and cell internalization of the reactive sites by an endocytosis pathway (saturation mechanism) (Wilhelm, Gazeau et al. 2002, Wilhelm, Billotey et al. 2003). The cell surface in monolayer culture contains large domains of

anionic glycan sites ((King 1981, Erik I. Finkelstein 2007) which could attract the cationized particles more than native and anionized adsorbate. That is why aminated MNPs, which are highly positively charged, are more likely to be adsorbed and further “swallowed” by the CHO cells. In other word, the electrostatic interaction between positively charged particles and the cell membrane could enhance cell uptake.

The PEG coating at the modified surfaces will effectively depress both the plasma protein adsorption and cell attachment (Zalipsky and Harris 1997, Zhang, Desai et al. 1998). The hydrophilic character of PEG would lead to a larger contact angle, which makes PEG film stable in water. On the other hand, the PEG Chain is unlikely to absorb cell adhesive proteins, due to the lack of ionic interaction between them and due to the chains’ steric hindrance effect. In this way, the cells are less able to swallow particles with a high content of PEG on their coating.

5.4.2 - Triplicate Experiments

Triplicate experiments were done to test the reproducibility and accuracy of the test method using magnetophoresis. Table 5.3 and Figure 5.4 suggest a good agreement among parallel tests.

Table 5.3 - Statistical calculations for results of triplicate experiments.

100 nm sample	average mobility ($10^{-12} \text{m}^3/\text{T A s}$)	SD* ($10^{-12} \text{m}^3/\text{T A s}$)	SD/mean (%)	50 nm sample	average mobility ($10^{-12} \text{m}^3/\text{T A s}$)	SD* ($10^{-12} \text{m}^3/\text{T A s}$)	SD/mean (%)
starch	10.70	1.19	11.15	starch	0.50	0.21	41.12
aminated	16.71	0.26	1.54	aminated	6.42	0.44	6.92
2k PEG	0.92	0.09	9.43	2k PEG	0.37	0.09	24.53
5k PEG	4.89	0.65	13.33	5k PEG	0.58	0.16	26.98
20k PEG	15.80	0.54	3.42	20k PEG	3.46	0.72	20.91

*SD is based on three samples. Incubation condition: 24h, 100 $\mu\text{g}/\text{mL}$. Cells with high particle capture have relatively less variation than the case of low particle uptake.

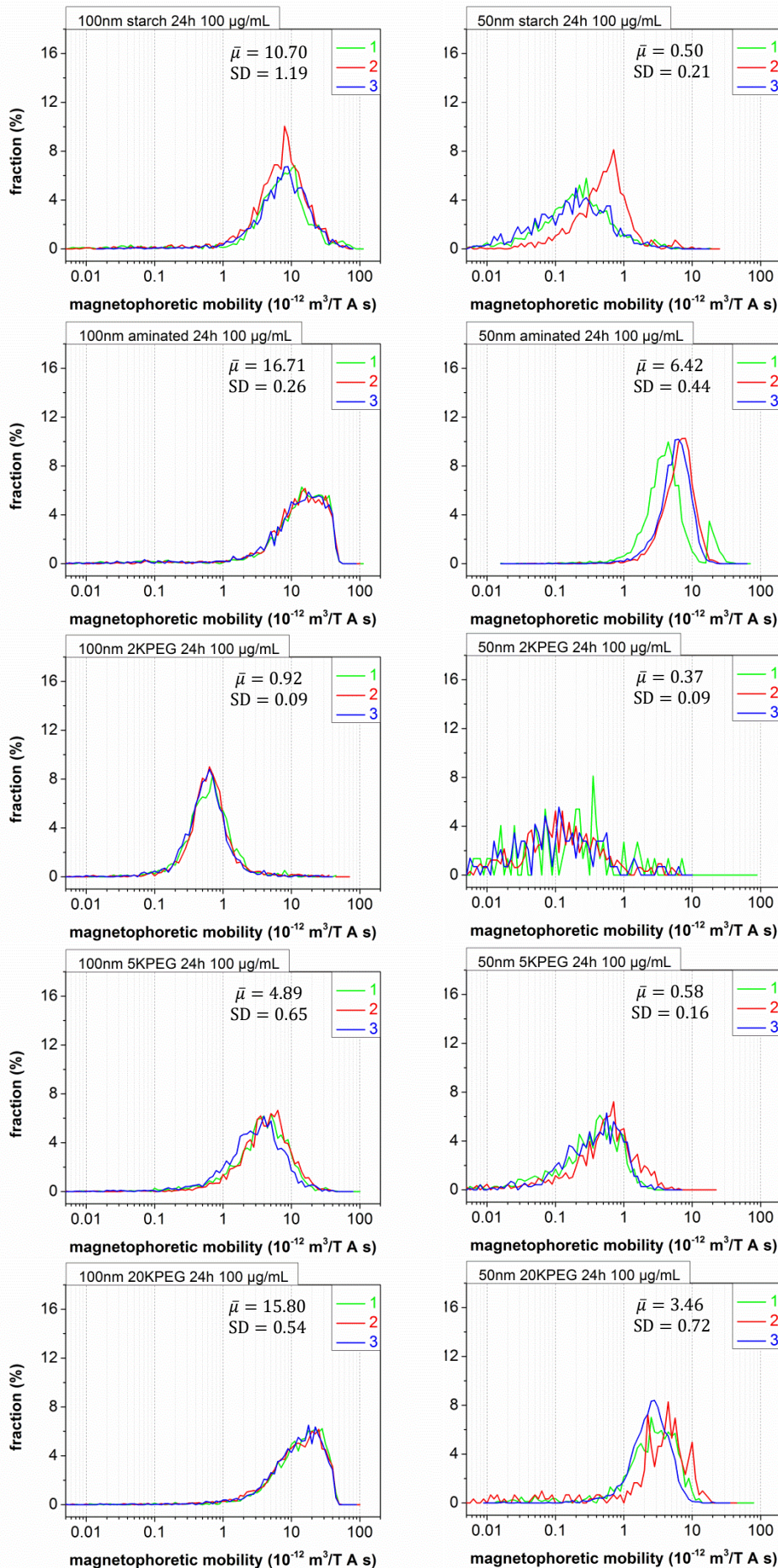


**Figure 5.4 -
 Triplicate
 experiment:
 magnetophoretic
 mobility
 distributions of
 CHO cells labeled
 by 100 and 50nm
 SPIONs coated
 with starch,
 primary amine
 groups or
 2k/5k/20k Da
 PEG
 PEGpoly(ethylene
 glycol) (PEG),
 iron incubation
 time = 24h,
 incubation
 concentration =
 100 μ g/mL**

5.4.3 - Flow cytometry analysis

As Table 5.4 illustrates, the surface chemistry of particles is changed when the particles undergo dye conjugation. From aminated fluidMag to the aminated fluidMag - AF488 particles, the zeta potential decreased significantly, and the size significantly enlarges. In other words, the conjugation of particles with dye results in aggregation. On the other hand, aggregation is not obvious when the particles are pretreated by PEGylated process. The zeta potential only drops a little for PEGylated FluidMAG-AF488.

Table 5.4 - Particles with and without fluorescent label used in phagocytosis assays

PARTICLE TYPE	DIAMETER Z-Avenm)	Zeta (mv)	Potential	Fluorescent Dye	SURFACE COMPOSITION
100nm aminated fluidMAG	170.6	36		no	NHS (Succinimidyl)
100nm aminated fluidMAG+AF488	398	18.5		Alexa Fluor® 488 dye	NHS, AF488
100nm 2k PEGylated fluidMAG	189.4	23.5		no	NHS, 2k PEG
100nm 2k PEGylated fluidMAG+AF488	200.7	21.8		Alexa Fluor® 488 dye	NHS, AF488, 2k PEG
100nm 5k PEGylated fluidMAG	174.7	32		no	NHS, 5k PEG
100nm 5k PEGylated fluidMAG+AF488	228.4	24.1		Alexa Fluor® 488 dye	NHS, AF488, 5k PEG
100nm 20k PEGylated fluidMAG	185.0	26.4		no	NHS, 20K PEG
100nm 20k PEGylated fluidMAG+AF488	211.7	24.8		Alexa Fluor® 488 dye	NHS, AF488, 20k PEG

Table 5.5 summarizes the alexafluor 488 fluorescent signals of labeled cells determined from flow cytometry and the corresponding magnetophoretic mobility values determined from magnetophoretic velocimetry of cells labeled for 24 hours with 100 nm SPIONs. The relatively low fluorescent intensity and mobility value of fluorescent aminated SPIONs-CHO Cells confirm the chemistry change of the particle surface. The PEG content just prevents or weakens the decreased trend due to fluorescent dye. In other words, the NHS groups as active spots could react with PEG and fluorescent dye (which is anionic) and CHO cells. The three options compete against each other. Thus we could control the synthesis orders and chemical charge to optimize the testing method and particles' quality.

Table 5.5 - Fluorescent assay and magnetophoresis of cells

LABEL CELL TYPE	GeoMean fluorescence alexa 488	SD alexa 488	average mobility (10^{-12} m ³ /TAs)	SD (10^{-12} m ³ /TAs)
Unstained cell (ghost dye 780)	5104	3479	0.19	0.56
100nm aminated fluidMAG	2941	15552	16.58	11.0
100nm aminated fluidMAG+AF488	355499	360949	5.21	5.43
100nm 2k PEGylated fluidMAG	4286	2392	0.92	2.15
100nm 2k PEGylated fluidMAG+AF488	23577	27969	0.63	2.37
100nm 5k PEGylated fluidMAG	2217	15180	4.98	3.87
100nm 5k PEGylated fluidMAG+AF488	74395	87977	1.28	3.39
100nm 20k PEGylated fluidMAG	3070	42743	15.5	12.27
100nm 20k PEGylated fluidMAG+AF488	6.94E5	7.35E5	10.77	9.92

Figures 5.5 and 5.6 provide information on the cell suspension samples, especially the health status of the cells. We found that the samples, aminated 20k PEGylated fluidMAG and 20k PEGylated fluidMAG+AF488, have the data dots shifted upward. The fall in FSC signal and

increase in SSC signal will suggest death or dying of the cells. These cells are unhealthy due to large amount of cell uptake of particles. Per cent live cells is displayed on each chart based on a designated 2-parameter live-cell window.

Table 5.6 compares these two analytical methods, both cell by cell methods, from many aspects. Flow cytometry could provide more detail about the cell condition. However, the restrictions such as test cost and sample fluorescent requirement should be considered when choosing flow cytometry as measuring tool to characterize labeled cells.

Table 5.6 - Comparison of the two analytical methods based on study of magnetic carriers

	Flow cytometry	Hyperflux™ Velocimeter
Assay type	Individual cell assay	Individual cell assay
Cell Health	Could detect if viability dye used	Can't tell but could exclude some dead cells data by size gating and total cell count
Test cost	Expensive (fluorescent dye)	Economical after instrument purchase
Sample requirement	Fluorescent Yes. Limit on fluorescent magnetic particles. Also, the fluorescent marker will change the properties of particles, which is not what we need in quantification.	No, so the test range is wide.

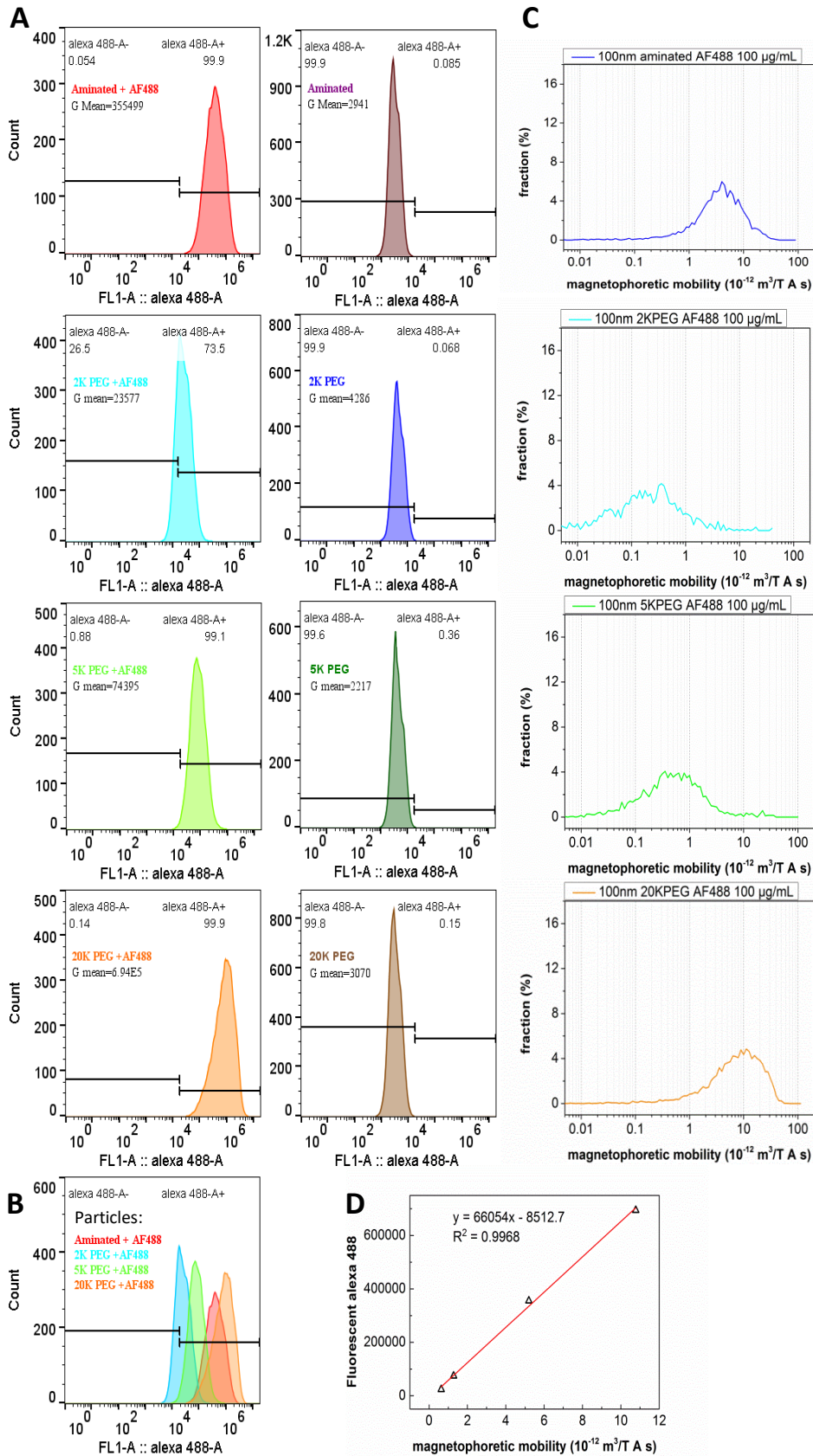


Figure 5.5 - Cell uptake study by flow cytometry (Accuri C6 Flow Cytometer®) and Hyperflux™ Velocimetry. (A) Fluorescence intensity distributions of labeled cells before and after fluorescent marking with different fluorescent SPIONs. (C) Magnetophoretic mobility distribution of labeled cells captured by fluorescent SPIONs (100nm aminated, 2k, 5k and 20k PEGylated MNPs-AF488). (B) Comparison of fluorescence intensities between labeled cells capturing fluorescent SPIONs. (D) The linear relationship between mean fluorescence intensities and average mobility suggest a good agreement between the two methods of phagocytosis assay.

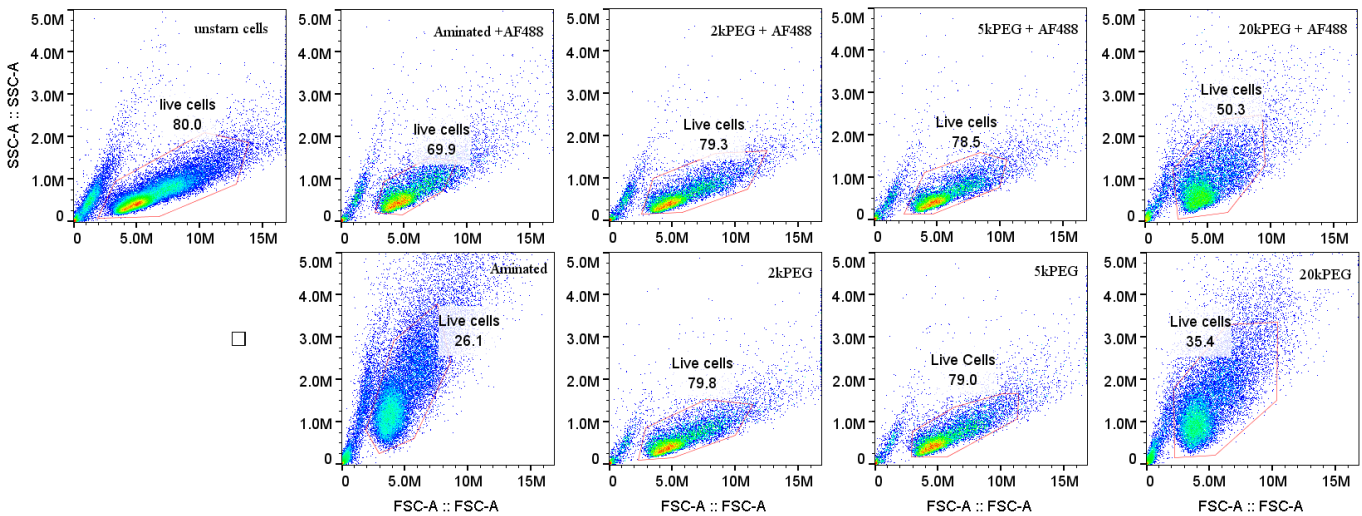


Figure 5.6 Side scatter and forward scatter dot plots.

5.4.4 - Ferrozine Assay

Ferrozine assay for total iron content was also done to evaluate the accuracy of our method.

Table 5.7 - Results of Ferrozine Assay

Labeled cell type	cell number (10^6/mL)	Iron concentration ($\mu\text{g/ml}$)	cell uptake (10^{-6} $\mu\text{g/cell}$)	Average mobility (Hyperflux) (10^{-12} m^3/TAs)
100nm starch	8.38	11.22	1.34	10.70
100nm aminated	9.31	24.36	2.62	16.71
100nm 2k PEGylated	8.67	0.82	0.09	0.92
100nm 5k PEGylated	7.75	3.34	0.43	4.89
100nm 20k PEGylated	8.02	13.69	1.71	15.8
50nm starch	8.94	0.86	0.10	0.50
50nm aminated	8.46	11.95	1.41	6.42
50nm 2k PEGylated	8.29	0.26	0.03	0.37
50nm 5k PEGylated	7.30	0.34	0.05	0.58
50nm 20k PEGylated	7.36	3.61	0.49	3.46

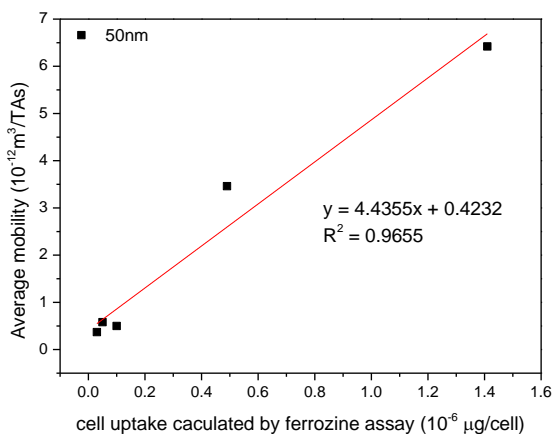
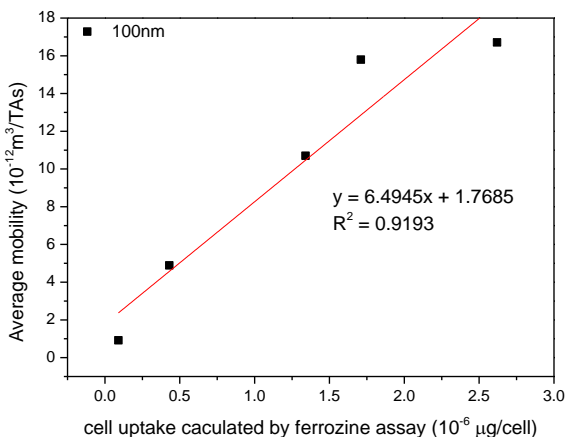


Figure 5.7 - Comparison between magnetophoresis and ferrozine assay

As shown in Figure 5.7, the agreement of results between the ferrozine assay and the Hyperflux analysis is good, but not as good as between Hyperflux and FACS assay, as the latter two are individual assays. Unlike magnetophoresis or flow cytometry assay which is an individual cell assay, the ferrozine assay is a bulk assay. The ferrozine assay doesn't require live cells for testing, so we can prepare or test more samples at the same time. However this method can't exclude the dead cells or debris, which will also contain SPIONs. This result will produce significant error in the data. The FACS assay reveals the dead cell data impact the final result. In addition, the 50 mM NaOH can't dissolve whole cells. There will be flocculence left in the

solution which will aggregate large amounts of the iron, making it more difficult for subsequent sample transfers and tests.

5.5 - Conclusions

The experimental results confirm the ability of the velocimeter to accurately describe the magnetic properties of magnetically labeled cells. The methods have good reproducibility and accuracy as evidenced by triplicate experiments, FACS analysis and Ferrozine Assay. Through investigating the motion behavior of CHO cells labeled by 10 types of unmodified or modified particles (50 and 100 nm paramagnetic-core beads coated with starch, primary amine groups or 2k/5k/20k Da poly(ethylene glycol) (PEG)) in a defined magnetic field, the impact of incubation condition such as particles types, incubation time and incubation concentration are discussed. The mobility distribution results also reveal the cell uptake mode of different types of particles. The phenomena could be explained by the interaction between particle and cell membrane. During the adsorption and intercellular processes, the particle surface charge and composition profoundly affect their uptake by cells in vitro.

The velocimeter provides new opportunities for the application of cell magnetic labeling to investigate the cell uptake mode. Labeling conditions (iron concentration and incubation time) could be chosen to control product quality. FACS assay has a strong ability to reveal the cell health. Ferrozine assay could be used to roughly estimate the cell uptake situation when large amounts of samples are needed to measure at the same time, especially at the stage of experiment design. Both these two methods could be complement of magnetophoresis to comprehensively characterize the properties of labeled cells.

References

Erik I. Finkelstein, P.-h. G. C., Clark T. Hung, and Jeannette Chloe "Bulinski (2007). "Electric Field-Induced Polarization of Charged Cell Surface Proteins Does Not Determine the Direction of Galvanotaxis." Cell Motility and the Cytoskeleton **64**: 833–846.

King, B. F. (1981). "The Distribution and Mobility of Anionic Sites on the Surface of Human Placental Syncytial Trophoblast." Anatomical Record **199**(1): 15-22.

Wilhelm, C., C. Billotey, J. Roger, J. N. Pons, J. C. Bacri and F. Gazeau (2003). "Intracellular uptake of anionic superparamagnetic nanoparticles as a function of their surface coating." Biomaterials **24**(6): 1001-1011.

Wilhelm, C., F. Gazeau, J. Roger, J. N. Pons and J. C. Bacri (2002). "Interaction of anionic superparamagnetic nanoparticles with cells: Kinetic analyses of membrane adsorption and subsequent internalization." Langmuir **18**(21): 8148-8155.

Zalipsky, S. and J. M. Harris (1997). "Introduction to chemistry and biological applications of poly(ethylene glycol)." Poly(Ethylene Glycol) **680**: 1-13.

Zhang, M. Q., T. Desai and M. Ferrari (1998). "Proteins and cells on PEG immobilized silicon surfaces." Biomaterials **19**(10): 953-960.

Chapter 6 – Summary

A magnetophoretic velocimeter (HyperfluxTM velocimeter) was successfully employed to directly measure the magnetophoretic mobility, size and other parameters of magnetic particle suspensions. The instrument, equipped with high-definition microscope system, can collect large amounts of imagery data, showing the trajectory of each particle in an isodynamic magnetic field. The mobility distribution, produced by fast image analysis software, effectively describes magnetism properties of particle samples. The analysis result provides a better understanding and quality control of particle samples(Chen Zhou, Eugene D. Boland et al. 2016).

The magnetophoresis method was introduced to the particle/cell system. As a surrogate for fluorescence activated cell sorters (FACS) in quantitative labeled cell analysis, the velocimeter effectively characterized the cells labeled by the particles without producing a fluorescence signal. In this way, the instrument provides a rapid and convenient tool for the study of cell labeling, without considering the particle selection. The triplicate experiments and comparison experiments confirmed that the velocimeter has accurately described the magnetism properties of labeled cells. In addition, the cell uptake modes were revealed through investigating the motion behavior of CHO cells labeled by 10 types of unmodified/modified particles in a defined magnetic field. The particles' surface charge and composition are key factors that impact their uptake by cells.

The velocimeter provides new opportunities for the application of magnetic carriers to quantitative cell analysis. Two examples are listed to illustrate the point. Cultured *Gallus* lymphoma cells were immunolabeled with commercial magnetic beads and shown to have adequate magnetophoretic mobility to be separated by a novel flowing magnetic separator(Qian

2016, Chen Zhou, Zhixi Qian et al. 2017). Phagocytosis of starch nanoparticles having magnetic cores by cultured Chinese hamster ovary (CHO) cells was quantified on the basis of magnetophoretic mobility. The kinetics of particle phagocytosis, which could be studied by magnetophoretic mobility distribution analysis, provides data suitable for theoretical modeling. The cell labeling system can be optimized for specific application by the control of particle type and labeling conditions such as concentration and incubation time.

Reference

- Chen Zhou, Eugene D. Boland, Paul W. Todd and T. R. Hanley (2016). "Magnetic particle characterization—magnetophoretic mobility and particle size." Cytometry Part A **89**(6): 585-593.
- Chen Zhou, Zhixi Qian, Young Suk Choi, Allan E. David, Paul Todd and T. R. Hanley (2017). "Application of magnetic carriers to two examples of quantitative cell analysis." Journal of Magnetism and Magnetic Materials **427**: pp 25-28.
- Qian, Z. (2016). "Design and Simulation of a Circulating Tumor Cell Detector." Auburn University Dissertations.